Mathematical Modelling of Phage Dynamics

Thesis submitted in accordance with the requirements of
the University of Liverpool for the degree of Doctor in Philosophy
by

Thomas W. Evans

April 2009

Abstract

Shiga toxin-converting (Stx) phages are viruses of the bacterium *Escherichia coli*. They are 'temperate' which means that they may replicate either via the lytic or the lysogenic pathway. A molecular switch determines which of the two pathways is selected. Following lysis of the host cell, toxin molecules are released which can cause potentially fatal diseases in humans.

Three different timescales are considered: cellular time, ecological time and evolutionary time. In ecological time, a population dynamical model is used to derive conditions under which virulent phages (i.e. phages which are only able to replicate lytically) can coexist with temperate phages, and conditions when temperate phages can invade a population of virulent phages and vice versa. The outcome of competition between temperate and virulent phage strains depends on the model parameter values, in particular the relative adsorption rates and burst sizes of the two strains, and also the probability of lysogeny and the induction rate of the temperate phages.

The population dynamical model then forms the basis for modelling the evolution of temperate phages, using an adaptive dynamics approach. Two key parameters relating to the temperate phage population (namely the probability of lysogeny and the lysogen induction rate) are allowed to evolve over time. The adaptive dynamics analysis is used to identify evolutionary singularities which evolution is either directed towards or away from. It is shown that attractor and repellor singularities do arise. However, evolutionary branching does not occur within this framework.

At the cellular level, molecular models are used to consider three problems. Firstly, the stability of Stx lysogens and lysogens of the related phage lambda is modelled and compared. The modelling results show that certain known differences between the molecular switches of Stx and lambda phages can account for the lower stability of certain Stx phages.

The same model is also used to determine the impact of selected environmental factors (nutrient level and temperature) on lysogen stability. An increase in nutrient level or temperature will increase the growth rate of the host cell, which tends to increase the stability of the lysogen. However, it is found that there are circumstances

in which increases in nutrient level or temperature can result in a decrease in lysogen stability.

Finally, a stochastic modelling approach is used to compare the probability of lysogeny in Stx and lambda phages. The results show that a weaker binding energy at the molecular switch in Stx phages leads to a lower probability of lysogeny, and hence a higher rate of toxin release.

Contents

Contents iv

List of Figures ix

1 Background 1

1.1 Introduction to phages 1
1.2 Stx phages 2
1.3 Population Dynamics of Bacteria and Virulent Phages 3
1.4 Adaptive Dynamics 7
1.5 The Lambda Molecular Switch 12
1.6 Thesis Outline 14

2 The Population Dynamics of Temperate and Virulent Bacteriophages 15

2.1 Model 1. Lysogens and free phage 16
2.2 Model 2. Temperate phage, lysogens, and sensitive cells 18
2.3 Model 3. Temperate phage, lysogens, sensitive, and resistant bacteria . 25
2.4 Model 4. Lysogens and sensitive bacteria with virulent and temperate phage 34
2.5 Model 5. The Full Model 42
2.6 Discussion 56

3 Adaptive Dynamics of Temperate Phages 59

3.1 Introduction 59
3.2 A two-strain model 60
3.3 The adaptive dynamics approach 62
3.4 Some examples 66
3.5 Discussion 68
3.6 Appendix A: The fitness function 70
3.7 Appendix B: The Q function 72
3.8 Appendix C: Derivatives of μ and Q at p^* 73

4 Modelling the Stability of Stx Lysogens **81**
4.1 Introduction 81
4.2 Modelling the switch 82
4.3 Phage scenarios 87
4.4 Results 88
4.5 Discussion 91

5 Modelling lysogen stability under varying environmental conditions 104
5.1 Introduction 104
5.2 Derivation of the average number of genome equivalents per cell 107
5.3 Results and Discussion 111

6 Stochastic modelling of the intial decision between lysis and lysogeny in Stx phages **126**
6.1 Introduction 126
6.2 The lambda lysis-lysogeny switch 127
6.3 The stochastic modelling framework 129
6.4 The model 132
6.5 Results and Discussion 135

7 Conclusion **140**

Bibliography **151**

List of Figures

1.1 An example of a Pairwise Invasibility Plot. The horizontal axis corresponds to the resident strategy (x) and the vertical axis corresponds to the mutant strategy (y). In each region of the plot, the sign of the mutant fitness function is indicated. 9

2.1 Numerical simulations for Model 1 (R=resources, L=lysogens, T=temperate phages). Two equilibrium types are shown:(A) Resources (R) only; (B) Resources, lysogens (L) and temperate phages (T). In (A) the parameter settings are $i = 0.4$ and $\omega = 0.5$, while in (B) $i = 0.1$ and $\omega = 0.2$. The remaining parameter values (same for (A) and (B)) are: $R_0 = 100$, $\epsilon = 5 \times 10^{-7}$, $r = 0.7$, $k = 4$, $\beta_T = 100$, $\delta_T = 10^{-9}$, $\alpha_S = 0$, $\xi = 0$ 19

2.2 Numerical simulations for Model 2 (R=resources, L=lysogens, S=sensitive bacteria, T=temperate phages). Three equilibrium types are shown:(A) Resources only ($\omega = 0.8$, $\beta_T = 100$, $\delta_T = 10^{-9}$); (B) Resources and sensitive bacteria ($\omega = 0.65$, $\beta_T = 50$, $\delta_T = 10^{-10}$); (C) Resources, sensitive bacteria, lysogens and temperate phages ($\omega = 0.2$, $\beta_T = 100$, $\delta_T = 10^{-9}$). The remaining parameter values are: $R_0 = 100$, $\epsilon = 5 \times 10^{-7}$, $r = 0.7$, $k = 4$, $\alpha_S = -0.02$, $\xi = 0.0001$, i=0.1, p=0.4 26

2.3 Numerical simulations for Model 3 (R=resources, L=lysogens, S=sensitive bacteria, B=resistant bacteria, T=temperate phages). Five equilibrium types are shown:(A) Resources only ($\omega = 0.8$); (B) Resources and resistant bacteria ($\delta_T = 10^{-5}$); (C) Resources and sensitive bacteria ($\alpha_B = 0.5$, $\beta_T = 10$, $\delta_T = 10^{-11}$). (D) Resources, sensitive cells, temperate phages and their lysogens ($\alpha_B = 0.5$) (E) Resources and all four populations ($\alpha_B = 0.32$). Except where otherwise indicated, the parameter values are: $R_0 = 100$, $\epsilon = 5 \times 10^{-7}$, $r = 0.7$, $k = 4$, $\beta_T = 100$, $\delta_T = 10^{-9}$, $\alpha_S = -0.02$, $\alpha_B = 0$, $\xi = 0.0001$, i=0.1, $\omega = 0.2$ 35

2.4 Numerical simulations for Model 4 (R=resources, L=lysogens, S=sensitive bacteria, T=temperate phages, V=virulent phages). Five equilibrium types are shown:(A) Resources only ($\delta_V = 10^{-12}, \beta_T = 10. \delta_T = 10^{-12}, R_0 = 50, \omega = 0.8$). (B) Resources and sensitive bacteria ($\delta_V = 10^{-11}, \beta_T = 10, \delta_T = 10^{-12}, \alpha_S = -0.1, \omega = 0.2$). (C) Resources, sensitive bacteria and virulent phages ($\beta_V = 150, \delta_V = 2 \times 10^{-11}, \beta_T = 10, \delta_T = 10^{-12}, \alpha_S = -0.1, \omega = 0.2$). (D) Resources, sensitive bacteria, lysogens and temperate phages ($\delta_V = 10^{-11}$). (E) Resources, sensitive cells, lysogens, temperate phages and virulent phages ($\delta_V = 10^{-10}$). Except where otherwise indicated, the parameter values are: $R_0 = 100, \epsilon = 5 \times 10^{-7}, r = 0.7, k = 4, \beta_T = 80, \beta_V = 100, \delta_T = 8 \times 10^{-10}, \alpha_S = -0.02, \xi = 0.001, i = 0.001$ 43

2.5 Numerical simulations for Model 5 (R=resources, B=resistant bacteria, V=virulent phages, L=lysogens, S=sensitive bacteria, T=temperate phages). Nine equilibrium types are shown: (A) Resources only ($\omega = 0.7, \alpha_S = -0.02$) (B) Resources and sensitive cells ($\omega = 0.7$) (C) Resources and resistant cells ($\alpha_S = -0.032, \alpha_B = -0.025, \omega = 0.69, \delta_V = 10^{-3}$) (D) Resources, sensitive cells, and virulent phages ($\alpha_B = 0.7, \delta_T = 10^{-11}$) (E) Resources, sensitive cells, lysogens, and temperate phages ($\beta_T = 100, \delta_T = 10^{-9}, \delta_V = 10^{-11}$) (F) Resources, sensitive cells, resistant cells, and virulent phages ($\alpha_B = 0.1, \delta_T = 10^{-11}$) (G) All populations apart from virulent phages ($\alpha_B = 0, \beta_T = 100, \delta_T = 10^{-9}, \delta_V = 10^{-11}$) (H) All populations apart from resistant cells ($\alpha_B = 0.7$) (I) All populations. Except where otherwise indicated, the parameter values are: $R_0 = 100, \epsilon = 5 \times 10^{-7}, r = 0.7, k = 4, \beta_T = 80, \beta_V = 100, \delta_T = 8 \times 10^{-10}, \delta_V = 10^{-10}, \alpha_S = -0.04, \alpha_B = 0.4, \xi = 0.001, i = 0.001, p = 0.001, \omega = 0.5$. 55

3.1 Contour plots for the function Q. Each contour is labelled with its respective Q value. The contours are all straight lines, and the gradient of each line is equal to the value of the function μ along that line. Parameter values: $R_0 = 100$, $S_0 = 2 \times 10^8$, $\delta = 10^{-9}$, $\beta = 100$, $\xi = 0.0001$, $r = 0.7$, $k = 4.0$, $\epsilon = 5 \times 10^{-7}$, $\omega = 0.2$. 75

3.2 An attractor singularity (A) PIP showing the attractor at $p = 0.6$. (B) Plot of trade-off curve and the line $Q = 0$ line. The tangent to the trade-off curve at the singularity is also shown. (C) Dynamical simulation. Parameter values: $\alpha = -0.7$, other parameters as in Figure 3.1. 76

3.3 A repellor singularity. (A) PIP showing the repellor at $p = 0.24$. (B) Plot of trade-off curve and the line $Q = 0$ line. The tangent to the trade-off curve at the singularity is also shown. (C) Dynamical simulation. Parameter values: $\alpha = 10$, other parameters as in Figure 3.1. 77

3.4 Multiple singularities (I). (A) PIP showing a repellor at $p = 0.73$, and two marginally ESS attractors (at $p = 0.53$ and $p = 0.85$). (B) Plot of trade-off curve and the line $Q = 0$ line. The tangent to the trade-off curve at the repellor singularity is also shown. (C) Dynamical simulation. Parameter values: $\alpha = -0.85$, other parameters as in Figure 3.1. 78

3.5 Multiple singularities (II). (A) PIP showing a repellor at $p = 0.65$, and two marginally ESS attractors (at 0.53 and 0.84). (B) Plot of trade-off curve and the line $Q = 0$ line. The tangent to the trade-off curve at the repellor singularity is also shown. (C) Dynamical simulation. Parameter values: $\alpha = 1.5$, other parameters as in Figure 3.1. 79

3.6 Constraining i to be a decreasing function of p. (A) PIP showing a marginally ESS attractor at $p = 0.58$. (B) Plot of trade-off curve and the line $Q = 0$ line. (C) Dynamical simulation. Parameter values: $\alpha = 5$, other parameters as in Figure 3.1. 80

4.1 The region of lambda DNA which comprises the molecular switch between lysis and lysogeny. It includes the left and right operators, which are regions of DNA which can regulate gene transcription. There are three binding sites at the right operator (O_R1, O_R2, and O_R3) and another three binding sites at the left operator (O_L1, O_L2, and O_L3). The promoters for the genes *cI* and *cro* are labelled P_{RM} and P_R respectively. Repressor molecules are shown bound at all six operator sites. The diagram shows how adjacent repressor molecules interact cooperatively, so as to increase the stability of the molecular configuration. In the configuration shown, transcription of both *cI* and *cro* is blocked. (After Ptashne, 2004). 97

4.2 Plots of the equilibrium equations $\Theta = 0$ (thick black line) and $\Phi = 0$ (with γ_{cI}=0 min^{-1}) for lambda (A, B, and C) and Stx 1 (D, E, and F). The graphs in B, C, E, and F show close ups of the regions where the curves intersect. These points of intersection correspond to the steady states of the models. 98

4.3 Plots of the equilibrium equations $\Theta = 0$ (thick black line) and $\Phi = 0$ (with γ_{cI}=0.061 min^{-1}) for lambda (A), Stx 2 (B), and Stx 3 (C). The graphs in D, E, and F show close-ups of the regions where the lytic and unstable equilibria first appear via a saddle node bifurcation 99
4.4 Plots of the equilibrium equations $\Theta = 0$ (thick black line) and $\Phi = 0$ (with γ_{cI}=0 min^{-1}) for lambda (A), Stx 4(i) (B), and Stx 4(iii) (C). . . 100
4.5 Projections in (CI_T, Cro_T) space of the model trajectories for lambda (A) and Stx 4(iii) (B), with $\gamma_{cI} = 0.20$, obtained by numerically solving the model delay differential equations. Filled circles indicate stable equilibria, while the empty circle in A represents an unstable equilibrium. 101
4.6 Bifurcation diagram for Stx 4 in $(\Delta G_{O_R2}^{CI_2}, \gamma_{cI})$ space. There is no region of lysogenic monostability, so the only possible stability structures are bistability or lytic monostability. 102
4.7 Graphs showing three numerical measures of the stability of lysogenic equilibria: (A) Concentration of Cro_T; (B) Leading eigenvalue; and (C) P_R repression. 103

5.1 Modelling changes in lysogen stability in response to changes in the nutrient level. (a) The example relationship between nutrient level and *E. coli* growth rate which has been adopted for modelling purposes. (b) Leading eigenvalues of the lysogenic equilibrium versus nutrient level (phage lambda). (c) Leading eigenvalues of the lysogenic equilibrium versus nutrient level (Stx3). The curves are labelled with the appropriate value of γ_{cI}. 114
5.2 Plots of the four eigenvalues of the lysogenic equilibrium against *E. coli* growth rate for different values of the CI degradation rate, γ_{cI} (phage lambda only). (a) $\gamma_{cI} = 0.0$. (b) $\gamma_{cI} = 0.05$. (c) $\gamma_{cI} = 0.10$. (d) $\gamma_{cI} = 0.20$. (e) $\gamma_{cI} = 0.30$. (f) $\gamma_{cI} = 0.37$. 115
5.3 Plots of the leading eigenvalue of the lysogenic equilibrium against γ_{cI} for phage lambda and the four Stx scenarios, at three different nutrient levels (a) Low nutrient level. (b) Medium nutrient level. (c) High nutrient level. 116
5.4 Modelling changes in lysogen stability in response to changes in temperature. (a) The relationship between temperature and *E. coli* growth rate reported by Bremer and Dennis (1996). (b) Leading eigenvalue of the lysogenic equilibrium versus temperature (phage lambda). (c) Leading eigenvalue of the lysogenic equilibrium versus temperature (Stx3). . . . 119

5.5 Plots of the four eigenvalues of the lysogenic equilibrium against temperature for different values of the CI degradation rate, γ_{cI} (phage lambda only). (a) $\gamma_{cI} = 0.0$. (b) $\gamma_{cI} = 0.05$. (c) $\gamma_{cI} = 0.10$. (d) $\gamma_{cI} = 0.35$. (e) $\gamma_{cI} = 0.45$. (f) $\gamma_{cI} = 0.50$. 120

5.6 Plots of the leading eigenvalue of the lysogenic equilibrium against γ_{cI} for phage lambda and the four Stx scenarios, at three different temperatures. (a) 20 °C. (b) 30 °C. (c) 40 °C. 121

5.7 Plots of the leading eigenvalue of the lysogenic equilibrium against γ_{cI} for phage lambda and the four Stx scenarios. (a) 1 prophage per lysogen. (b) 2 prophages per lysogen. (c) 3 prophages per lysogen. (d) 4 prophages per lysogen. 123

6.1 The region of lambda DNA which comprises the molecular switch between lysis and lysogeny. After Ptashne (1986). 127

6.2 The model algorithm. (The notation $j \in C0$, for example, means that reaction j is a member of the gamma class, C0). 133

6.3 Scatter plots of the final numbers of molecules of CI_2 and Cro_2 for phage lambda (A), Stx1 (B), and Stx2 (C). Points above the diagonal line correspond to lysis, points below the line correspond to lysogeny. 139

Acknowledgements

I would like to thank my supervisors Roger and Martin for their tremendous support and guidance during the project. Thanks also to my family, and to the friends I have made in Liverpool over the last three years.

Chapter 1

Background

1.1 Introduction to phages

Bacteriophages (also known as phages) are viruses which infect bacteria. They were discovered independently by the bacteriologists Frederick Twort (1915) and Felix d'Herelle (1917). D'Herelle coined the name bacteriophage, which means 'bacteria-eater' (the Greek word $\phi\alpha\gamma\epsilon\iota\nu$ - *phagein* - is the verb 'to eat').

A typical phage consists of a head, which contains the genetic material, and a tail. Bacterial infection begins when the phage tail attaches itself to the outer cell wall of the bacteria, a process known as adsorption. The phage genome (a molecule of either DNA or RNA, depending on the phage type) then passes through the tail and is inserted into the bacterial cell. There are then two possible pathways by which the infection may subsequently proceed, known as the lytic and lysogenic pathways.

The *lytic* pathway involves the construction of many copies of the original phage, followed by the bursting open (lysis) of the host cell and the release of the new phage particles; in this case the host is destroyed. In a *lysogenic* infection, the phage genome is inserted into the bacterial genome (and is then known as a prophage). In this case the host cell survives and is known as a lysogen. Following normal cell division of the host, the two daughter cells each contain a copy of the prophage within their genomes. Lysogens are generally immune to superinfection by phages of the same strain as the resident prophage.

Phage strains may be either virulent or temperate. A virulent phage is only capable of replicating itself via the lytic pathway, while temperate phages are capable of both lytic and lysogenic reproduction. A temperate phage which initially forms a lysogen with its host may later initiate the lytic cycle via a process known as induction. One of the most extensively studied temperate phages is lambda (λ) phage, a virus of *Escherichia coli* (*E. coli*) first isolated by Esther Lederberg (1951). The mechanisms by which phage lambda selects between the lytic and lysogenic pathways, and by which

it maintains the lysogenic state, have been determined at the level of individual genes and proteins (Ptashne, 1986).

1.2 Stx phages

Shiga toxin-producing *E. coli* (STEC), and in particular the O157:H7 serotype, are well known human pathogens. The STEC O157:H7 serotype was discovered to be a foodborne pathogen in 1982, when it was identified as the cause of an outbreak of hemorrhagic colitis in Oregon and Michigan in the U.S.A. (Karmali et al., 1983; Riley et al., 1983). Since then, it has been associated with further outbreaks of hemorrhagic colitis and other diseases, including hemolytic uremic syndrome (HUS), which can be fatal in humans. For example, *E. coli* O157:H7 infections occurred in primary schools in Japan in 1996 and 1998, affecting over 6,000 children and resulting in two deaths from HUS (Watarai et al., 1998). Healthy cattle constitute a major reservoir of STEC, and infection in humans is often the result of the contamination of food or water by manure (Gyles, 2007).

The major virulence factors of STEC are Shiga toxin 1 (Stx1) and Shiga toxin 2 (Stx2). The genome sequence of Stx1 is almost identical to that of the *S. dysenteriae* toxin, while there is a greater degree of diversity in the sequence of Stx2. The sequence identity of some Stx2 variants to the *S. dysenteriae* toxin is only 60% (Allison, 2007). The ability of *E. coli* to produce Shiga toxins is conferred by temperate lambdoid phages known as Shiga toxin-converting (Stx) phages. The term 'lambdoid' signifies that these phages share a similar genome structure and life history with phage lambda (Ptashne, 2004). Each Stx phage encodes only one Shiga toxin, which is either of type Stx1 or Stx2 (Allison, 2007); for example, the strains known as 933W and H-19B encode Stx2 and Stx1 respectively.

It has been reported that freely existing Stx phages persist in the environment (especially soil and water) more successfully than their bacterial hosts, and also that they are more resistant to chlorination, heat treatment and composting processes (Muniesa et al, 1999; Johanessen et al 2005), thus promoting the survival of *stx* genes. In six river water studies, it was found that over a one week period the numbers of *E. coli* cells decreased between 2 and 3 log units while the numbers of free Stx phages decreased between 1 and 2 log units (Muniesa et al, 1999). Free Stx phages may begin the infection process as soon as a suitable host cell is encountered.

An *E. coli* cell which has been infected by an Stx phage will only release Shiga toxins when lysis occurs. Thus, if the lysogenic pathway is selected there will be no release of toxins initially. However, if the lysogen is later induced (i.e. the lytic pathway is initiated), then toxins will be released when the host cell is lysed. Thus, the proportion

of infections which result in lysogeny (the 'probability of lysogeny'), and the rate at which lysogens are induced (the 'induction rate'), have an important impact on the rate at which Shiga toxins are released into the environment. Studies have shown that lysogens of 933W and H19-B are subject to higher rates of induction than lambda lysogens (Livny and Friedman, 2004). In Stx phages, a genetic switch similar to that of phage lambda determines whether the lytic or lysogenic pathway is selected.

Using models at both the population and the molecular levels, this thesis investigates some of the factors which influence the probability of lysogeny and the induction rate of Stx phages over three different timescales: cellular time (Chapters 4, 5 and 6), ecological time (Chapter 2) and evolutionary time (Chapter 3). Over cellular time, the levels of key regulatory proteins within a single infected host cell are modelled, while populations of bacteria and phages and their interactions are considered in ecological time. Over evolutionary time, the evolution of characteristics within a phage population is modelled. The following sections introduce the main mathematical techniques which will be used, with the help of some examples, beginning with a consideration of population dynamics.

1.3 Population Dynamics of Bacteria and Virulent Phages

In the Malthusian growth model, named after Thomas Malthus (1766-1834), the size of a population at time t can be expressed as

$$B(t) = B_0 e^{rt}$$

where B_0 is the initial population size and r is a constant known as the growth rate. Differentiating with respect to t, we obtain

$$B'(t) = rB_0 e^{rt} = rB(t)$$

so that the rate at which the population size increases is proportional to the current population size. This is also known as exponential growth.

Exponential growth of a population cannot continue indefinitely since the supply of resources needed for growth, such as food, is limited. In the logistic model of population growth (Verhulst, 1838) there is an initial period of (approximately) exponential growth, but over time the growth slows down and eventually stops altogether. This model is given by the following first-order differential equation:

$$\frac{dB}{dt} = rB(1 - \frac{B}{C})$$

where r and C (the 'carrying capacity') are constants. This model has two steady states or equilibria (obtained by setting the above equation equal to zero): $B_1^* = 0$ and $B_2^* = C$.

Novick and Szilard (1950) developed a device known as a chemostat which may be used to maintain a bacterial population at a steady state. The bacteria are held in a container called the 'growth tube'. A supply of nutrients flows into the growth tube from a storage tank at a rate ω. Bacteria and unused nutrient also flow out of the growth tube at a rate of ω so that the amount of fluid in the tube remains constant. The nutrient contains high concentrations of all but one of the growth factors needed by the bacteria for growth. The single exception is the controlling growth factor, whose concentration is relatively low. The concentration of the controlling growth factor within the nutrient will determine the concentration of bacteria at the steady state.

The following expression was proposed by Monod (1949) for the per capita bacterial growth rate (ψ) in the presence of a limiting nutrient or resource (R):

$$\psi(R) = \frac{rR}{k + R}$$

where r is the maximum growth rate and k is the nutrient concentration at which the population grows at half of the maximum rate. This model will appear in the chemostat models of phage and bacteria interactions discussed later on.

1.3.1 A model of bacteria and virulent phages

Campbell (1961) modelled populations of virulent phages (V) and their bacterial hosts (B) in a chemostat as follows:

$$\frac{dB}{dt} = rB(1 - \frac{B}{C}) - \omega B - \delta BV \tag{1.1}$$

$$\frac{dV}{dt} = \delta\beta B(t-l)V(t-l) - \delta BV - k_V V - \omega V \tag{1.2}$$

Here the normal growth of the bacteria is assumed to be logistic with growth rate r and carrying capacity C. The rate at which bacteria are infected by phages, δ, is known as the adsorption rate. The burst size β is the number of new phages which are released following lysis of the host cell. The chemostat flow rate is denoted by ω. Phages are spontaneously deactiveated at a rate of k_V. The time delay between the initial infection of a cell and the release of new phage particles is denoted by l, and the terms $B(t-l)$ and $V(t-l)$ are the values of B and V at time $t-l$.

By setting (1.1) and (1.2) equal to zero, with $B(t-l)V(t-l) = BV$, Campbell (1961) obtained four possible equilibria:

(i) $\hat{B} = 0, \hat{V} = 0$

(ii) $\hat{B} = 0, \hat{V} = V_0$ (in the special case $k_V = \omega = 0$)

(iii) $\hat{V} = 0, \hat{B} = C\left(1 - \frac{\omega}{r}\right)$

(iv) $\hat{B} = \frac{k_V + \omega}{\delta(\beta - 1)}, \hat{V} = \frac{r}{C\delta}\left[C\left(1 - \frac{\omega}{r}\right) - \frac{k_V + \omega}{\delta(\beta - 1)}\right]$ (1.3)

Given a set of such equilibria, it is natural to ask under what conditions each equilibrium is feasible (i.e. $\hat{B}$ and $\hat{V}$ are both non-negative) and stable (i.e. given a small perturbation to the system at equilibrium, the system will return to the original equilibrium). The feasibility conditions for the four equilibria are as follows:

(i) Always feasible

(ii) Feasible provided $V_0 > 0$

(iii) Feasible provided $\omega/r < 1$

(iv) Feasible provided $\beta > 1$ and $C\delta(\beta - 1)(1 - \omega/r) \geq k_V + \omega$

The stability of an equilibrium can be determined from the eigenvalues of the Jacobian matrix. In order to simplify the analysis we can ignore the time delay between infection and lysis (i.e. set $l = 0$ in (1.1) and (1.2) so that $B(t - l)V(t - l) = BV$); then the Jacobian is given by:

$$J = \begin{pmatrix} r - 2r\hat{B}/C - \omega - \delta\hat{V} & -\delta\hat{B} \\ \delta\hat{V}(\beta - 1) & \delta\hat{B}(\beta - 1) - k_V - \omega \end{pmatrix}$$

The stability conditions are obtained by requiring the eigenvalues of the Jacobian to be negative. For the equilibria (i) to (iii), these conditions turn out to be:

(i) $k_V + \omega > 0$ and $r < \omega$

(ii) $k_V + \omega > 0$ and $V_0 > (r - \omega)/\delta$ (which cannot be satisfied, since $k_V = \omega = 0$ for this equilibrium)

(iii) $r > \omega$ and $\delta C(\beta r + \omega) > (\delta\beta C\omega + \delta C r + k_V r + \omega r)$

The stability conditions for the fourth equilibrium are rather lengthy and are therefore not repeated here.

Another question we can ask is whether it is possible for mutant strains of bacteria to invade a stable equilibrium of type (iv), consisting of a resident bacterial strain and

a resident phage strain. Let B_1 and V be the resident strains, and let B_2 represent a mutant bacterial strain. Let strains B_1 and B_2 be subject to different adsorption rates (δ_1 and δ_2 respectively) and growth rates (r_1 and r_2 respectively). Consider a small number of invading bacterial cells from B_2. Using (1.1), we can write down the rate at which this mutant population will grow as follows:

$$r_2(1 - \hat{B}_1/C) - \omega - \delta_2\hat{V} \tag{1.4}$$

where $\hat{B}_1$ (> 0) and $\hat{V}$ (> 0) are given by (1.3). If the above expression is greater than zero, then the mutants will be able to invade.

Similarly, suppose that B and V_1 are the resident strains, and that a small number of mutant phages from strain V_2 emerge in the population. If V_1 and V_2 are subject to different deactivation rates (k_{V1} and k_{V2}) and have different burst sizes (β_1 and β_2), then using (1.2) the rate at which the mutant population will grow is given by:

$$\delta\beta_2\hat{B} - \delta\hat{B} - k_{V2} - \omega \tag{1.5}$$

where $\hat{B}$ (> 0) is given by the expression in (1.3). If the above quantity is positive, then the mutant phages can invade.

1.3.2 A model of resources, bacteria and virulent phages

Levin et al (1977) present a model of virulent phages (V) and bacteria (B) which includes a term representing the availability of resources (R) required by the bacteria. Another term, B_v, represents infected bacteria which have not yet been lysed. The model allows for multiple types of each population, but with one resource, one bacterium and one phage it reduces to:

$$\frac{dR}{dt} = \omega(R_0 - R) - \phi(R)(B + B_v) \tag{1.6}$$

$$\frac{dB}{dt} = B\phi(R)/e_B - \omega B - \delta BV \tag{1.7}$$

$$\frac{dB_v}{dt} = \delta BV - \omega B_v - e^{-\omega l}\delta B(t-l)V(t-l) \tag{1.8}$$

$$\frac{dV}{dt} = \beta c^{-\omega l}\delta B(t-l)V(t-l) - \omega V - \delta BV \tag{1.9}$$

Here ϕ is the bacterial growth function (not specified), and its value depends on the availability of resources. Resources are assumed to flow into the habitat from a reservoir at a rate ω; unused resources also flow out of the habitat at the same rate ω. The

concentration of resources in the reservoir is denoted by R_0. The amount of resources which a bacterium must consume in order to replicate (i.e. divide into two daughter cells) is e_B, and the other parameters are the adsorption rate (δ) and the burst size (β).

This model formed the basis for later work by Stewart and Levin (1984) in which time delays between infection and lysis are ignored (hence neither the B_c population nor the parameter l appear), but populations of temperate phages and their lysogens are introduced; this later model will be analysed in detail in Chapter 2. The following section illustrates how a population dynamical model can be used to model evolution within the framework of adaptive dynamics, which is the subject of Chapter 3.

1.4 Adaptive Dynamics

The theory of Adaptive Dynamics (Geritz *et al*, 1998) is concerned with the evolution of a population whose individuals are subject to small mutations. Suppose that there is a resident population of identical individuals which reproduce asexually, such that offspring are identical to the parent. We are interested in the evolution of a particular one-dimensional trait or strategy. Initially, the resident population is assumed to have reached a locally stable equilibrium (the demographic attractor), and so all individuals have the same strategy, denoted by x.

The long-term exponential growth rate of the population is denoted by $r(x, E_x)$, where E_x is the environment given that all individuals follow strategy x. At the demographic attractor, we have $r(x, E_x) = 0$.

Now suppose that the population is subject to mutations, so that an offspring may be born with a different strategy to its parent. We assume that such mutations are small and infrequent, and therefore the effect on the overall population will be negligible, initially. If a particular mutation represents an improvement in fitness compared to the resident strategy, then this mutant strategy may begin to spread within the population.

Suppose that a small number of mutants emerge with strategy y. At this stage, the predominant population behaviour is still determined by the resident strategy x, and so the mutant fitness function can be written as

$$s_x(y) = r(y, E_x)$$

If $s_x(y) < 0$ then the mutant population will simply die out. If $s_x(y) > 0$, then the small number of mutants may still die out owing to random extinctions; however, there is also the possibility that the mutant population will begin to grow. If $s_x(y) > 0$ and $s_y(x) < 0$, then once the mutant population becomes large enough, the resident

population will not be able to recover and will eventually be replaced by the mutant population. On the other hand, if both $s_x(y)$ and $s_y(x)$ are positive then the two populations may coexist.

Since mutations are assumed to be small, we can write down the following linear approximation of the mutant fitness:

$$s_x(y) = s_x(x) + D(x)(y - x)$$

where $D(x)$ is the local fitness gradient, given by

$$D(x) = \left.\frac{\partial s_x(y)}{\partial y}\right|_{y=x}$$

We know that $s_x(x) = r(x, E_x) = 0$, and so it is the sign of $D(x)$ which determines whether a particular mutant may invade. If $D(x)$ is positive then a mutant strategy y may invade if $y > x$, and it may not invade if $y < x$. Similarly, if $D(x)$ is negative then a mutant strategy y will only be able to invade if $y < x$.

Evolution will proceed over time in the direction of the local fitness gradient until either (i) the maximum or minimum value of x is reached, or (ii) a value of x is reached at which the local fitness gradient is zero. If $D(x) = 0$ then x is said to be an 'evolutionary singularity', and is denoted by x^*.

1.4.1 Pairwise invasibility plots

Pairwise invasibility plots (PIPs) (Christiansen and Loeschcke, 1980; Metz et al, 1992) provide a geometrical method of locating evolutionary singularities. A PIP shows the regions in (x, y) space in which the function $s_x(y)$ is positive, and the regions where it is negative. An example is shown in Figure 1.1.

For a given resident strategy, x_1 say, we can see which mutant strategies may invade by drawing a vertical line through x_1. Those parts of the line which fall in a region of the PIP labelled '+' indicate mutant strategies with positive fitness, and therefore these mutants are capable of invading.

On the principal diagonal of a PIP the mutant and resident strategies are the same, and so the mutant fitness is zero along this line. The sign of the local fitness function can be deduced from the pattern of signs around the principal diagonal. Consider a particular point on the principal diagonal, (x_1, x_1), and suppose that there is a '+' above this point and a '-' below. In this case, the mutant fitness is increasing as y increases and therefore the sign of $D(x_1)$ is positive. Similarly, for a point on the principal diagonal with a '-' above and a '+' below, the sign of the local fitness gradient will be negative.

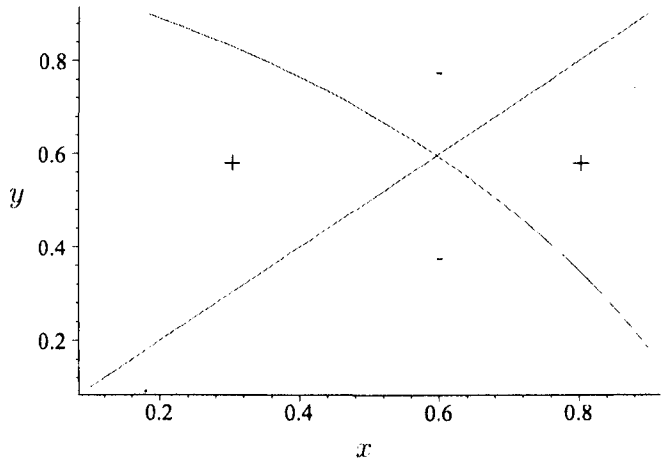

Figure 1.1: An example of a Pairwise Invasibility Plot. The horizontal axis corresponds to the resident strategy (x) and the vertical axis corresponds to the mutant strategy (y). In each region of the plot, the sign of the mutant fitness function is indicated.

1.4.2 Properties of evolutionary singularities

A point at which the principal diagonal in the PIP intersects with another line along which $s_x(y) = 0$ corresponds to an evolutionary singularity, x^*. At the point (x^*, x^*) on the principal diagonal, the signs above and below are the same (i.e. both positive or both negative) and so the value of $D(x^*)$ must be zero. In other words, at a singularity x^* the mutant fitness function reaches either a local maximum or a local minimum value; the pattern of signs around (x^*, x^*) indicates which of these possibilities is the case, as described below.

If the regions above and below the point (x^*, x^*) are labelled '-' in the PIP, then we know that $s_x(y)$ as a function of y reaches a local maximum at the singularity, and therefore the second-order derivative of $s_x(y)$ with respect to y must be negative:

$$\left.\frac{\partial^2 s_x(y)}{\partial y^2}\right|_{y=x=x^*} < 0 \tag{1.10}$$

In this case any nearby mutant will have lower fitness than the singularity x^*, and x^* is said to be ES-stable (ESS; Maynard Smith and Price, 1973). Thus a nearby mutant cannot invade an ESS singularity, and once such a singularity has been reached no further evolutionary change is possible.

The singularity x^* is convergence-stable (CS; Eshel, 1983; Christiansen, 1991) if a nearby resident population can be invaded by a mutant which is even closer to the singularity. If there is a neighbourhood of x^* such that $s_x(y) > 0$ for all x and y

satisfying either $x < y < x^*$ or $x^* < y < x$, then x^* is CS. On the PIP there will be a '+' above and a '-' below the leading diagonal for $x < y < x^*$, and a '-' above and a '+' below the leading diagonal for $x^* < y < x$. Thus evolution will proceed towards the singularity.

If x^* is CS, then the sign of $D(x)$ changes from positive to negative at this point, i.e. :

$$\left.\frac{dD(x)}{dx}\right|_{y=x=x^*} = \left.\frac{\partial^2 s_x(y)}{\partial x \partial y} + \frac{\partial^2 s_x(y)}{\partial y^2}\right|_{y=x=x^*} < 0. \tag{1.11}$$

Using the following relationship (Geritz et al, 1998)

$$\frac{\partial^2 s_x(y)}{\partial x^2} + 2\frac{\partial^2 s_x(y)}{\partial x \partial y} + \frac{\partial^2 s_x(y)}{\partial y^2} = 0$$

we can re-write the CS condition as:

$$\left.\frac{\partial^2 s_x(y)}{\partial x^2}\right|_{y=x} > \left.\frac{\partial^2 s_x(y)}{\partial y^2}\right|_{y=x=x^*}$$

Given the definitions of the ESS and CS properties, we are now able to distinguish between different types of evolutionary singularity.

1.4.3 Evolutionary outcomes

The properties of ESS and CS enable us to identify four types of singularity, namely: attractors, branching points, repellors, and 'Garden of Eden' points.

An attractor is a singularity which is both ESS and CS. Evolution is directed towards an attractor, and once the attractor is reached no further evolutionary change is possible. Thus attractors are associated with evolution towards intermediate values of the evolving parameter

Branching points are CS but not ESS. Evolution proceeds towards a branching point, but once this point is reached it is possible for nearby mutants to invade. This may lead to evolutionary branching and coexistence of different strains.

Repellors are neither ESS nor CS. If the resident population is at or close to a repellor, evolution will be directed away from this point. Repellors are associated with evolution towards extreme values of the evolving parameter.

'Garden of Eden' points are ESS but not CS. These are strategies which are unbeatable, but which cannot be reached from any other point via small mutations.

1.4.4 An example of the use of adaptive dynamics

As a brief and novel example we can consider the evolution of a bacterial population in the presence of a fixed (i.e. non-evolving) strain of virulent phages. To do this, we can return to the Cambell (1961) model of bacteria and virulent phages given by (1.1) and (1.2), with the assumption of zero time delays (i.e. $l = 0$ and $B(t-l)V(t-l) = BV$). Resident and mutant bacterial strains are denoted by B_1 and B_2, and are subject to different adsorption rates (δ_1 and δ_2) and growth rates (r_1 and r_2). In this case the fitness function is given by (1.4), i.e.

$$s_x(y) = r_2(1 - \hat{B}_1/C) - \omega - \delta_2\hat{V} \tag{1.12}$$

where x denotes the resident parameters (r_1 and δ_1) and y denotes the mutant parameters (r_2 and δ_2). Now suppose that there is a trade-off relationship f between the parameters δ and r, such that $r = f(\delta)$ (where f is monotonic increasing). This represents the assumption that if resistance to infection increases (i.e. the value of the parameter δ decreases), then the ability of the bacteria to take in resources will be impaired (and so the value of r will also decrease). We can re-write the fitness function as:

$$s_x(y) = f(\delta_2)(1 - \hat{B}_1/C) - \omega - \delta_2\hat{V}, \tag{1.13}$$

where x now denotes δ_1 and y, δ_2. At an evolutionary singularity $\delta_1 = \delta_2 = \delta^*$, we have

$$\left.\frac{\partial s_x(y)}{\partial y}\right|_* = f'(\delta^*)\left(1 - \frac{\hat{B}(\delta^*)}{C}\right) - \hat{V}(\delta^*) = 0 \tag{1.14}$$

So the evolutionary singularities are the values of δ at which the slope of the trade-off function is equal to $\hat{V}C/(C - \hat{B})$. Note that for positive values of $\hat{B}$, the value of $(C - \hat{B})$ must be positive (otherwise the right hand side of (1.1) will not be equal to zero). Once the singularities have been identified, they can be classified according to whether they satisfy the ESS and CS conditions. Differentiating $s_x(y)$ twice with respect to the mutant:

$$\frac{\partial^2 s_x(y)}{\partial y^2} = f''(\delta_2)(1 - \hat{B}_1/C) \tag{1.15}$$

Since $C > \hat{B}$, the sign of this quantity depends only on the sign of $f''(\delta_2)$. Therefore (using (1.10)), a singularity δ^* is ESS if $f''(\delta^*)$ is negative.

Differentiating $s_x(y)$ with respect to the mutant and again with respect to the resident yields, and evaluating the result at a singularity δ^* yields:

$$\left.\frac{\partial^2 s_x(y)}{\partial y \partial x}\right|_* = \frac{2\hat{B}}{C}\left[\frac{f'(\delta^*)}{\delta^*} - \frac{f(\delta^*)}{\delta^{*2}}\right] + \frac{f(\delta^*) - \delta^* f'(\delta^*) - \omega}{\delta^{*2}}$$

Here we have assumed that the resident equilibrium inludes non-zero populations of both bacteria and phages, so that $\hat{B}$ is given by (1.3). Then the CS condition is satisfied if the sign of $\frac{\partial^2 s_x(y)}{\partial x \partial y} + \frac{\partial^2 s_x(y)}{\partial y^2}$ is negative (from (1.11)). Once the ES and CS conditions have been determined it is possible to classify the singularity as a repellor, attractor, branching point or 'Garden of Eden'.

The above example considers the evolution of the host bacterium in the presence of virulent phages. In Chapter 3 the evolution of temperate phage strains (in the presence of a single fixed bacterial population) will be modelled using adaptive dynamics, which is a more complicated problem in the sense that the presence of lysogens be allowed for, in addition to the bacterial and phage populations.

The following section introduces the topic of molecular level modelling of phage infections, which is the approach used in Chapters 4, 5 and 6.

1.5 The Lambda Molecular Switch

A genetic switch enables phage lambda to select between lysis and lysogeny, and also to exit the lysogenic state via induction. A brief description of the components of the lambda switch is given below, and further details can be found in the relevant later chapters.

The switch centres around the right operator, O_R, on the lambda genome. This operator includes three binding sites (labelled O_R1, O_R2 and O_R3) and is situated between the genes *cI* and *cro*. These genes code for the regulatory proteins CI (known as the repressor) and Cro. Dimers of CI and Cro (i.e. CI_2 and Cro_2 molecules) can bind to the O_R binding sites, and thus regulate the expression of the two genes. For example, with molecules of CI_2 bound to O_R1 and O_R2 (and O_R3 unbound), *cI* is on and *cro* is off. This means that a molecule of the enzyme RNAP can transcribe the *cI* gene to produce a mRNA transcript which can then be translated by a ribosome to produce a molecule of CI. Similarly, with a Cro_2 molecule bound to O_R3 (and O_R1 and O_R2 unbound) *cI* is off and *cro* is on, leading to the synthesis (via transcription and translation) of Cro molecules.

The balance between the concentrations of CI and Cro within the cell determines the outcome of the initial decision between lysis and lysogeny, and also the rate at which lysogens undergo induction. Following an initial infection event, a high level of

cI expression and a low level of *cro* expression will lead to lysogeny; low *cI* expression and high *cro* expression will lead to lysis.

In a lysogen there is a relatively high concentration of CI_2, while the concentration of Cro_2 is almost nil. If the CI_2 concentration falls, this will lead to the *cro* gene being expressed. If synthesis of Cro_2 proceeds at a high enough rate, then this will lead to a further reduction in the level of CI_2, since repression of *cI* will occur more frequently.

Santillan and Mackey (2004) presented the following delay differential equation model of the lambda switch:

$$\begin{aligned}
\frac{d[M_{cI}]}{dt} &= k^q_{cI}[O_R]f^q_{RM}([CI_2]_{\tau_M}, [Cro_2]_{\tau_M}) + k^s_{cI}[O_R]f^s_{RM}([CI_2]_{\tau_M}, [Cro_2]_{\tau_M}) \\
&\quad - (\gamma_M + \mu)[M_{cI}] \\
\frac{d[M_{cro}]}{dt} &= k_{cro}[O_R]f_R([CI_2]_{\tau_M}, [Cro_2]_{\tau_M}) - (\gamma_M + \mu)[M_{cro}] \\
\frac{d[CI_T]}{dt} &= \rho_{cI}[M_{cI}]_{\tau_{cI}} - (\gamma_{cI} + \mu)[CI_T] \\
\frac{d[Cro_T]}{dt} &= \rho_{cro}[M_{cro}]_{\tau_{cro}} - (\gamma_{cro} + \mu)[Cro_T]
\end{aligned}$$

where M_{cI} and M_{cro} are the concentrations of the mRNA transcripts of the genes *cI* and *cro* respectively, and CI_T and Cro_T are the total concentrations (i.e. monomers plus dimers) of the proteins CI and Cro. The remaining terms in the model are described in Chapter 4.

In Chapter 4 the above model is used to find equilibria corresponding to the lysogenic state, and the leading eigenvalue of each equilibria is used as a measure of its stability. The model is then adjusted to allow for known characteristics of the molecular switch in Stx phages, so that the stability of lambda and Stx lysogens can be compared.

The ability of a prophage to initiate the lytic cycle provides a means of escape from a host whose survival is threatened by adverse environmental conditions, such as the presence of ultra-violet light, low resource levels, or extreme temperatures. Bremer and Dennis (1996) presented data on the growth rate and chemical composition of *E. coli* at different nutrient levels and temperatures. By incorporating this data into the Santillan and Mackey (2004) model, Chapter 5 investigates the impact of some environmental conditions on lysogen stability.

Arkin et al (1998) developed a stochastic model of the initial decision between lysis and lysogeny of phage lambda. This model used the Gillespie (1977) algorithm to simulate reaction events such as protein dimerization, dissociation and degradation. In Chapter 6, this model is used as the basis for comparing the probability of lysogeny in Stx and lambda phages. In order to speed up the simulation process, the algorithm used incorporates a simplification proposed by Gibson and Bruck (2000) whereby tran-

scription of genes and translation of mRNA molecules are modelled as single reaction events, rather than as series of reactions representing movement of the enzyme (in the case of transcription) or ribosome (in the case of translation) from one nucleotide to the next.

1.6 Thesis Outline

To summarize, this thesis considers the dynamics of phage infections over cellular, ecological, and evolutionary timescales. In the following Chapter an existing population dynamical model of bacteria and phages (Stewart and Levin, 1984) is analysed in a more mathematically rigorous way than the original authors. Building on the work of Chapter 2, the methods of Adaptive Dynamics are applied in Chapter 3 to model the evolution of temperate phages.

Chapter 4 considers whether known differences between the genetic switches of lambda and Stx phages can account for the lower stability of Stx lysogens, while Chapter 5 is concerned with the impact on lysogen stability of environmental factors such as temperature and nutrient levels. The stability of lysogens containing multiple prophages is also considered.

Finally, Chapter 6 extends the findings in Chapter 4 and uses a stochastic model to compare the probability of lysogeny in lambda and Stx phages.

Chapter 2

The Population Dynamics of Temperate and Virulent Bacteriophages

Stewart and Levin (1984) developed a model of bacteriophage dynamics consisting of resources (R), sensitive bacteria (S), resistant bacteria (B), lysogens (L), temperate phage (T), and virulent phage (V). Four sub-models of the full model exclude one or more of these populations. Based on a chemostat approach, resources enter at a rate of ωR_0 per hour (where R_0 is the resource concentration in the input reservoir), and the contents of the chemostat are washed out at a rate proportional to ω. The parameter ϵ reflects the efficiency with which cells consume the resource. Populations of lysogens, sensitive bacteria, and resistant bacteria grow at per capita rates $\psi_L(R)$, $(1 - \alpha_S)\psi_L(R)$, and $(1 - \alpha_B)\psi_L(R)$ respectively, where ψ_L is a monotonic increasing funtion of R (we generally assume that sensitive cells have a higher growth rate than lysogens, i.e. $\alpha_S < 0$; clearly $(1 - \alpha_S)$ and $(1 - \alpha_B)$ are positive). Temperate phages adsorb to sensitive bacteria and lysogens at rates of $\delta_T ST$ and $\delta_T LT$ respectively, where δ_T is a constant of proportionality. The corresponding adsorption rates for virulent phages are $\delta_V SV$ and $\delta_V LV$. Note that lysogens can be infected and lysed by virulent phages, but a temperate phage which adsorbs to a lysogen is simply lost from the system. A proportion p of temperate phage adsorptions result in lysogeny, while the remaining $(1 - p)$ lead to lysis. Lysogens are induced, i.e. enter the lytic cycle, at a rate of i per hour, and lysogens lose their prophage and thus become sensitive bacteria again at a rate of ξ per hour (ξ is known as the segregation rate). The temperate and virulent phage burst sizes are represented by the parameters β_T and β_V respectively.

A hyperbolic model (Monod, 1949) is used for the growth function ψ_L:

$$\psi_L(R) = rR/(R + k)$$

where r is the maximum growth rate of lysogens in unlimited resources and k is the concentration of resources at which cells grow at half of the maximum rate.

Given the above definitions and assumptions, the differential equations governing the system are as follows:

$$\frac{dR}{dt} = \omega(R_0 - R) - \epsilon\psi_L(R)[L + (1-\alpha_S)S + (1-\alpha_B)B] \quad (2.0.1)$$

$$\frac{dL}{dt} = \psi_L(R)L + p\delta_T ST - \delta_V LV - (\omega + i + \xi)L \quad (2.0.2)$$

$$\frac{dS}{dt} = (1-\alpha_S)\psi_L(R)S - \delta_T ST - \delta_V SV + \xi L - \omega S \quad (2.0.3)$$

$$\frac{dB}{dt} = (1-\alpha_B)\psi_L(R)B - \omega B \quad (2.0.4)$$

$$\frac{dT}{dt} = i\beta_T L + \beta_T(1-p)\delta_T ST - \delta_T LT - \omega T \quad (2.0.5)$$

$$\frac{dV}{dt} = \beta_V\delta_V(S+L)V - \omega V \quad (2.0.6)$$

Following Stewart and Levin (1984) we consider four sub-models (Models 1-4) of the full model, before addressing the full model itself. Much of the material presented here is adapted from their work (note that the notation used here is modified in order to be consistent with later material). For each model we identify the possible equilibria, and then systematically carry out feasibility and stability analyses for these equilibria, using Maple as necessary. Thus we have extended the work of Stewart and Levin as far as possible in order to provide a more complete analysis. This chapter will also lay the foundations for the modelling of phage evolution in Chapter 3, where the methods of adaptive dynamics are applied to the sub-model of temperate phages, lysogens, and sensitive cells (Model 2).

2.1 Model 1. Lysogens and free phage

The simplest model contains only resources (R) and two populations: lysogens (L) and free temperate phage (T). In this case the possibility of lysogens losing their prophages is excluded (i.e. the parameter $\xi = 0$), and equations (2.0.1) - (2.0.6) are reduced to the following:

$$\frac{dR}{dt} = \omega(R_0 - R) - \epsilon\psi_L(R)L \quad (2.1.1)$$

$$\frac{dL}{dt} = \psi_L(R)L - iL - \omega L \quad (2.1.2)$$

$$\frac{dT}{dt} = i\beta_T L - \delta_T LT - \omega T \quad (2.1.3)$$

with Jacobian matrix

$$J = \begin{pmatrix} -\omega - \epsilon\psi_L'(R)L & -\epsilon\psi_L(R) & 0 \\ \psi_L'(R)L & \psi_L(R) - i - \omega & 0 \\ 0 & i\beta_T - \delta_T T & -\delta_T L - \omega \end{pmatrix}$$

2.1.1 Deriving and interpreting the equilibria

Setting (2.1.2) equal to zero, we find that either $\hat{L} = 0$ or

$$\psi_L(\hat{R}) = i + \omega, \tag{2.1.4}$$

at equilibrium. If $\hat{L} = 0$, then (2.1.3) implies that $\hat{T} = 0$, and (2.1.1) implies that $\hat{R} = R_0$. On the other hand, if $\psi_L(\hat{R}) = (i+\omega)$ then $\hat{R} = \psi_L^{-1}(i+\omega)$. Then from (2.1.1):

$$\hat{L} = \frac{\omega(R_0 - \hat{R})}{\epsilon\psi_L(\hat{R})} = \frac{\omega}{i+\omega}.\frac{R_0 - \hat{R}}{\epsilon} \tag{2.1.5}$$

and from (2.1.3):

$$\hat{T} = \frac{i\beta_T \hat{L}}{\omega + \delta_T \hat{L}} \tag{2.1.6}$$

Thus there are two types of equilibria for Model 1:

E1 : Resources only - $(R_0, 0, 0)$

E2 : Resources, lysogens and temperate phages - $(\hat{R}, \hat{L}, \hat{T})$

2.1.2 Feasibility and stability of the equilibria

Equilibrium E1 (i.e. $\hat{R} = R_0, \hat{L} = 0, \hat{T} = 0$) corresponds to extinction of the lysogen and phage populations. The equilibrium is clearly feasible because R_0 is a positive constant. The Jacobian matrix at this point is

$$J(E1) = \begin{pmatrix} -\omega & -\epsilon\psi_L(R_0) & 0 \\ 0 & \psi_L(R_0) - i - \omega & 0 \\ 0 & i\beta_T & -\omega \end{pmatrix}$$

with eigenvalues $-\omega$ (repeated) and $\psi_L(R_0) - i - \omega$. Since ω is always positive, it follows that the equilibrium will be stable provided that $\psi_L(R_0) < i + \omega$, i.e. the growth rate

of the lysogens is less than the rate at which they are lost owing to induction and being washed out of the system. If this is the case then the lysogen population cannot survive, and if there are no lysogens then the phage population will also be eliminated.

Now we turn to Equilibrium E2. From (2.1.5), this equilibrium is feasible if and only if

$$R_0 \geq \hat{R} \iff \psi_L(R_0) > \psi_L(\hat{R}) \tag{2.1.7}$$

(since ψ_L is monotonic increasing). Using (2.1.4), we can rewrite this feasibility condition as $\psi_L(R_0) \geq i + \omega$.

The Jacobian for E2 is

$$J(E2) = \begin{pmatrix} -\omega - \epsilon\psi'_L(\hat{R})\hat{L} & -\epsilon(i+\omega) & 0 \\ \psi'_L(\hat{R})\hat{L} & 0 & 0 \\ 0 & i\beta_T - \delta_T\hat{T} & -\delta_T\hat{L} - \omega \end{pmatrix}$$

We can read off one of the eigenvalues as $-\delta_T\hat{L} - \omega$, which is negative provided that E2 is feasible. Now consider the top left 2x2 submatrix of J(E2). The remaining two eigenvalues will have negative real parts provided that the submatrix has a positive determinant and negative trace, and this is the case provided that $\hat{L} > 0$. Thus, if E2 is feasible then it must also be stable.

Figure 2.1 provides an example dynamical simulation of both types of equilibria for Model 1. This simulation was obtained by choosing a set of parameter values and the initial sizes of the phage and lysogen populations, and then numerically integrating the model differential equations in order to determine how the population sizes vary over time. The simulations for the other models in this chapter were carried out using the same procedure. In this example, we have $\psi_L(R_0) = rR_0/(R_0 + k) = 0.67$ (to 2 d.p.). The above theory shows that equilibria of type E1 are feasible and stable when $i + \omega > \psi_L(R_0)$, and equilibria of type E2 are feasible and stable when $i + \omega < \psi_L(R_0)$. In Figure 2.1(A) we have $i + \omega = 0.9 > \psi_L(R_0)$, and the equilibria is of type E1; in Figure 2.1(B) we have $i + \omega = 0.3 < \psi_L(R_0)$ and the equilibria is of type E2. Thus the simulations are in agreement with the theory.

2.2 Model 2. Temperate phage, lysogens, and sensitive cells

This model includes a population of sensitive bacteria (S), and the segregation rate for lysogens is strictly positive.

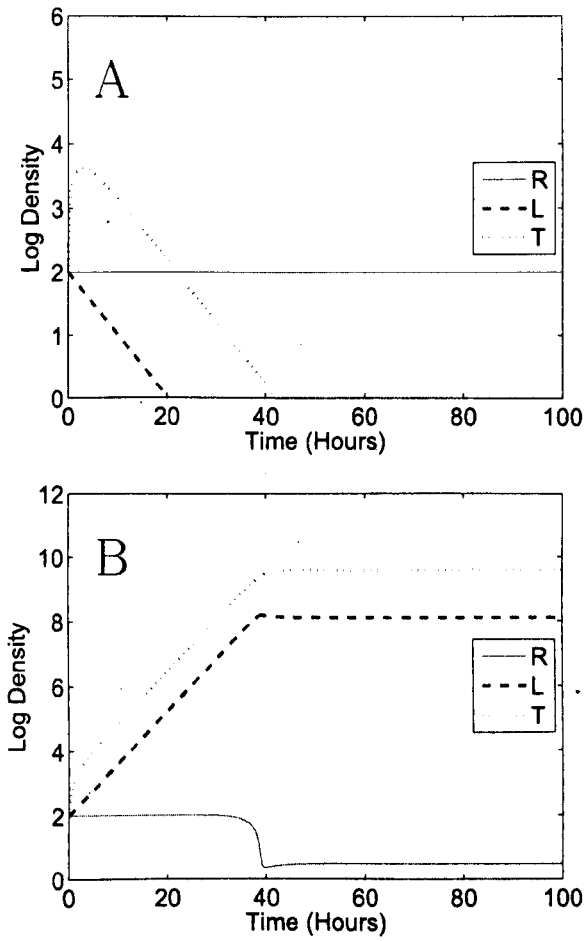

Figure 2.1: Numerical simulations for Model 1 (R=resources, L=lysogens, T=temperate phages). Two equilibrium types are shown:(A) Resources (R) only; (B) Resources, lysogens (L) and temperate phages (T). In (A) the parameter settings are $i = 0.4$ and $\omega = 0.5$, while in (B) $i = 0.1$ and $\omega = 0.2$. The remaining parameter values (same for (A) and (B)) are: $R_0 = 100$, $\epsilon = 5 \times 10^{-7}$, $r = 0.7$, $k = 4$, $\beta_T = 100$, $\delta_T = 10^{-9}$, $\alpha_S = 0$, $\xi = 0$

$$\frac{dR}{dt} = \omega(R_0 - R) - \epsilon\psi_L(R)(L + (1-\alpha_S)S) \tag{2.2.1}$$

$$\frac{dL}{dt} = \psi_L(R)L + p\delta_T ST - (\omega + i + \xi)L \tag{2.2.2}$$

$$\frac{dS}{dt} = (1-\alpha_S)\psi_L(R)S - \delta_T ST + \xi L - \omega S \tag{2.2.3}$$

$$\frac{dT}{dt} = i\beta_T L + \beta_T(1-p)\delta_T ST - \delta_T LT - \omega T \tag{2.2.4}$$

The Jacobian matrix for this model is:

$$J = \begin{pmatrix} -\omega - \epsilon\psi_L'(R)L - \epsilon\psi_L'(R)(1-\alpha_S)S & -\epsilon\psi_L(R) & -\epsilon\psi_L(R)(1-\alpha_S) & 0 \\ \psi_L'(R)L & \psi_L(R) - i - \omega - \xi & p\delta_T T & p\delta_T S \\ (1-\alpha_S)\psi_L'(R)S & \xi & (1-\alpha_S)\psi_L(R) - \delta_T T - \omega & -\delta_T S \\ 0 & i\beta_T - \delta_T T & \beta_T(1-p)\delta_T T & \beta_T(1-p)\delta_T S - \delta_T L - \omega \end{pmatrix}$$

2.2.1 Deriving and interpreting the equilibria

Model 2 contains the four species R, S, L, and T, and so there are 2^4 potential types of equilibria. However, we will show that many of these potential equilibria are not feasible, irrespective of the parameter values. Other equilibria will turn out to be feasible provided that the parameter values satisfy certain conditions.

First we set Equations (2.2.1) - (2.2.4) equal to zero. If we multiply the right hand side of (2.2.3) by p, and add the result to the right hand side of (2.2.2), we obtain

$$\psi_L(\hat{R})\hat{L} - (\omega + i + \xi)\hat{L} + p(1-\alpha_S)\psi(\hat{R})\hat{S} + p\xi\hat{L} - p\omega\hat{S} = 0 \tag{2.2.5}$$

It is convenient to consider the cases $\hat{L} = 0$ and $\hat{L} > 0$ separately; we begin by looking for equilibria with $\hat{L} = 0$. In this case, we find from (2.2.5) that either $\hat{S} = 0$ or $\omega = (1-\alpha_S)\psi_L(\hat{R})$. If $\hat{S} = 0$, then $\hat{R} = R_0$ (from (2.2.1)) and $\hat{T} = 0$ (from (2.2.4)). On the other hand if $\omega = (1-\alpha_S)\psi_L(\hat{R})$, then

$$\hat{R} = \frac{k\omega}{(1-\alpha_S)r - \omega} \tag{2.2.6}$$

and we find that

$$\hat{S} = (R_0 - \hat{R})/\epsilon \tag{2.2.7}$$

(from (2.2.1)) and $\hat{T} = 0$ (from (2.2.3)).

Now we will look for equilibria with $\hat{L} > 0$. In this case we can use the substitution $\hat{S} = x\hat{L}$ to write Equation (2.2.5) as follows:

$$\hat{L}\left(\psi_L(\hat{R}) - (\omega + i + \xi) + p(1 - \alpha_S)\psi(\hat{R})x + p\xi - p\omega x\right) = 0 \tag{2.2.8}$$

Since we are assuming that $\hat{L}$ is non-zero, the expression inside the large brackets in the above expression must be equal to zero. This tells us that

$$\hat{x} = \frac{\hat{S}}{\hat{L}} = \frac{\psi_L(\hat{R}) - \omega - i - (1-p)\xi}{p\left(\omega - (1 - \alpha_S)\psi_L(\hat{R})\right)}, \tag{2.2.9}$$

and therefore

$$\psi_L(\hat{R}) = \frac{\omega + i + (1-p)\xi + p\omega\hat{x}}{1 + p(1 - \alpha_S)\hat{x}} \tag{2.2.10}$$

which implies that ψ is a monotone function of $\hat{x}$ and lies between

$$\psi_m = \frac{\omega}{1 - \alpha_S} \tag{2.2.11}$$

and

$$\psi_M = \omega + i + (1-p)\xi \tag{2.2.12}$$

From (2.2.2) we find

$$\delta_T\hat{S}\hat{T} = \frac{(\omega + i + \xi - \psi_L(\hat{R}))\hat{L}}{p}, \tag{2.2.13}$$

and so

$$\hat{T} = \frac{\omega + i + \xi - \psi_L(\hat{R})}{p\delta_T\hat{x}}. \tag{2.2.14}$$

From (2.2.4), we have

$$\hat{L} = \omega\hat{T}/(i\beta_T + \delta_T[\hat{x}\beta_T(1-p) - 1]\hat{T}) \tag{2.2.15}$$

and clearly

$$\hat{S} = \hat{x}\hat{L}, \text{ and } \hat{R} = k\hat{\psi}_L/(r - \hat{\psi}_L). \tag{2.2.16}$$

So for a given value of $\hat{\psi}_L$, there is a corresponding unique equilibrium. Using (2.2.1), the following relationship between the parameter R_0 and the equilibrium values can be obtained:

$$R_0 = \hat{R} + (\epsilon\hat{\psi}_L/\omega)[\hat{L} + (1+\alpha_S)\hat{S}] \tag{2.2.17}$$

Thus there are three possible types of equilibria:

E1 : Resources only - $(R_0, 0, 0, 0)$

E2 : Resources and sensitive cells - $(\hat{R}, \hat{S}, 0, 0)$

E3 : Resources and all three populations - $(\hat{R}, \hat{S}, \hat{L}, \hat{T})$

2.2.2 Feasibility and stability of the equilibria

The equilibrium E1 (i.e. $(R_0, 0, 0, 0)$) is clearly feasible (since R_0 is always positive). To establish its stability we can examine the Jacobian at E1:

$$J(E1) = \begin{pmatrix} -\omega & -\epsilon\psi_L(R_0) & -\epsilon\psi_L(R_0)(1-\alpha_S) & 0 \\ 0 & \psi_L(R_0) - i - \omega - \xi & 0 & 0 \\ 0 & \xi & (1-\alpha_S)\psi_L(R_0) - \omega & 0 \\ 0 & i\beta_T & 0 & -\omega \end{pmatrix}$$

The eigenvalues of $J(E1)$ are: $(1-\alpha_S)\psi_L(R_0) - \omega$; $\psi_L(R_0) - i - \omega - \xi$; and $-\omega$ (repeated). So E1 is stable provided that the following conditions are satisfied:

$$\psi_L(R_0) < \frac{\omega}{(1-\alpha_S)} \tag{2.2.18}$$

$$\psi_L(R_0) < i + \omega + \xi \tag{2.2.19}$$

Clearly if $(1-\alpha_S) > 1$, and (2.2.18) is satisfied, then (2.2.19) will also be satisfied. The analysis of the E2 equilibrium will reveal that (2.2.18) is equivalent to $R_0 < \hat{R}(E2)$.

Now we consider equilibrium E2 (i.e. $(\hat{R}, \hat{S}, 0, 0)$). From (2.2.6) and (2.2.7), we see that E2 is feasible provided that

$$\omega < (1-\alpha_S)r \tag{2.2.20}$$

$$\omega < \frac{(1-\alpha_S)r}{1+k/R_0} \tag{2.2.21}$$

Clearly if the second of these conditions holds, then the first condition will also hold. Note that the second condition is equivalent to $(R_0 > \hat{R})$.

The Jacobian matrix for E2 (in the order (R, S, L, T)) is as follows:

$$J(E2) = \begin{pmatrix} -\epsilon\psi_L'(\hat{R})(1-\alpha_S)\hat{S} - \omega & -\epsilon\psi_L(\hat{R})(1-\alpha_S) & -\epsilon\psi_L(\hat{R}) & 0 \\ (1-\alpha_S)\psi_L'(\hat{R})\hat{S} & (1-\alpha_S)\psi_L(\hat{R}) - \omega & \xi & -\delta_T\hat{S} \\ 0 & 0 & \psi_L(\hat{R}) - i - \omega - \xi & p\delta_T\hat{S} \\ 0 & 0 & i\beta_T & \beta_T(1-p)\delta_T\hat{S} - \omega \end{pmatrix}$$

The expressions for the eigenvalues of the $J(E2)$ are rather long and complicated, but we can proceed by splitting the matrix into two parts: intrinsic (R and S) and extrinsic (L and T). The intrinsic Jacobian is

$$I(E2) = \begin{pmatrix} -\epsilon\psi_L'(\hat{R})(1-\alpha_S)\hat{S} - \omega & -\epsilon\psi_L(\hat{R})(1-\alpha_S) \\ (1-\alpha_S)\psi_L'(\hat{R})\hat{S} & (1-\alpha_S)\psi_L(\hat{R}) - \omega \end{pmatrix}$$

with eigenvalues

$$-\omega \tag{2.2.22}$$

and

$$-\omega + (1-\alpha_S)\psi_L(\hat{R}) - \epsilon\psi_L'(\hat{R})(1-\alpha_S)\hat{S}. \tag{2.2.23}$$

If these eigenvalues are both negative, then the equilibrium is intrinsically stable.

The extrinsic Jacobian is

$$E(E2) = \begin{pmatrix} \psi_L(\hat{R}) - i & p\delta_T\hat{S} \\ -\omega - \xi & \\ & \\ i\beta_T & \beta_T(1-p)\delta_T\hat{S} \\ & -\omega \end{pmatrix}$$

with trace given by

$$Tr(E(E2)) = \psi_L(\hat{R}) - 2\omega - i - \xi + \beta_T(1-p)\delta_T\hat{S}. \tag{2.2.24}$$

If the trace is positive then there must be at least one eigenvalue with a positive real part, which means that the equilibrium is extrinsically unstable and the phages and lysogens can invade. Even if the trace is negative the equilibrium will still be extrinsically unstable if the determinant, given by

$$\begin{aligned} Det(E(E2)) &= \beta_T\delta_T\hat{S}\left(\psi_L(\hat{R}) - \omega - i - \xi - p\psi_L(\hat{R}) + p\omega + p\xi\right) \\ &\quad +\omega\left(\omega + i + \xi - \psi_L(\hat{R})\right), \end{aligned}$$

is negative.

For E3, we are not able to obtain simple feasibility and stability criteria.

Figure 2.2 illustrates the three types of equilibria for Model 2. In these examples we have $\psi_L(R_0) = rR_0/(R_0+k) = 0.67$ (to 2 d.p.). For the equilibrium of type E1 (Figure 2.2(A)) we have $\omega/(1-\alpha_S) = 0.78$ and $i+\omega+\xi = 0.90$, so that the stability conditions (i.e. (2.2.18) and (2.2.18)) are satisfied.

For the E2 equilibrium (Figure 2.2(B)), the parameter values are such that $\omega = 0.65$, $(1-\alpha_S)r = 0.71$, and $(1-\alpha_S)r/(1+k/R_0) = 0.69$, and so the feasibility conditions (i.e. (2.2.20) and (2.2.21)) are satisfied. The eigenvalues of the intrinsic Jacobian (obtained by evaluating (2.2.22) and (2.2.23)) are both negative, which means that the equilibrium is intrinsically stable. Furthermore, by evaluating (2.2.24) we find that the extrinsic Jacobian has a negative trace and a positive determinant, which means that the real parts of the eigenvalues of this matrix must be negative. Thus, the lysogens and phages are unable to invade the equilibrium of resources and sensitive bacteria.

By varying the parameter values (in particular by lowering the value of ω to 0.2), we are also able to obtain a stable equilibrium with all populations present, as shown in Figure 2.2(C)

2.3 Model 3. Temperate phage, lysogens, sensitive, and resistant bacteria

The above model may be extended to include a population of resistant bacteria (B) which are immune to phage infection, and whose selection coefficient is α_B. Here, the rates of change of the populations are given by:

$$\frac{dR}{dt} = \omega(R_0 - R) - \epsilon\psi_L(R)(L + (1-\alpha_S)S + (1-\alpha_B)B) \quad (2.3.1)$$

$$\frac{dL}{dt} = \psi_L(R)L + p\delta_T ST - (\omega + i + \xi)L \quad (2.3.2)$$

$$\frac{dS}{dt} = (1-\alpha_S)\psi_L(R)S - \delta_T ST + \xi L - \omega S \quad (2.3.3)$$

$$\frac{dB}{dt} = (1-\alpha_B)\psi_L(R)B - \omega B \quad (2.3.4)$$

$$\frac{dT}{dt} = i\beta_T L + \beta_T(1-p)\delta_T ST - \delta_T LT - \omega T \quad (2.3.5)$$

The Jacobian for this model is:

$$J = \begin{pmatrix} -\omega - \epsilon\psi_L'(R)L & -\epsilon\psi_L(R) & -\epsilon\psi_L(R)(1-\alpha_S) & -\epsilon\psi_L(R)(1-\alpha_B) & 0 \\ -\epsilon\psi_L'(R)(1-\alpha_S)S & & & & \\ -\epsilon\psi_L'(R)(1-\alpha_B)B & & & & \\ \psi_L'(R)L & \psi_L(R) - i & p\delta_T T & 0 & p\delta_T S \\ & -\omega - \xi & & & \\ (1-\alpha_S)\psi_L'(R)S & \xi & (1-\alpha_S)\psi_L(R) & 0 & -\delta_T S \\ & & -\delta_T T - \omega & & \\ (1-\alpha_B)\psi_L'(R)B & 0 & 0 & (1-\alpha_B)\psi_L(R) & 0 \\ & & & -\omega & \\ 0 & i\beta_T & \beta_T(1-p)\delta_T T & 0 & \beta_T(1-p)\delta_T S \\ & -\delta_T T & & & -\delta_T L - \omega \end{pmatrix}$$

2.3.1 Deriving and interpreting the equilibria

This model is very similar to the previous one. In fact, Equations (2.2.2), (2.2.3), and (2.2.4) are identical to (2.3.2), (2.3.3), and (2.3.5). By setting (2.3.4) equal to zero, we see that either $\hat{B} = 0$ or

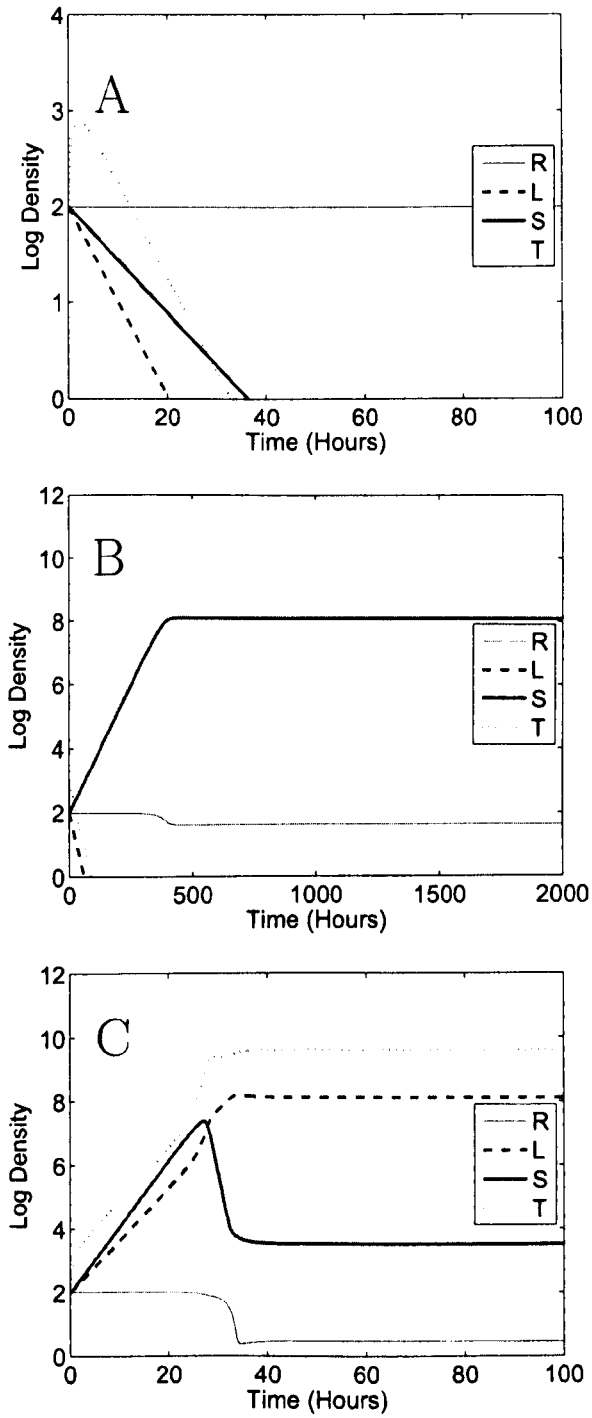

Figure 2.2: Numerical simulations for Model 2 (R=resources, L=lysogens, S=sensitive bacteria, T=temperate phages). Three equilibrium types are shown:(A) Resources only ($\omega = 0.8$, $\beta_T = 100$, $\delta_T = 10^{-9}$); (B) Resources and sensitive bacteria ($\omega = 0.65$, $\beta_T = 50$, $\delta_T = 10^{-10}$); (C) Resources, sensitive bacteria, lysogens and temperate phages ($\omega = 0.2$, $\beta_T = 100$, $\delta_T = 10^{-9}$). The remaining parameter values are: $R_0 = 100$, $\epsilon = 5 \times 10^{-7}$, $r = 0.7$, $k = 4$, $\alpha_S = -0.02$, $\xi = 0.0001$, i=0.1, p=0.4

$$\psi_L(\hat{R}) = \omega/(1-\alpha_B) \tag{2.3.6}$$

at equilibrium. If $\hat{B} = 0$, then (2.2.1) and (2.3.1) are identical; in this case, there are three potential equilibria as described in Section 2.2.1.

To identify the remaining equilibria for Model 3 we assume that (2.3.6) holds, and therefore

$$\hat{R} = \frac{\omega k}{r(1-\alpha_B) - \omega}. \tag{2.3.7}$$

As we did in Model 2, we multiply the right hand side of Equation (2.3.3) by p, and add the result to the right hand side of (2.3.2), and we obtain

$$\psi_L(\hat{R})\hat{L} - (\omega + i + \xi)\hat{L} + p(1-\alpha_S)\psi(\hat{R})\hat{S} + p\xi\hat{L} - p\omega\hat{S} = 0 \tag{2.3.8}$$

(which is identical to (2.2.5)). As before, we will consider the cases $\hat{L} = 0$ and $\hat{L} > 0$ separately.

If $\hat{L} = 0$, then (2.3.8) implies that either $\hat{S} = 0$ or $\omega = (1-\alpha_S)\psi_L(\hat{R})$. If $\hat{S} = 0$, it follows that $\hat{B} = \omega(R_0 - \hat{R})/[\epsilon\psi_L(\hat{R})(1-\alpha_B)]$ (from (2.3.1)) and $\hat{T} = 0$ (from (2.3.5)). On the other hand, if $\omega = (1-\alpha_S)\psi_L(\hat{R})$ then using (2.3.6) we must have $\alpha_S = \alpha_B$ - but this contradicts our assumption that sensitive cells grow faster than resistant cells, and so this particular type of equilibrium can be discounted.

Now we look for equilibria with $\hat{L} > 0$. The expression for $\hat{S}/\hat{L}$ for Model 3 is the same as in Model 2, i.e. Equation (2.2.9). Using (2.3.6), we can now write $\hat{S}/\hat{L}$ as

$$\frac{\hat{S}}{\hat{L}} = \frac{\omega - (1-\alpha_B)(\omega + i + (1-p)\xi)}{\omega p(\alpha_S - \alpha_B)} \tag{2.3.9}$$

The expressions for $\hat{T}$, $\hat{L}$, $\hat{S}$ are the same as in Model 2, i.e. Equations (2.2.14), (2.2.15), and (2.2.16) (remember that in these equations, $\hat{x}$ is used to denote $\hat{S}/\hat{L}$). Finally, by substituting (2.3.7) into (2.3.1) (set equal to zero) and rearranging, we obtain:

$$\hat{B} = \frac{(R_0 - \hat{R})(1-\alpha_B) - \epsilon\hat{L} - \epsilon(1-\alpha_S)\hat{S}}{\epsilon(1-\alpha_B)} \tag{2.3.10}$$

The list of possible equilibrium types is as follows:

E1 : Resources only - $(R_0, 0, 0, 0, 0)$

E2 : Resources and resistant cells - $(\hat{R}, 0, 0, 0, \hat{B})$

E3 : Resources and sensitive cells - $(\hat{R}, \hat{S}, 0, 0, 0)$

E4 : Resources, sensitive cells, lysogens and temperate phages - $(\hat{R}, \hat{S}, \hat{L}, \hat{T}, 0)$

E5 : Resources and all four populations - $(\hat{R}, \hat{S}, \hat{L}, \hat{T}, \hat{B})$

2.3.2 Feasibility and stability of the equilibria

E1 is clearly feasible. The Jacobian at this equilibrium is:

$$J(E1) = \begin{pmatrix} -\omega & -\epsilon\psi_L(R_0) & -\epsilon\psi_L(R_0)(1-\alpha_S) & -\epsilon\psi_L(R_0)(1-\alpha_B) & 0 \\ 0 & \psi_L(R_0) - i - \omega - \xi & 0 & 0 & 0 \\ 0 & \xi & (1-\alpha_S)\psi_L(R_0) - \omega & 0 & 0 \\ 0 & 0 & 0 & (1-\alpha_B)\psi_L(R_0) - \omega & 0 \\ 0 & i\beta_T & 0 & 0 & -\omega \end{pmatrix}$$

The eigenvalues of J(E1) are:

$$(1-\alpha_S)\psi_L(\hat{R}_0) - \omega \tag{2.3.11}$$

$$(1-\alpha_B)\psi_L(\hat{R}_0) - \omega \tag{2.3.12}$$

$$\psi_L(\hat{R}_0) - \omega - i - \xi \tag{2.3.13}$$

$$-\omega \quad \text{(twice)} \tag{2.3.14}$$

Thus, E1 will be stable provided that (i) the growth rates of both the sensitive and resistant bacteria ($(1-\alpha_S)\psi_L(R_0)$ and $(1-\alpha_B)\psi_L(R_0)$ respectively) are lower than the flow rate, and (ii) the growth rate of the lysogens ($\psi_L(R_0)$) is lower than their rate of loss owing to induction, loss of prophage, and flowing out.

E2 is feasible provided that the following conditions are satisfied:

$$r > \omega/(1-\alpha_B) \tag{2.3.15}$$

$$R_0 > \hat{R} \tag{2.3.16}$$

Note that these are similar to the feasibility conditions for equilibrium E2 of model 2.

The Jacobian matrix for E2, in the order (R, B, S, L, T), is:

$$J(E2) = \begin{pmatrix} \underset{-\omega}{-\epsilon\psi_L'(\hat{R})(1-\alpha_B)\hat{B}} & -\epsilon\psi_L(\hat{R})(1-\alpha_B) & -\epsilon\psi_L(\hat{R})(1-\alpha_S) & -\epsilon\psi_L(\hat{R}) & 0 \\ (1-\alpha_B)\psi_L'(\hat{R})\hat{B} & \underset{-\omega}{(1-\alpha_B)\psi_L(\hat{R})} & 0 & 0 & 0 \\ 0 & 0 & \underset{-\omega}{(1-\alpha_S)\psi_L(\hat{R})} & \xi & 0 \\ 0 & 0 & 0 & \underset{-\omega-\xi}{\psi_L(\hat{R})-i} & 0 \\ 0 & 0 & 0 & i\beta_T & -\omega \end{pmatrix}$$

The eigenvalues of J(E2) are as follows:

$$\psi_L(\hat{R})(1-\alpha_S) - \omega \tag{2.3.17}$$

$$\psi_L(\hat{R}) - \omega - i - \xi \tag{2.3.18}$$

$$(\psi_L(\hat{R}) - \epsilon\psi_L'(\hat{R})\hat{B})(1-\alpha_B) - \omega \tag{2.3.19}$$

$$-\omega \quad \text{(twice)} \tag{2.3.20}$$

and these must all be negative for the equilibrium E2 to be stable. From the first eigenvalue we see that the growth rate of sensitive cells must be lower than the flow rate, while the second eigenvalue shows that the growth rate of lysogens must be lower than the sum of the flow, induction and segregation rates.

The E3 equilibrium is feasible provided that the following conditions are satisfied:

$$r(1-\alpha_S) > \omega \tag{2.3.21}$$

$$R_0 > \hat{R} \tag{2.3.22}$$

The Jacobian for E3, in the order (R, S, B, L, T), is:

$J(E3) =$

$$\begin{pmatrix} \alpha_S\epsilon\psi_L'(\hat{R})\hat{S} & -\epsilon\psi_L(\hat{R})(1-\alpha_S) & -\epsilon\psi_L(\hat{R})(1-\alpha_B) & -\epsilon\psi_L(\hat{R}) & 0 \\ -\epsilon\psi_L'(\hat{R})\hat{S} & & & & \\ -\omega & & & & \\ \psi_L'(\hat{R})\hat{S} & (1-\alpha_S)\psi_L(\hat{R}) & 0 & \xi & -\delta_T\hat{S} \\ -\alpha_S\psi_L'(\hat{R})\hat{S} & -\omega & & & \\ 0 & 0 & (1-\alpha_B)\psi_L(\hat{R}) & 0 & 0 \\ & & -\omega & & \\ 0 & 0 & 0 & \psi_L(\hat{R}) - i & p\delta_T\hat{S} \\ & & & -\omega-\xi & \\ 0 & 0 & 0 & i\beta_T & \beta_T(1-p)\delta_T\hat{S} \\ & & & & -\omega \end{pmatrix}$$

To examine the stability of E3, we can look at the intrinsic (R, S) and extrinsic (B, L, T) sub-matrices of J(E3). The intrinsic Jacobian (i.e. the intersection of the 1st and 2nd rows and columns of $J(E3)$) has the following eigenvalues:

$$-\omega \tag{2.3.23}$$

$$-\omega - \epsilon\psi_L'(\hat{R})S(1-\alpha_S) + \psi_L(\hat{R})(1-\alpha_S) \tag{2.3.24}$$

and these must both be negative for the equilibrium to be intrinsically stable.

The extrinsic Jacobian is as follows:

$$E(E3) = \begin{pmatrix} (1-\alpha_B)\psi_L(R) & 0 & 0 \\ -\omega & & \\ 0 & \psi_L(\hat{R}) - i & p\delta_T\hat{S} \\ & -\omega-\xi & \\ 0 & i\beta_T & \beta_T(1-p)\delta_T\hat{S} \\ & & -\omega \end{pmatrix}$$

The first eigenvalue is clearly $(1-\alpha_B)\psi_L(R)-\omega$, and if this is positive then the resistant bacteria will be able to invade. To determine whether one or both of the other two eigenvalues have positive real parts, we can examine further sub-matrix

$$\begin{pmatrix} \psi_L(\hat{R}) - i - \omega - \xi & p\delta_T\hat{S} \\ i\beta_T & \beta_T(1-p)\delta_T\hat{S} - \omega \end{pmatrix}$$

(i.e. the intersection of the second and third rows and columns of $E(E2)$). Since this matrix is the same as the extrinsic Jacobian of Section 2.2.2 (Model 2, E2), the conditions for determining whether there is an eigenvalue with a positive real part are the same as in the earlier case.

At an E4 type equilibrium of resources, sensitive bacteria, temperate phages, and lysogens, the Jacobian matrix (in the order R, S, L, T, B) is given by:

$J(E4) =$

$$\begin{pmatrix} -\omega - \epsilon\psi_L'(\hat{R})\hat{L} - \epsilon\psi_L'(\hat{R})(1-\alpha_S)\hat{S} & -\epsilon\psi_L(\hat{R})(1-\alpha_S) & -\epsilon\psi_L(\hat{R}) & 0 & -\epsilon\psi_L(\hat{R})(1-\alpha_B) \\ (1-\alpha_S)\psi_L'(\hat{R})\hat{S} & (1-\alpha_S)\psi_L(\hat{R}) - \delta_T\hat{T} - \omega & \xi & -\delta_T\hat{S} & 0 \\ \psi_L'(\hat{R})\hat{L} & p\delta_T\hat{T} & \psi_L(\hat{R}) - i - \omega - \xi & p\delta_T\hat{S} & 0 \\ 0 & \beta_T(1-p)\delta_T\hat{T} & i\beta_T - \delta_T\hat{T} & \beta_T(1-p)\delta_T\hat{S} - \delta_T\hat{L} - \omega & 0 \\ 0 & 0 & 0 & 0 & (1-\alpha_B)\psi_L(\hat{R}) - \omega \end{pmatrix}$$

The intrinsic section of this Jacobian is the same as the full Jacobian for Model 2 (although the order of the variables is different). The extrinsic section of $J(E4)$ is the single element

$$(1-\alpha_B)\psi_L(\hat{R}) - \omega. \tag{2.3.25}$$

If this quantity is positive, then the resistant bacteria will be able to invade.

An E5 equilibrium includes resources and all four populations. Notice that (2.3.2), (2.3.3), and (2.3.5) are identical to (2.2.2), (2.2.3), and (2.2.4) respectively, and this means that some of the results already obtained for Model 2 (E3) will be useful in analysing the present case.

Suppose we begin with an equilibrium $(\hat{R}, \hat{L}, \hat{S}, \hat{T})$ with no resistant cells present initially, and then introduce a small number of resistant cells. As usual, we assume $\alpha_S < \alpha_B$. For the resistant cells to invade, we must have (from (2.3.25)):

$$\alpha_S < \alpha_B < 1 - \omega/\hat{\psi}_L \tag{2.3.26}$$

which implies that

$$\omega < (1 - \alpha_B)\hat{\psi}_L < (1 - \alpha_S)\hat{\psi}_L \tag{2.3.27}$$

where $\hat{\psi}_L$ is the lysogenic growth rate at the equilibrium involving no resistant cells.

Now we will investigate the feasibility of E5. Following Stewart and Levin (1984), let $(\hat{R}, \hat{L}, \hat{S}, \hat{T}, 0)$ be an equilibrium with no resistant cells present, and let $(\tilde{R}, \tilde{L}, \tilde{S}, \tilde{T}, \tilde{B})$ be an equilibrium involving all four populations. For the right hand side of (2.3.4) to be equal to zero we must have (since $\tilde{B} \neq 0$)

$$\tilde{R} = \frac{k\omega}{(1 - \alpha_B)r - \omega}$$

and

$$\psi_L(\tilde{R}) = \tilde{\psi}_L = \frac{\omega}{1 - \alpha_B}.$$

Using (2.3.27), together with (2.2.11) and (2.2.12), we see that $\tilde{\psi}_L$ is bounded as follows:

$$\psi_m = \frac{\omega}{1 - \alpha_S} < \tilde{\psi}_L < \hat{\psi}_L < \psi_M = \omega + i + (1 - p)\xi$$

For a given value of $\hat{\psi}_L$, we know from the analysis of Model 2 (E3) that there are unique values of $\tilde{L}$, $\tilde{S}$, and $\tilde{T}$ which satisfy the identical sets of equations (2.2.2), (2.2.3), (2.2.4) and (2.3.2), (2.3.3), (2.3.5). We also know that these values are feasible, i.e. positive. Now all we need to do is show that the value of $\tilde{B}$ is feasible as well.

From (2.2.17), we know that

$$R_0 = \hat{R} + (\epsilon\hat{\psi}_L/\rho)(\hat{L} + (1 - \alpha_S)\hat{S})$$

and we now let

$$\tilde{R}_0 = \tilde{R} + (\epsilon\tilde{\psi}_L/\omega)(\tilde{L} + (1 - \alpha_S)\tilde{S}).$$

Then from (2.3.4) we have

$$\tilde{B} = \frac{\omega(R_0 - \tilde{R}) - \epsilon\psi_L(\tilde{R})(\tilde{L} + (1-\alpha_S)\tilde{S})}{(1-\alpha_B)} \quad (2.3.28)$$

$$= \frac{\omega(R_0 - \tilde{R}_0)}{(1-\alpha_B)} \quad (2.3.29)$$

$$> 0 \quad (2.3.30)$$

The last step follows because we assume that $\tilde{\psi}_L < \hat{\psi}_L$ implies $\tilde{R}_0 < R_0$.

We are not able to derive straightforward stability conditions for E5.

Figure 2.3 illustrates the five types of equilibria. For the E1 simulation (Figure 2.3(A)), the high flow rate ($\omega = 0.8$) ensures that the growth rates of the sensitive cells and resistant cells are lower than the rates at which they are washed out of the system. The flow rate is also high enough to ensure that the growth rate of the lysogens is lower than the total rate at which lysogens are lost (via induction, segregation, and washing out). Thus, the E1 stability conditions (obtained by requiring the eigenvalue expressions (2.3.11)-(2.3.13) to be negative) are satisfied. To check the feasibility of E1 we simply observe that $\hat{R} = R_0 = 100 > 0$.

In Figure 2.3(B), the high adsorption rate of temperate phages to sensitive cells ($\delta_T = 10^{-5}$) means that the population of sensitive cells cannot survive, and this in turn leads to the extinction of the lysogens and temperate phages. Thus, a stable equilibrium of resources and resistant cells is established. Note that the E2 stability conditions, obtained by requiring the eigenvalues in (2.3.17)-(2.3.20) to be negative, are all satisfied. The E2 feasibility conditions given by (2.3.15) and (2.3.16) are also satisfied.

In Figure 2.3(C)), resistant cells have a very significant growth disadvantage ($\alpha_B = 0.5$) compared to lysogens and sensitive cells, and so the resistant population dies out very quickly. The low adsorption rate and burst size ($\delta_T = 10^{-11}$ and $\beta = 10$) mean that the temperate phage and lysogen populations cannot be sustained, and a stable equilibrium of resources and sensitive cells is established. Note that the feasibility conditions ((2.3.21) and (2.3.22)) are satisfied. The intrinsic stability conditions (obtained by requiring the eigenvalues (2.3.23) and (2.3.24) to be negative) and the extrinsic stability conditions (which are the same as the extrinsic stability conditions given in Section 2.2.2 for Model 2, E2) are also satisfied.

An E4 type equilibrium is shown in Figure 2.3(D). Here, the growth disadvantage of resistant cells leads to their extinction, and a stable equilibrium of resources and the other three populations is reached. We do not have straightforward feasibility and intrinsic stability conditions for E4, but we observe that the condition for extrinsic stability condition (obtained by requiring (2.3.25) to be negative) is satisfied.

Figure 2.3(E) shows a stable equilibrium with all populations present. We do not have feasibility and stability conditions for E5. The only difference in parameter values between E4 and E5 is that the growth disadvantage of the resistant cells is lower for E5 than it was for E4, so that the E4 extrinsic stability condition (obtained by requiring (2.3.25) to be negative) is no longer satisfied. Thus, we can regard this E5 equilibrium as the result of a successful invasion by resistant bacteria of the above E4 equilibrium.

2.4 Model 4. Lysogens and sensitive bacteria with virulent and temperate phage

Another variation of the model consists of lysogens, sensitive bacteria, and virulent and temperate phage. Virulent phage can grow on both lysogens and sensitive cells, and the adsorption rate δ_V is the same for both types of cell. The model is given by

$$\frac{dR}{dt} = \omega(R_0 - R) - \epsilon[\psi_L(R)L + (1-\alpha_S)\psi_L(R)S] \tag{2.4.1}$$

$$\frac{dL}{dt} = \psi_L(R)L + p\delta_T ST - \delta_V LV - (\omega + i + \xi)L \tag{2.4.2}$$

$$\frac{dS}{dt} = \psi_S(R)S - \delta_T ST - \delta_V SV + \xi L - \omega S \tag{2.4.3}$$

$$\frac{dT}{dt} = i\beta_T L + \beta_T(1-p)\delta_T ST - \delta_T LT - \omega T \tag{2.4.4}$$

$$\frac{dV}{dt} = \beta_V \delta_V (S+L)V - \omega V \tag{2.4.5}$$

where β_V is the burst size for the virulent phage. The Jacobian for this model is:

$J =$

$$\begin{pmatrix}
-\omega - \epsilon\psi_L'(R)L & -\epsilon\psi_L(R) & -\epsilon\psi_L(R)(1-\alpha_S) & 0 & 0 \\
-(1-\alpha_S)\epsilon\psi_L'(R)S & & & & \\
\psi_L'(R)L & \psi_L(R) - \delta_V V & p\delta_T T & p\delta_T S & -\delta_V L \\
 & -i - \omega - \xi & & & \\
(1-\alpha_S)\psi_L'(R)S & \xi & (1-\alpha_S)\psi_L(R) & -\delta_T S & -S\delta_V \\
 & & -\delta_T T - \delta_V V - \omega & & \\
0 & i\beta_T - \delta_T T & \beta_T(1-p)\delta_T T & \beta_T(1-p)\delta_T S & 0 \\
 & & & -\delta_T L - \omega & \\
0 & V\beta_V\delta_V & V\beta_V\delta V & 0 & \beta_V\delta_V(S+L) \\
 & & & & -\omega
\end{pmatrix}$$

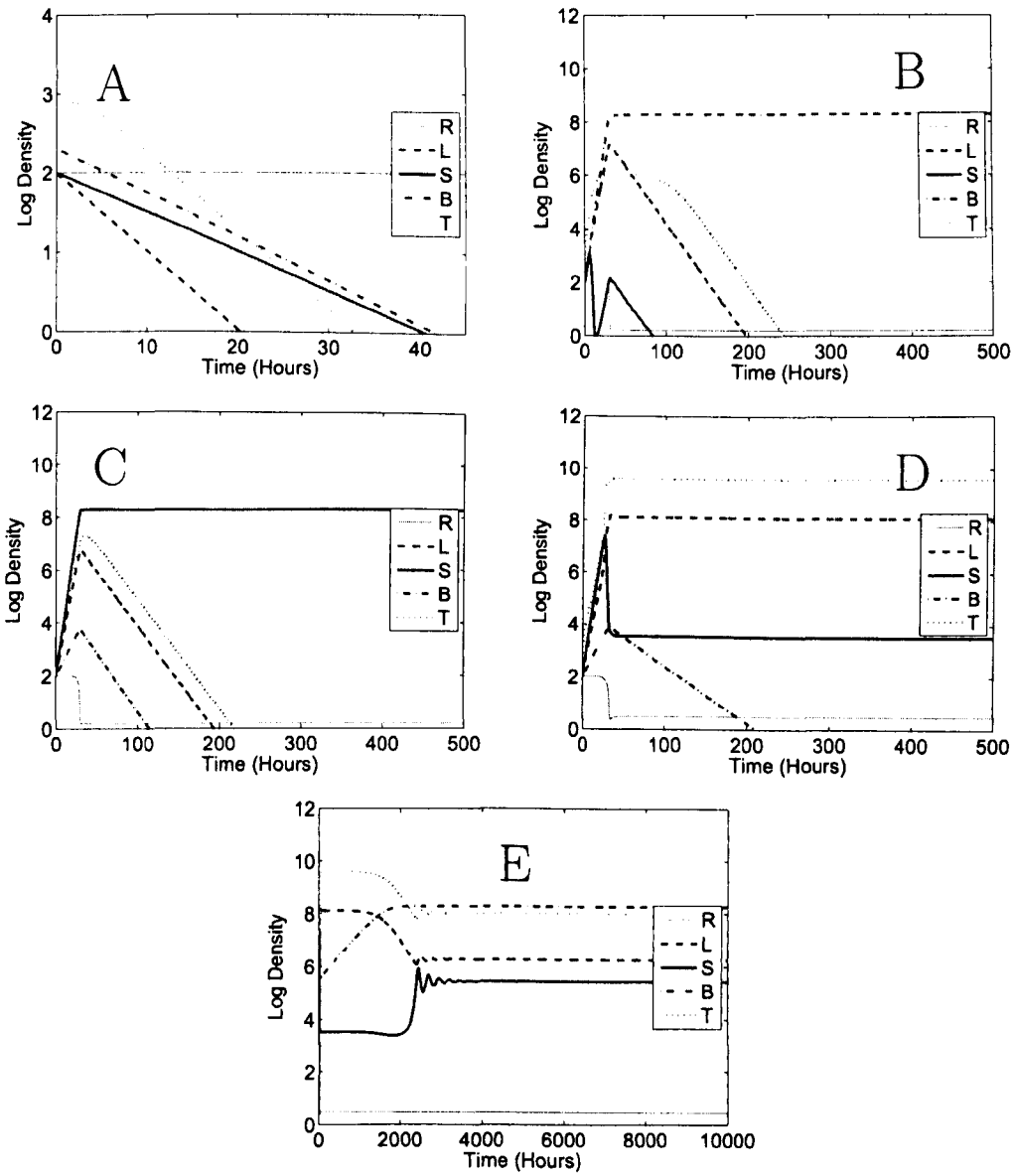

Figure 2.3: Numerical simulations for Model 3 (R=resources, L=lysogens, S=sensitive bacteria, B=resistant bacteria, T=temperate phages). Five equilibrium types are shown:(A) Resources only ($\omega = 0.8$); (B) Resources and resistant bacteria ($\delta_T = 10^{-5}$); (C) Resources and sensitive bacteria ($\alpha_B = 0.5$, $\beta_T = 10$, $\delta_T = 10^{-11}$). (D) Resources, sensitive cells, temperate phages and their lysogens ($\alpha_B = 0.5$) (E) Resources and all four populations ($\alpha_B = 0.32$). Except where otherwise indicated, the parameter values are: $R_0 = 100$, $\epsilon = 5 \times 10^{-7}$, $r = 0.7$, $k = 4$, $\beta_T = 100$, $\delta_T = 10^{-9}$, $\alpha_S = -0.02$, $\alpha_B = 0$, $\xi = 0.0001$, i=0.1, $\omega = 0.2$

2.4.1 Deriving and interpreting the equilibria

By setting (2.4.5) equal to zero, we see that either $\hat{V} = 0$ or $\omega = \beta_V \delta_V (\hat{S} + \hat{L})$. If $\hat{V} = 0$, then the model reduces to Model 2, in which case there are three possible equilibria as described in Section 2.2. Now suppose that $\hat{V} > 0$. As the equations for this model are somewhat intractable, we can begin by looking for equilibria in which one or more of the species populations (apart from V) are absent.

We can rule out the possibility of any equilibria existing with zero resources by setting (2.4.1) equal to zero and substituting $\hat{R} = 0$ and $\psi_L(\hat{R}) = 0$. This leaves us with the condition $\omega R_0 = 0$, which cannot be satisfied. Thus we can assume that $\hat{R}$ is strictly positive for all equilibria in this model.

We can also rule out the existence of equilibria with lysogens present but no temperate phages. Setting 2.4.4 equal to zero and substituting $T = 0$, we are left with the condition $i\beta_T \hat{L} = 0$, which is false when $\hat{L}$ is positive.

There are also no equilibria with $\hat{V} > 0$ and $\hat{S} = 0$. Equation (2.4.3) tells us that $\hat{L} = 0$, but if $\hat{V}$ is non-zero and both $\hat{S}$ and $\hat{L}$ are zero then there is no way that the right hand side of (2.4.5) can be zero. Therefore we can discount this type of equilibrium.

Now we look for an equilibrium with $\hat{V} > 0$ and $\hat{L} = 0$. Since $\hat{V}$ is non-zero, we know from (2.4.5) that

$$\hat{S} = \omega/(\beta_V \delta_V). \tag{2.4.6}$$

Thus, setting Equation (2.4.3) equal to zero, we obtain

$$\frac{\omega}{\beta_V \delta_V} \Big((1 - \alpha_S)\psi_L(\hat{R}) - \delta_T \hat{T} - \delta_V \hat{V} - \omega \Big) = 0, \tag{2.4.7}$$

and so we must have

$$(1 - \alpha_S)\psi_L(\hat{R}) - \delta_T \hat{T} - \delta_V \hat{V} - \omega = 0. \tag{2.4.8}$$

Since $\hat{L}$ is zero and $\hat{S}$ is non-zero, Equation (2.4.2) tells us that $\hat{T} = 0$, and so the above expression becomes

$$(1 - \alpha_S)\psi_L(\hat{R}) - \delta_V \hat{V} - \omega = 0 \tag{2.4.9}$$

and so

$$\hat{V} = \frac{(1 - \alpha_S)\psi_L(\hat{R}) - \omega}{\delta_V}. \tag{2.4.10}$$

By substituting $\hat{S} = \omega/(\beta_V \delta_V)$ into (2.4.1) (set equal to zero) and re-arranging, we obtain

$$\psi_L(\hat{R}) = \frac{(R_0 - \hat{R})\beta_V \delta_V}{\epsilon(1 - \alpha_S)} \tag{2.4.11}$$

which can be solved to find the value of $\hat{R}$. Note that the above equilibrium is also obtained if we search for an equilibrium with $\hat{V} > 0$ and $\hat{I} = 0$.

The final potential equilibrium has all populations present, although we are not able to derive expressions for the population densities at such an equilibrium.

The full list of equilibrium types for this model is:

E1 : Resources only -$(R_0, 0, 0, 0, 0)$

E2 : Resources and sensitive cells -$(\hat{R}, \hat{S}, 0, 0, 0)$

E3 : Resources, sensitive cells and virulent phages -$(\hat{R}, \hat{S}, 0, 0, \hat{V})$

E4 : Resources, sensitive cells and both phage populations -$(\hat{R}, \hat{S}, \hat{L}, \hat{T}, 0)$

E5 : Resources and all four populations -$(\hat{R}, \hat{S}, \hat{L}, \hat{T}, \hat{V})$

2.4.2 Feasibility and stability of the equilibria

The equilibrium E1 is feasible. The Jacobian at this point is:

$$J(E1) = \begin{pmatrix} -\omega & -\epsilon\psi_L(R_0) & -\epsilon\psi_L(R_0)(1-\alpha_S) & 0 & 0 \\ 0 & \psi_L(R_0) - i - \omega - \xi & 0 & 0 & 0 \\ 0 & \xi & (1-\alpha_S)\psi_L(R_0) - \omega & 0 & 0 \\ 0 & i\beta_T & 0 & -\omega & 0 \\ 0 & 0 & 0 & 0 & -\omega \end{pmatrix}$$

The eigenvalues of $J(E1)$ are:

$$-\omega \quad \text{(three-fold)} \tag{2.4.12}$$

$$(1 - \alpha_S)\psi_L(R_0) - \omega \tag{2.4.13}$$

$$\psi_L(R_0) - \omega - i - \xi. \tag{2.4.14}$$

It follows that E1 will be stable provided that (i) the growth rate of the sensitive cells is less than the flow rate, and (ii) the growth rate of the lysogens is less than the rate at which they are lost owing to induction, segregation and flowing out.

For E2, the feasibility conditions are:

$$r(1-\alpha_S) > \omega \tag{2.4.15}$$

$$R_0 > \hat{R}. \tag{2.4.16}$$

Note that these are the same as the feasibility conditions for Model 2, E2. The Jacobian for E2, in the order (R, S, V, L, T), is:
$J(E2) =$

$$\begin{pmatrix}
\alpha_S\epsilon\psi_L'(\hat{R})\hat{S} - \epsilon\psi_L'(\hat{R})\hat{S} - \omega & -\epsilon\psi_L(\hat{R})(1-\alpha_S) & 0 & -\epsilon\psi_L(\hat{R}) & 0 \\
\psi_L'(\hat{R})(1-\alpha_S)\hat{S} & \psi_L(\hat{R})(1-\alpha_S) - \omega & -\delta_V\hat{S} & \xi & -\delta_T\hat{S} \\
0 & 0 & \beta_V\delta_V\hat{S} - \omega & 0 & 0 \\
0 & 0 & 0 & \psi_L(\hat{R}) - \omega - i - \xi & p\delta_T\hat{S} \\
0 & 0 & 0 & i\beta_T & \beta_T(1-p)\delta_T\hat{S} - \omega
\end{pmatrix}$$

The intrinsic section of the Jacobian (i.e. the 2×2 matrix at the top left corner of $J(E2)$) has the following eigenvalues:

$$-\omega \tag{2.4.17}$$

$$(1-\alpha_S)(\psi_L(\hat{R}) - \epsilon\psi_L'(\hat{R})\hat{S}) - \omega \tag{2.4.18}$$

Note that these are the same as the eigenvalues of the intrinsic Jacobian of Model 2, E2. If these eigenvalues are negative, then the system is intrinsically stable.

The first eigenvalue of the (3×3) extrinsic section of the Jacobian is $\beta_V\delta_V\hat{S} - \omega$. If this is positive, then the virulent phages will be able to invade. To check whether the lysogens and temperate phages can invade, we must determine whether or not the 2×2 matrix at the bottom right corner of $J(E2)$ has an eigenvalue with a positive real part; in fact, this matrix is the same as the extrinsic matrices of sections (1.2.2) and (1.3.3), with trace and determinant given by (2.2.24) and 2.2.25 respectively. If the

determinant is negative, then there will be one eigenvalue with a positive real part; if the determinant and the trace are both positive then both eigenvalues will have positive real parts.

For E3, the value of $\hat{S}$ given by (2.4.6) is always feasible. From (2.4.10) we see that $\hat{V}$ will be feasible provided that

$$(1-\alpha_S)\psi_L(\hat{R}) > \omega \tag{2.4.19}$$

From (2.4.10), we must also have $\hat{R} > R_0$ in order for E3 to be feasible.

The Jacobian for E3, in the order (R, S, V, L, T), is:

$J(E3) =$

$$\begin{pmatrix}
\alpha_S\epsilon\psi_L'(\hat{R})\hat{S} - \epsilon\psi_L'(\hat{R})\hat{S} - \omega & -\epsilon\psi_L(\hat{R})(1-\alpha_S) & 0 & -\epsilon\psi_L(\hat{R}) & 0 \\
(1-\alpha_S)\psi_L'(\hat{R})\hat{S} & (1-\alpha_S)\psi_L(\hat{R}) - \delta_V\hat{V} - \omega & -\delta_V\hat{S} & \xi & -\delta_T\hat{S} \\
0 & \hat{V}\beta_V\delta_V & \beta_V\delta_V\hat{S} - \omega & \hat{V}\beta_V\delta_V & 0 \\
0 & 0 & 0 & \psi_L(\hat{R}) - \delta_V\hat{V} - \omega - i - \xi & p\delta_T\hat{S} \\
0 & 0 & 0 & i\beta_T & \beta_T(1-p)\delta_T\hat{S} - \omega
\end{pmatrix}$$

The intrinsic section of $J(E3)$ is the 3×3 matrix at the top left corner; the system will be intrinsically stable if this matrix has no eigenvalue with a positive real part (one of these eigenvalues is $-\omega$; the expressions for the other two eigenvalues are rather complicated). The 2×2 extrinsic section of the Jacobian (bottom right corner) has trace

$$\psi_L(\hat{R}) - \delta_V\hat{V} - 2\omega - i - \xi + \beta_T(1-p)\delta_T\hat{S}.$$

If the trace is positive then there must be at least one eigenvalue with a positive real part, which means that the system is extrinsically unstable and the phages and lysogens

can invade. Even if the trace is negative the system will still be extrinsically unstable if the determinant, given by

$$\beta_T\delta_T\hat{S}\left(\psi_L(\hat{R})-\omega-i-\xi-p\psi_L(\hat{R})+p\omega+p\xi-\delta_V\hat{V}(1-p)\right)$$
$$+\omega\left(\omega+i+\xi-\psi_L(\hat{R})+\delta_V\hat{V}\right),$$

is negative.

For E4, we know from the analysis of Model 2 that for realistic parameter values there will be a unique feasible equilibrium. The Jacobian for this model, in the order (R, L, S, T, V), is:

$J(E4) =$

$$\begin{pmatrix}
\begin{matrix}\alpha_S\epsilon\psi_L'(\hat{R})\hat{S}\\ -\epsilon\psi_L'(\hat{R})\hat{S}\\ -\epsilon\psi_L'(\hat{R})\hat{L}\\ -\omega\end{matrix} & -\epsilon\psi_L(\hat{R}) & -\epsilon\psi_L(\hat{R})(1-\alpha_S) & 0 & 0\\
\psi_L'(\hat{R})\hat{L} & \begin{matrix}\psi_L(\hat{R})\\ -\omega-i-\xi\end{matrix} & p\delta_T\hat{T} & p\delta_T\hat{S} & -\delta_V\hat{L}\\
\psi_L'(\hat{R})(1-\alpha_S)\hat{S} & \xi & \begin{matrix}\psi_L(\hat{R})(1-\alpha_S)\\ -\delta_T\hat{T}-\omega\end{matrix} & -\delta_T\hat{S} & -\delta_V\hat{S}\\
0 & i\beta_T-\delta_T\hat{T} & \beta_T(1-p)\delta_T\hat{T} & \begin{matrix}\beta_T(1-p)\delta_T\hat{S}\\ -\delta_T\hat{L}-\omega\end{matrix} & 0\\
0 & 0 & 0 & 0 & \begin{matrix}\beta_V\delta_V(\hat{S}+\hat{L})\\ -\omega\end{matrix}
\end{pmatrix}$$

The (4×4) intrinsic section of the Jacobian is identical to the full Jacobian of Model 2 (Section 2.2.2); the equilbrium will be intrinsically stable if this matrix has no eigenvalues with positive real parts (note that in Section 2.2.2 we were unable to obtain straightforward expressions for these eigenvalues). The extrinsic section of the Jacobian is the single element

$$\beta_V\delta_V(\hat{S}+\hat{L})-\omega. \tag{2.4.20}$$

If this quantity is positive, then the virulent phages will be able to invade.

For E5, we are not able to derive straightforward feasibility or stability conditions.

Figure 2.4 shows examples of the five equilibrium types. In Figure 2.4(A), an equilibrium of type E1 is shown. The high flow rate ($\omega = 0.8$) ensures that the populations of lysogens, sensitive cells, and phages are all washed out of the system at a faster rate than they can grow. This equilibrium is feasible since $\hat{R} = R_0 > 0$. The eigenvalues of the Jacobian matrix (given by (2.4.12)-(2.4.14)) are all negative, so the equilibrium is stable.

In Figure 2.4(B), an equilibrium of type E2 is shown. Here, the flow rate is lower than for E1 ($\omega = 0.2$) and the growth rate of sensitive cells is high enough for this population to survive ($\alpha_S = -0.1$). The feasibility conditions (2.4.15) and (2.4.16) are satisfied. The eigenvalues of the intrinsic Jacobian (given by (2.4.17) and (2.4.18) are both negative, so the equilibrium is intrinsically stable. The extrinsic stability conditions, as described in Section 2.4.2, are also satisfied.

In Figure 2.4(C), an equilibrium of type E3 is shown. Here, the higher burst size ($\beta_V = 150$) and adsorption rate ($\delta_V = 2 \times 10^{-11}$) of the virulent phages enables them to coexist with the sensitive bacteria. The feasibility condition 2.4.19 is satisfied. The intrinsic and extrinsice stability conditions, as described in Section 2.4.2, are also satisfied.

In Figure 2.4(D), an equilibrium of type E4 is shown. The faster adsorption rate of temperate phages compared to virulent phages leads to the extinction of the virulent phage population. We do not have straightforward feasibility and intrinsic stability conditions for this equilibrium. The condition for extrinsic stability (obtained by requiring (2.4.20) to be negative) is satisfied.

In Figure 2.4(E), an equilibrium of type E5 is shown, with all four populations coexisting. We did not obtain feasibility or stability conditions for this type of equilibrium.

2.5 Model 5. The Full Model

This model includes sensitive and resistant bacteria, virulent phages, and temperate phages and their lysogens. The full model equations are given by (2.0.1)-(2.0.6). The Jacobian for Model 5 (in the order R, L, S, T, V, B) is:

$J =$

$$\begin{pmatrix}
\begin{array}{c} -\epsilon\psi'_L(R)L \\ -\epsilon\psi'_L(R)S \\ +\alpha_S\epsilon\psi'_L(R)S \\ -\epsilon\psi'_L(R)B \\ +\alpha_B\epsilon\psi'_L(R)B \\ -\omega \end{array} & -\epsilon\psi_L(R) & \begin{array}{c} -\epsilon\psi_L(R) \\ +\alpha_S\epsilon\psi_L(R) \end{array} & 0 & 0 & \begin{array}{c} -\epsilon\psi_L(R) \\ +\alpha_B\epsilon\psi_L(R) \end{array} \\
\psi'_L(R)L & \begin{array}{c} \psi_L(R) - \delta_V V \\ -\omega - i - \xi \end{array} & p\delta_T T & p\delta_T S & -\delta_V L & 0 \\
\begin{array}{c} \psi'_L(R)S \\ -\alpha_S\psi'_L(R)S \end{array} & \xi & \begin{array}{c} \psi_L(R) \\ -\alpha_S\psi_L(R) \\ -\delta_T T - \delta_V V \\ -\omega \end{array} & -\delta_T S & -\delta_V S & 0 \\
0 & i\beta_T - \delta_T T & \begin{array}{c} \beta_T\delta_T T \\ -p\beta_T\delta_T T \end{array} & \begin{array}{c} \beta_T\delta_T S \\ -p\beta_T\delta_T S \\ -\delta_T L \\ -\omega \end{array} & 0 & 0 \\
0 & \beta_V\delta_V V & \beta_V\delta_V V & 0 & \begin{array}{c} \beta_V\delta_V S \\ \beta_V\delta_V L \\ -\omega \end{array} & 0 \\
\begin{array}{c} \psi'_L(R)B \\ -\alpha_B\psi'_L(R)B \end{array} & 0 & 0 & 0 & 0 & \begin{array}{c} \psi_L(R) \\ -\alpha_B\psi_L(R) \\ -\omega \end{array}
\end{pmatrix}$$

2.5.1 Deriving and interpreting the equilibria

We can rule out the existence of equilibria with $\hat{R} = 0$ by setting (2.0.1) equal to zero and substituting $\hat{R} = 0$ and $\psi_L(\hat{R}) = 0$. This leaves us with the expression $\omega R_0 = 0$, which is false. Other potential equilibria in which either $\hat{B} = 0$ or $\hat{V} = 0$ (or $\hat{B} = \hat{V} = 0$) have been covered in the analysis of the previous models. Thus we need only look for equilibria with $\hat{B} > 0$ and $\hat{V} > 0$.

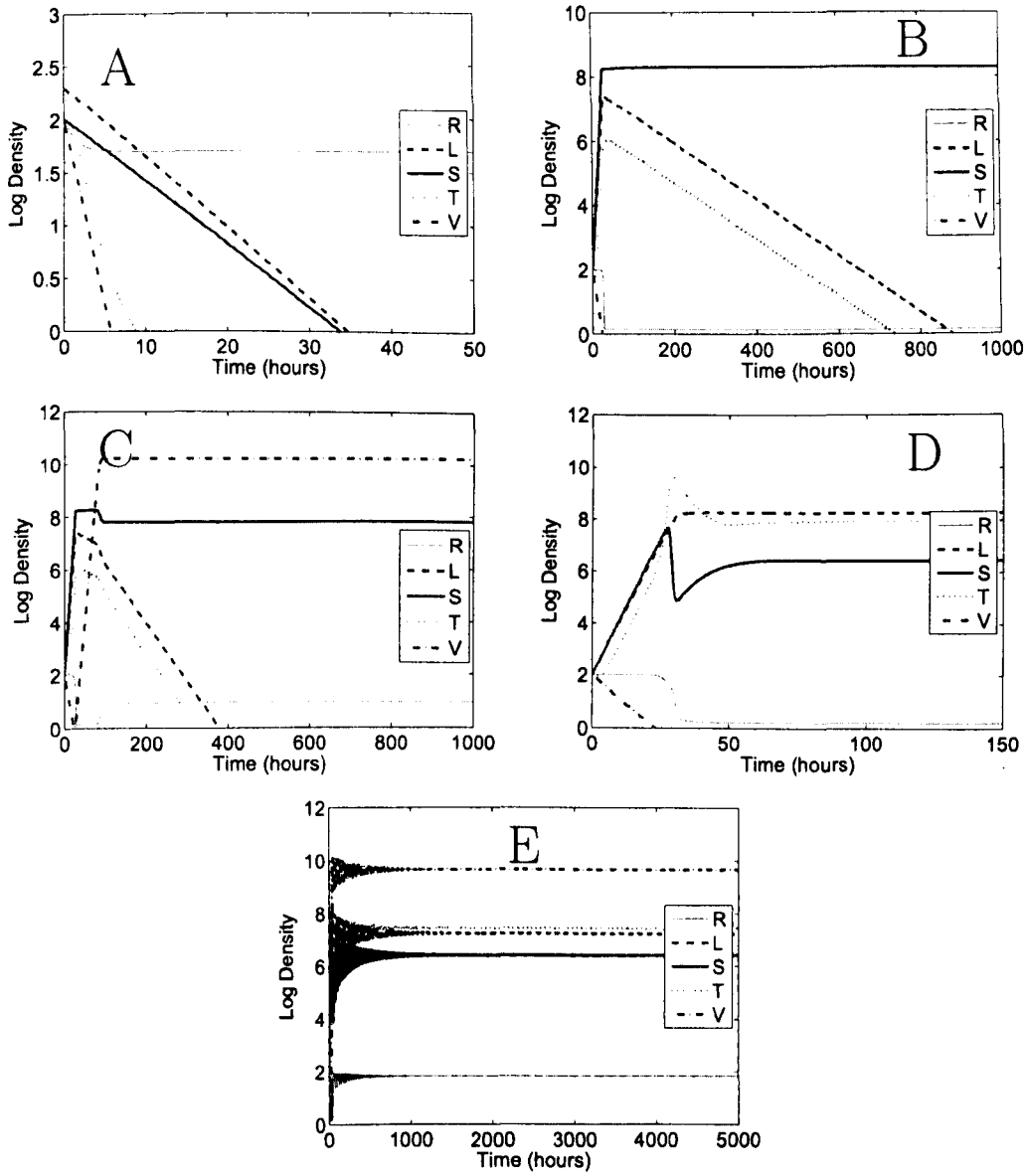

Figure 2.4: Numerical simulations for Model 4 (R=resources, L=lysogens, S=sensitive bacteria, T=temperate phages, V=virulent phages). Five equilibrium types are shown:(A) Resources only ($\delta_V = 10^{-12}, \beta_T = 10, \delta_T = 10^{-12}, R_0 = 50, \omega = 0.8$). (B) Resources and sensitive bacteria ($\delta_V = 10^{-11}, \beta_T = 10, \delta_T = 10^{-12}, \alpha_S = -0.1, \omega = 0.2$). (C) Resources, sensitive bacteria and virulent phages ($\beta_V = 150, \delta_V = 2 \times 10^{-11}, \beta_T = 10, \delta_T = 10^{-12}, \alpha_S = -0.1, \omega = 0.2$). (D) Resources, sensitive bacteria, lysogens and temperate phages ($\delta_V = 10^{-11}$). (E) Resources, sensitive cells, lysogens, temperate phages and virulent phages ($\delta_V = 10^{-10}$). Except where otherwise indicated, the parameter values are: $R_0 = 100, \epsilon = 5 \times 10^{-7}, r = 0.7, k = 4, \beta_T = 80, \beta_V = 100, \delta_T = 8 \times 10^{-10}, \alpha_S = -0.02, \xi = 0.001, i = 0.001$

First suppose that $\hat{B}$ and $\hat{V}$ are positive, but $\hat{S}$ is zero. Then (2.0.3) (set equal to zero) implies that $\hat{L} = 0$. But if $\hat{S} = \hat{L} = 0$ and $\hat{V} > 0$, then the right hand side of (2.0.6) cannot be equal to zero. Therefore, there are no equilibria of this type.

Next we look for equilibria in which all populations apart from $\hat{L}$ are present. Setting (2.0.2) equal to zero, we are left with $p\delta_T \hat{S}\hat{T} = 0$, which cannot be satisfied if $\hat{S}$ and $\hat{T}$ are both positive. So we can discount this type of equilibria.

Now we look for equilibria containing all populations apart from $\hat{T}$. In this case, setting (2.0.5) equal to zero we have $i\beta_T \hat{L} = 0$, which is false if $\hat{L} > 0$.

Suppose now that there is an equilibrium with all populations present apart from lysogens and temperate phages. Using (2.0.6) (set equal to zero) we find $\hat{S} = \omega/(\beta_V \delta_V)$, and from (2.0.4) we find $\psi_L(\hat{R}) = \omega/(1 - \alpha_B)$ (from which we can obtain the value of $\hat{R}$). The expression for $\hat{V}$ is obtained from (2.0.3):

$$\hat{V} = \frac{\omega}{\delta_V}\left(\frac{\alpha_B - \alpha_S}{1 - \alpha_B}\right) \tag{2.5.1}$$

and the expression for $\hat{B}$ is obtained from (2.0.1):

$$\hat{B} = \frac{(R_0 - \hat{R})(1 - \alpha_B)\beta_V \delta_V - (1 - \alpha_S)\omega\epsilon}{\epsilon(1 - \alpha_B)\beta_V \delta_V} \tag{2.5.2}$$

The remaining possibility is an equilibrium with resources and all five populations present.

The full list of equilibrium types for this model is:

E1 : Resources only - $(R_0, 0, 0, 0, 0, 0)$

E2 : Resources and sensitive cells - $(\hat{R}, \hat{S}, 0, 0, 0, 0)$

E3 : Resources and resistant cells - $(\hat{R}, 0, 0, 0, \hat{B}, 0)$

E4 : Resources, sensitive cells and virulent phages - $(\hat{R}, \hat{S}, 0, 0, 0, \hat{V})$

E5 : Resources, sensitive cells, lysogens and temperate phages - $(\hat{R}, \hat{S}, \hat{L}, \hat{T}, 0, 0)$

E6 : Resources, sensitive cells, resistant cells and virulent phages - $(\hat{R}, \hat{S}, 0, 0, \hat{B}, \hat{V})$

E7 : Resources and all populations except virulent phages - $(\hat{R}, \hat{S}, \hat{L}, \hat{T}, \hat{B}, 0)$

E8 : Resources and all populations except resistant cells - $(\hat{R}, \hat{S}, \hat{L}, \hat{T}, 0, \hat{V})$

E9 : Resources and all five populations - $(\hat{R}, \hat{S}, \hat{L}, \hat{T}, \hat{B}, \hat{V})$

2.5.2 Feasibility and stability of the equilibria

The equilibrium E1 is feasible because R_0 is always positive. The Jacobian for E1, in the order (R, S, B, V, L, T), is:

$J(E1) =$

$$\begin{pmatrix} -\omega & -\epsilon\psi_L(R_0)(1-\alpha_S) & -\epsilon\psi_L(R_0)(1-\alpha_B) & 0 & -\epsilon\psi_L(R_0) & 0 \\ 0 & (1-\alpha_S)\psi_L(R_0)-\omega & 0 & 0 & \xi & 0 \\ 0 & 0 & (1-\alpha_B)\psi_L(R_0)-\omega & 0 & 0 & 0 \\ 0 & 0 & 0 & -\omega & 0 & 0 \\ 0 & 0 & 0 & 0 & \psi_L(R_0)-\omega-i-\xi & 0 \\ 0 & 0 & 0 & 0 & i\beta_T & -\omega \end{pmatrix}$$

with eigenvalues

$$(1-\alpha_S)\psi_L(R_0)-\omega \tag{2.5.3}$$

$$(1-\alpha_B)\psi_L(R_0)-\omega \tag{2.5.4}$$

$$\psi_L(R_0)-\omega-i-\xi \tag{2.5.5}$$

$$-\omega \quad \text{(repeated twice)} \tag{2.5.6}$$

and these must all be negative for E1 to be stable.

E2 is feasible provided that the following conditions are satisfied:

$$(1-\alpha_S)r-\omega>0 \tag{2.5.7}$$

$$R_0-\hat{R}(E2)>0. \tag{2.5.8}$$

The Jacobian for E2, in the order (R,S,B,V,L,T), is:
$J(E2) =$

$$\begin{pmatrix} -\epsilon\psi_L'(\hat{R})\hat{S} & -\epsilon\psi_L(\hat{R})(1-\alpha_S) & -\epsilon\psi_L(\hat{R})(1-\alpha_B) & 0 & -\epsilon\psi_L(\hat{R}) & 0 \\ +\alpha_S\epsilon\psi_L'(\hat{R})\hat{S} & & & & & \\ -\omega & & & & & \\ \psi_L'(\hat{R})(1-\alpha_S)\hat{S} & \psi_L(\hat{R})(1-\alpha_S) & 0 & -\delta_V\hat{S} & \xi & -\delta_T\hat{S} \\ & -\omega & & & & \\ 0 & 0 & \psi_L(\hat{R})(1-\alpha_B) & 0 & 0 & 0 \\ & & -\omega & & & \\ 0 & 0 & 0 & \beta_V\delta_V\hat{S} & 0 & 0 \\ & & & -\omega & & \\ 0 & 0 & 0 & 0 & \psi_L(\hat{R})-\omega & p\delta_T\hat{S} \\ & & & & -i-\xi & \\ 0 & 0 & 0 & 0 & i\beta_T & \beta_T(1-p)\delta_T\hat{S} \\ & & & & & -\omega \end{pmatrix}$$

The 2×2 intrinsic matrix (top left of $J(E2)$) has the following eigenvalues:

$$-\omega \tag{2.5.9}$$

$$(1-\alpha_S)\psi_L(\hat{R}) - \epsilon(1-\alpha_S)\psi_L'(\hat{R}) - \omega \tag{2.5.10}$$

Of the four eigenvalues of the (4×4) extrinsic matrix, we can read off the first two as $(1-\alpha_B)\psi_L(\hat{R}) - \omega$ and $\beta_V\delta_V\hat{S} - \omega$. The conditions for one of the other two eigenvalues to have positive real parts are the same as those given in Section 2.2.2 for the extrinsic matrix of Model 2, E2.

E3 is feasible provided that the following conditions are satisfied:

$$(1-\alpha_B)r - \omega > 0 \tag{2.5.11}$$

$$R_0 - \hat{R}(E3) > 0. \tag{2.5.12}$$

The Jacobian for E3, in the order (R, B, S, V, L, T), is:

$$\begin{pmatrix} -\omega - \epsilon\psi_L'(\hat{R})(1-\alpha_B)\hat{B} & -\epsilon\psi_L(\hat{R})(1-\alpha_B) & -\epsilon\psi_L(\hat{R})(1-\alpha_S) & 0 & -\epsilon\psi_L(\hat{R}) & 0 \\ \psi_L'(\hat{R})(1-\alpha_B)\hat{B} & \psi_L(\hat{R})(1-\alpha_B) - \omega & 0 & 0 & 0 & 0 \\ 0 & 0 & \psi_L(\hat{R})(1-\alpha_S) - \omega & 0 & \xi & 0 \\ 0 & 0 & 0 & -\omega & 0 & 0 \\ 0 & 0 & 0 & 0 & \psi_L(\hat{R}) - \omega - i - \xi & 0 \\ 0 & 0 & 0 & 0 & i\beta_T & -\omega \end{pmatrix}$$

with eigenvalues

$$(1-\alpha_S)\psi_L(\hat{R}) - \omega \tag{2.5.13}$$

$$\psi_L(\hat{R}) - \omega - i - \xi \tag{2.5.14}$$

$$(1-\alpha_B)(\psi_L(\hat{R}) - \epsilon\psi_L'(\hat{R})) - \omega \tag{2.5.15}$$

$$-\omega \quad \text{(three-fold)} \tag{2.5.16}$$

which must all be negative for E3 to be stable.

For E4, we see that the expression for $\hat{S}$, given by (2.4.6), is always feasible. Using (2.4.10), we also require that

$$(1-\alpha_S)\psi_L(\hat{R}) - \omega - \delta_V\hat{V} > 0 \tag{2.5.17}$$

for E4 to be feasible. The Jacobian for E4, in the order (R, S, V, B, L, T), is:
$J(E4) =$

$$\begin{pmatrix}
\begin{matrix}-\epsilon\psi_L'(\hat{R})\hat{S}\\ +\alpha_S\epsilon\psi_L'(\hat{R})\hat{S}\\ -\omega\end{matrix} & -\epsilon\psi_L(\hat{R})(1-\alpha_S) & 0 & -\epsilon\psi_L(\hat{R})(1-\alpha_B) & -\epsilon\psi_L(\hat{R}) & 0 \\
\begin{matrix}\psi_L'(\hat{R})\hat{S}\\ -\alpha_S\psi_L'(\hat{R})\hat{S}\end{matrix} & \begin{matrix}\psi_L(\hat{R})(1-\alpha_S)\\ -\delta_V\hat{V}-\omega\end{matrix} & -\delta_V\hat{S} & 0 & \xi & -\delta_T\hat{S} \\
0 & \beta_V\delta_V\hat{V} & \begin{matrix}\beta_V\delta_V\hat{S}\\ -\omega\end{matrix} & 0 & \beta_V\delta_V\hat{V} & 0 \\
0 & 0 & 0 & \begin{matrix}(1-\alpha_B)\psi_L(\hat{R})\\ -\omega\end{matrix} & 0 & 0 \\
0 & 0 & 0 & 0 & \begin{matrix}\psi_L(\hat{R})-\delta_V\hat{V}\\ -\omega-i-\xi\end{matrix} & p\delta_T\hat{S} \\
0 & 0 & 0 & 0 & i\beta_T & \begin{matrix}\beta_T(1-p)\delta_T\hat{S}\\ -\omega\end{matrix}
\end{pmatrix}$$

The intrinsic Jacobian does not have straightforward eigenvalue expression. The extrinsic matrix is the 3×3 matrix at the bottom right of $J(E4)$. We can see that the first eigenvalue is $(1-\alpha_B)\psi_L(\hat{R}) - \omega$. One of the other eigenvalues of the extrinsic matrix will have a positive real part if the quantity

$$\psi_L(\hat{R}) - \delta_V\hat{V} + \beta_T(1-p)\delta_T\hat{S} - i - \xi - 2\omega$$

(which is the trace of the 2×2 matrix at the bottom right of $J(E4)$) is positive.

We were not able to obtain straightforward feasibility conditions for E5. The Jacobian for E5, in the order (R, S, L, T, B, V), is:
$J(E5) =$

$$\begin{pmatrix}
\begin{matrix}-\epsilon\psi_L'(\hat{R})\hat{L}\\ -\epsilon\psi_L'(\hat{R})\hat{S}\\ +\alpha_S\epsilon\psi_L'(\hat{R})\hat{S}\\ -\omega\end{matrix} & -\epsilon\psi_L(\hat{R})(1-\alpha_S) & -\epsilon\psi_L(\hat{R}) & 0 & \begin{matrix}-\epsilon\psi_L(\hat{R})\\ +\alpha_B\epsilon\psi_L(\hat{R})\end{matrix} & 0 \\
\psi_L'(\hat{R})(1-\alpha_S)\hat{S} & \begin{matrix}\psi_L(\hat{R})(1-\alpha_S)\\ -\delta_T T-\omega\end{matrix} & \xi & -\delta_T\hat{S} & 0 & -\delta_V\hat{S} \\
\psi_L(\hat{R})\hat{L} & p\delta_T T & \begin{matrix}\psi_L(\hat{R})-i\\ -\xi-\omega\end{matrix} & p\delta_T\hat{S} & 0 & -\delta_V\hat{L} \\
0 & \beta_T(1-p)\delta_T\hat{T} & i\beta_T-\delta_T\hat{T} & \begin{matrix}\beta_T(1-p)\delta_T\hat{S}\\ -\delta_T\hat{L}-\omega\end{matrix} & 0 & 0 \\
0 & 0 & 0 & 0 & \begin{matrix}\psi_L(\hat{R})\\ -\alpha_B\psi_L(\hat{R})\\ -\omega\end{matrix} & 0 \\
0 & 0 & 0 & 0 & 0 & \begin{matrix}\beta_V\delta_V\hat{S}\\ +\beta_V\delta_V\hat{L}\\ -\omega\end{matrix}
\end{pmatrix}$$

There are no straightforward expressions for the eigenvalues of the 4×4 intrinsic Jacobian. The eigenvalues of the 2×2 extrinsic matrix for E5 are:

$$(1-\alpha_B)\psi_L(\hat{R}) - \omega \tag{2.5.18}$$

$$\beta_V\delta_V(\hat{S}+\hat{L}) - \omega. \tag{2.5.19}$$

If these are both negative, then the equilibrium cannot be invaded by resistant cells or virulent phages.

For E6, the feasibility condition for $\hat{R}$ is

$$(1-\alpha_B)\psi_L(\hat{R}) - \omega > 0 \tag{2.5.20}$$

(from (2.0.4)). The equilibrium density for S is $\omega/(\beta_V\delta_V)$, which is always positive. For $\hat{V}$ to be feasible, we must have $(\alpha_S - \alpha_B)/(\alpha_B - 1) > 0$; since we are assuming that $\alpha_S < \alpha_B$, this condition is equilivalent to

$$\alpha_B < 1 \tag{2.5.21}$$

Using (2.5.2), the final feasibility condition is:

$$\epsilon\psi_L(\hat{R})(1-\alpha_S)\hat{S} - \omega(R_0 - \hat{R}) > 0. \tag{2.5.22}$$

The Jacobian for E6, in the order (R, S, B, V, L, T), is:
$J(E6) =$

$$\begin{pmatrix}
\begin{array}{c} -\epsilon\psi_L'(\hat{R})\hat{S} \\ +\alpha_S\epsilon\psi_L'(\hat{R})\hat{S} \\ -\epsilon\psi_L'(\hat{R})\hat{B} \\ +\alpha_B\epsilon\psi_L'(\hat{R})\hat{B} \\ -\omega \end{array} & -\epsilon\psi_L(\hat{R})(1-\alpha_S) & -\epsilon\psi_L(\hat{R})(1-\alpha_B) & 0 & -\epsilon\psi_L(\hat{R}) & 0 \\
\begin{array}{c} \psi_L'(\hat{R})\hat{S} \\ -\alpha_S\psi_L'(\hat{R})\hat{S} \end{array} & \begin{array}{c} \psi_L(\hat{R})(1-\alpha_S) \\ -\delta_V\hat{V} - \omega \end{array} & 0 & -\delta_V\hat{S} & \xi & -\delta_T\hat{S} \\
\begin{array}{c} \psi_L'(\hat{R})\hat{B} \\ -\alpha_B\psi_L'(\hat{R})\hat{B} \end{array} & 0 & \begin{array}{c} \psi_L(\hat{R})(1-\alpha_B) \\ -\omega \end{array} & 0 & 0 & 0 \\
0 & \beta_V\delta_V\hat{V} & 0 & \begin{array}{c} \beta_V\delta_V\hat{S} \\ -\omega \end{array} & \beta_V\delta_V\hat{V} & 0 \\
0 & 0 & 0 & 0 & \begin{array}{c} \psi_L(\hat{R}) - \delta_V\hat{V} \\ -\omega - i - \xi \end{array} & p\delta_T\hat{S} \\
0 & 0 & 0 & 0 & i\beta_T & \begin{array}{c} \beta_T(1-p)\delta_T\hat{S} \\ -\omega \end{array}
\end{pmatrix}$$

The 4×4 intrinsic Jacobian does not have straightforward eigenvalue expressions. If the trace of the 2×2 extrinsic matrix (bottom right of $J(E6)$) is positive then this extrinsic matrix will have an eigenvalue whose real part is positive, and so the intrinsic system can be invaded by lysogens and temperate phages.

We are not able to obtain straightforward feasibility conditions for E7. The Jacobian for E7, in the order (R, S, B, L, T, V), is:
$J(E7) =$

$$\begin{pmatrix}
\begin{matrix}-\epsilon\psi_L'(\hat{R})\hat{L}\\ -\epsilon\psi_L'(\hat{R})\hat{S}\\ +\alpha_S\epsilon\psi_L'(\hat{R})\hat{S}\\ -\epsilon\psi_L'(\hat{R})\hat{B}\\ +\alpha_B\epsilon\psi_L'(\hat{R})\hat{B}\\ -\omega\end{matrix} & -\epsilon\psi_L(\hat{R})(1-\alpha_S) & -\epsilon\psi_L(\hat{R})(1-\alpha_B) & -\epsilon\psi_L(\hat{R}) & 0 & 0 \\
\begin{matrix}\psi_L'(\hat{R})\hat{S}\\ -\alpha_S\psi_L'(\hat{R})\hat{S}\end{matrix} & \begin{matrix}\psi_L(\hat{R})(1-\alpha_S)\\ -\delta_T\hat{T}-\omega\end{matrix} & 0 & \xi & -\delta_T\hat{S} & -\delta_V\hat{S} \\
\begin{matrix}\psi_L'(\hat{R})\hat{B}\\ -\alpha_B\psi_L'(\hat{R})\hat{B}\end{matrix} & 0 & \begin{matrix}\psi_L(\hat{R})(1-\alpha_B)\\ -\omega\end{matrix} & 0 & 0 & 0 \\
\psi_L'(\hat{R})\hat{L} & p\delta_T\hat{T} & 0 & \begin{matrix}\psi_L(\hat{R})-\omega\\ -i-\xi\end{matrix} & p\delta_T\hat{S} & -\delta_V\hat{L} \\
0 & \beta_T(1-p)\delta_T\hat{T} & 0 & i\beta_T-\delta_T\hat{T} & \begin{matrix}\beta_T(1-p)\delta_T\hat{S}\\ -\delta_T\hat{L}-\omega\end{matrix} & 0 \\
0 & 0 & 0 & 0 & 0 & \begin{matrix}\beta_V\delta_V\hat{S}\\ +\beta_V\delta_V\hat{L}\\ -\omega\end{matrix}
\end{pmatrix}$$

The 5×5 intrinsic Jacobian does not have straightforward eigenvalue expressions. The intrinsic system can be invaded by virulent phages if

$$\beta_V\delta_V(\hat{S}+\hat{L})-\omega>0. \tag{2.5.23}$$

We do not have feasibility conditions for E8. The Jacobian for E8, in the order (R,S,L,T,V,B), is:
$J(E8)=$

$$\begin{pmatrix}
\begin{matrix}-\epsilon\psi_L'(\hat{R})\hat{L}\\ -\epsilon\psi_L'(\hat{R})\hat{S}\\ +\alpha_S\epsilon\psi_L'(\hat{R})\hat{S}\\ -\omega\end{matrix} & -\epsilon\psi_L(\hat{R})(1-\alpha_S) & -\epsilon\psi_L(\hat{R}) & 0 & 0 & \begin{matrix}-\epsilon\psi_L(\hat{R})\\ +\alpha_B\epsilon\psi_L(\hat{R})\end{matrix} \\
\begin{matrix}\psi_L'(\hat{R})\hat{S}\\ -\alpha_S\psi_L'(\hat{R})\hat{S}\end{matrix} & \begin{matrix}\psi_L(\hat{R})(1-\alpha_S)\\ -\delta_T\hat{T}-\delta_V\hat{V}\\ -\omega\end{matrix} & \xi & -\delta_T\hat{S} & -\delta_V\hat{S} & 0 \\
\psi_L(\hat{R})\hat{L} & p\delta_T\hat{T} & \begin{matrix}\psi_L(\hat{R})\\ -i-\xi\\ -\delta_V\hat{V}-\omega\end{matrix} & p\delta_T\hat{S} & -\delta_V\hat{L} & 0 \\
0 & \beta_T(1-p)\delta_T\hat{T} & \begin{matrix}i\beta_T\\ -\delta_T\hat{T}\end{matrix} & \begin{matrix}\beta_T(1-p)\delta_T\hat{S}\\ -\delta_T\hat{L}-\omega\end{matrix} & 0 & 0 \\
0 & \beta_V\delta_V\hat{V} & \beta_V\delta_V\hat{V} & 0 & \begin{matrix}\beta_V\delta_V(\hat{S}+\hat{L})\\ -\omega\end{matrix} & 0 \\
0 & 0 & 0 & 0 & 0 & \begin{matrix}(1-\alpha_B)\psi_L(\hat{R})\\ -\omega\end{matrix}
\end{pmatrix}$$

The 5×5 intrinsic Jacobian does not have straightforward eigenvalue expressions. The intrinsic system can be invaded by resistant cells if

$$(1-\alpha_B)\psi_L(\hat{R}) > \omega. \tag{2.5.24}$$

We are not able to derive straightforward feasibility and stability conditions for E9.

Figure 2.5 shows examples of all 9 equilibrium types. Figure 2.5(A) shows an E1 equilibrium, in which a high flow rate ($\omega = 0.7$) causes the extinction of all 5 populations. This equilibrium is feasible because $\hat{R} = R_0 > 0$. The stability conditions (obtained by requiring the eigenvalues (2.5.3)-(2.5.6) to be negative) are satisfied.

In the E2 equilibrium shown in Figure 2.5(B), the increased growth rate of sensitive cells ($\alpha_S = -0.04$) enables their population to survive. The feasibility conditions (2.5.7) and (2.5.8) are satisfied. The eigenvalues of the intrinsic stability matrix (given by (2.5.9) and (2.5.10)) are both negative, and the extrinsic stability conditions (as described in Section 2.5.2) are also satisfied.

Figure 2.5(C) shows an E3 equilibrium with only resistant cells present. Although sensitive cells have a growth rate advantage over resistant cells, sensitive cells are eliminated owing to the high adsorption rate of the virulent phages ($\delta_V = 10^{-3}$) (and with no sensitive cells present, the virulent phage population cannot survive either). The feasibility conditions (2.5.11) and (2.5.12) are satisfied, and the eigenvalues ((2.5.13)-(2.5.16)) of the E3 Jacobian are all negative.

Figure 2.5(D) shows an E4 equilibrium with sensitive cells and virulent phages present. Resistant cells have a significant growth disadvantage compared to sensitive cells, and temperate phages have a lower burst size and adsorption rate compared to virulent phages. The feasibility conditions (2.5.17) is satisfied. We do not have straightforward criteria for intrinsic stability, but the conditions for extrinsic stability (as described in Section 2.5.2) are satisfied.

In Figure 2.5(E), an E5 equilibrium with sensitive cells, lysogens and temperate phages is shown. The burst sizes of temperate and virulent phages are the same (they are both equal to 100), but the adsorption rate for temperate phages is much higher than for virulent phages. We do not have expressions for feasibility or intrinsic stability. The conditions for extrinsic stability (obtained by requiring the eigenvalues (2.5.18) and (2.5.19) to be negative) are satisfied.

An E6 equilibrium is shown in Figure 2.5(F), with sensitive and resistant cells coexisting with virulent phages. Here the growth rate disadvantage of resistant cells is lower ($\alpha_B = 0.1$) than for the preceding equilibria, and virulent phages have a superior burst size and adsorption rate compared to temperate phages. We do not have expressions for feasibility or intrinsic stability. The conditions for extrinsic stability, as described in Section 2.5.2, are satisfied.

Figure 2.5(G) shows all populations coexisting apart from virulent phages. Here temperate and virulent phages have the same burst size, but temperate phages have a much higher adsorption rate than virulent phages. We do not have expressions for feasibility or intrinsic stability. The condition for extrinsic stability (given by (2.5.23)) is satisfied.

Figure 2.5(H) shows all populations coexisting apart from resistant cells, whose growth rate disadvantage ($\alpha_B = 0.7$) is too great for them to survive. We do not have expressions for feasibility or intrinsic stability. The condition for extrinsic stability (given by (2.5.24)) is satisfied.

An E9 equilibrium with all 5 populations present is shown in Figure 2.5(I). We do not have straightforward feasbility and stability criteria for E9.

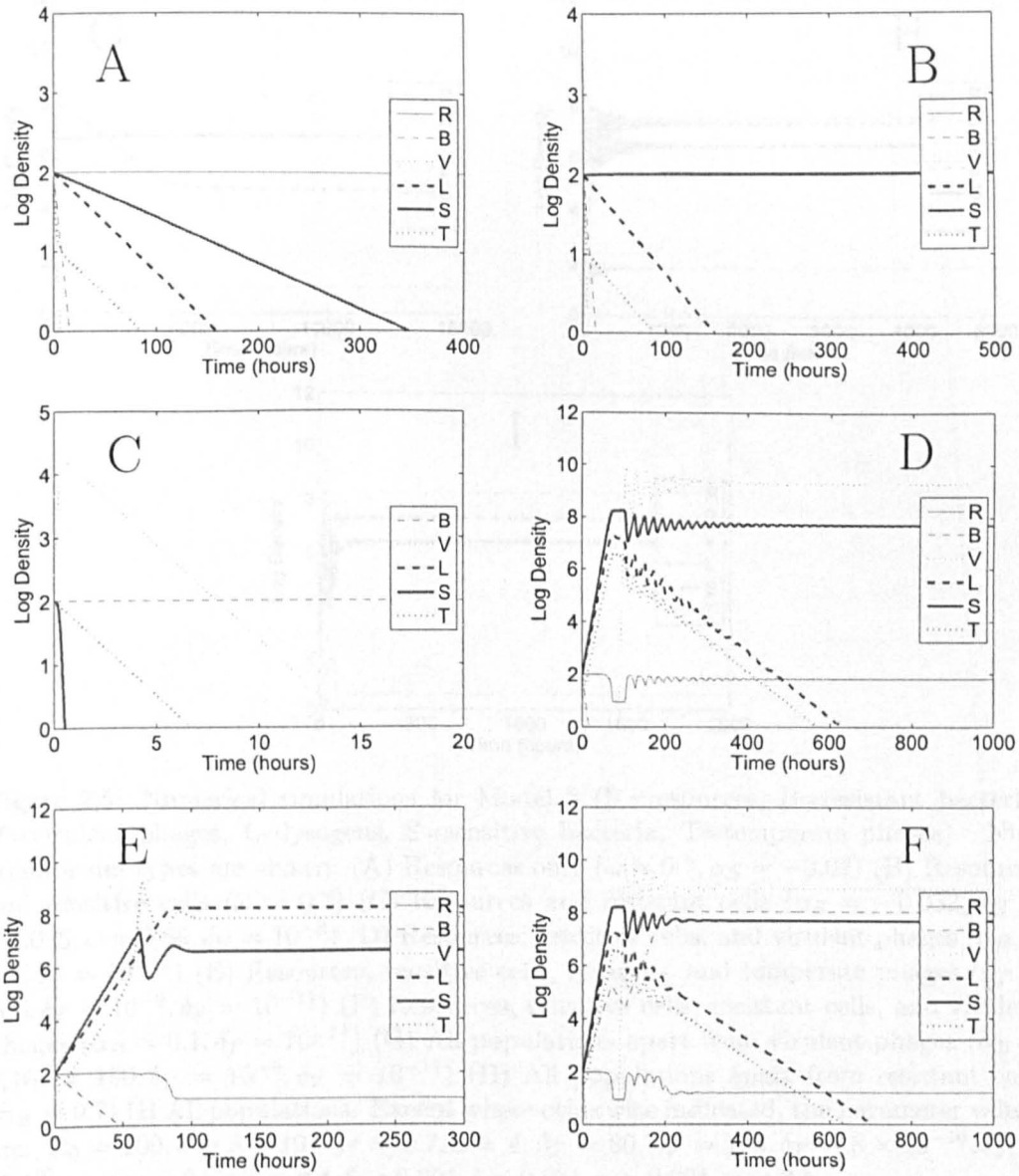
A
B
C
D
E
F
Log Density
Time (hours)
R
B
V
L
S
T

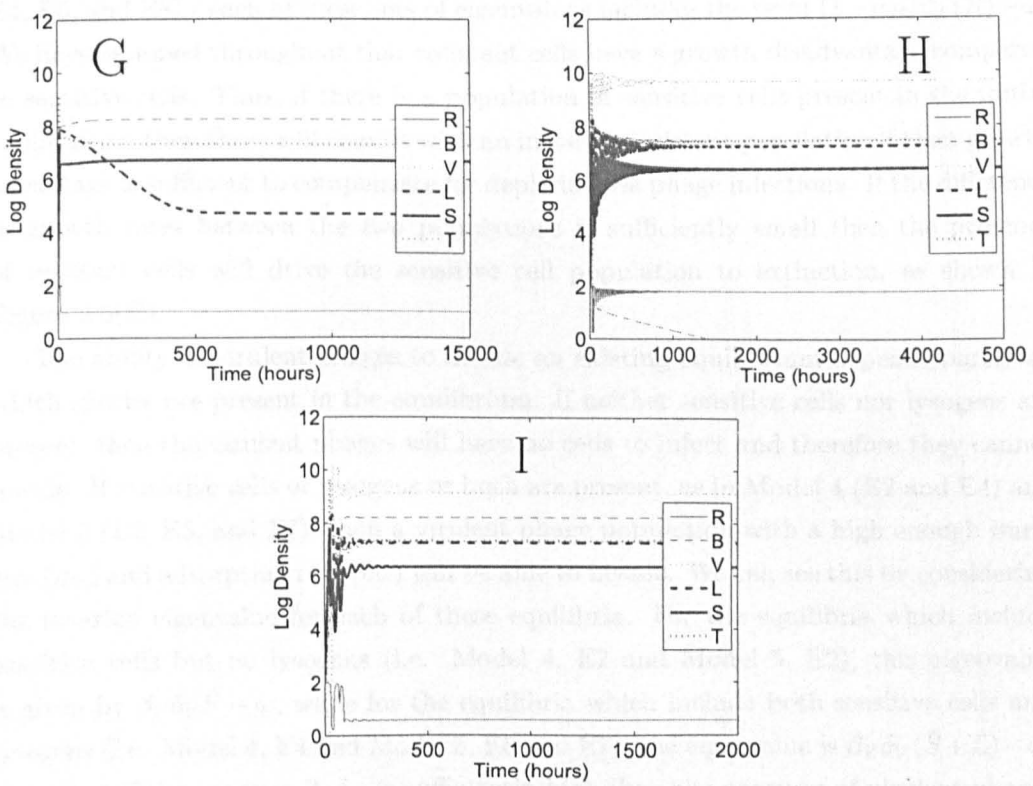

Figure 2.5: Numerical simulations for Model 5 (R=resources, B=resistant bacteria, V=virulent phages, L=lysogens, S=sensitive bacteria, T=temperate phages). Nine equilibrium types are shown: (A) Resources only ($\omega = 0.7, \alpha_S = -0.02$) (B) Resources and sensitive cells ($\omega = 0.7$) (C) Resources and resistant cells ($\alpha_S = -0.032, \alpha_B = -0.025, \omega = 0.69, \delta_V = 10^{-3}$) (D) Resources, sensitive cells, and virulent phages ($\alpha_B = 0.7, \delta_T = 10^{-11}$) (E) Resources, sensitive cells, lysogens, and temperate phages ($\beta_T = 100, \delta_T = 10^{-9}, \delta_V = 10^{-11}$) (F) Resources, sensitive cells, resistant cells, and virulent phages ($\alpha_B = 0.1, \delta_T = 10^{-11}$) (G) All populations apart from virulent phages ($\alpha_B = 0, \beta_T = 100, \delta_T = 10^{-9}, \delta_V = 10^{-11}$) (H) All populations apart from resistant cells ($\alpha_B = 0.7$) (I) All populations. Except where otherwise indicated, the parameter values are: $R_0 = 100, \epsilon = 5 \times 10^{-7}, r = 0.7, k = 4, \beta_T = 80, \beta_V = 100, \delta_T = 8 \times 10^{-10}, \delta_V = 10^{-10}, \alpha_S = -0.04, \alpha_B = 0.4, \xi = 0.001, i = 0.001, p = 0.001, \omega = 0.5$.

2.6 Discussion

Characteristically resistant cells will always invade an existing equilibrium, provided that their growth rate is greater than the flow rate. This is clear from the eigenvalues of the full or extrinsic Jacobians for Model 3 (E1, E3, and E4) and Model 5 (E1, E2, E4, E5, and E8) - each of these sets of eigenvalues includes the term $(1-\alpha_B)\psi_L(\hat{R})-\omega$. We have assumed throughout that resistant cells have a growth disadvantage compared to sensitive cells. Thus, if there is a population of sensitive cells present in the initial equilibrium, then these will coexist with an invading resistant population if their growth advantage is sufficient to compensate for depletion via phage infections. If the difference in growth rates between the two populations is sufficiently small then the presence of resistant cells will drive the sensitive cell population to extinction, as shown in Figure 2.5(C).

The ability of virulent phages to invade an existing equilibrium depends partly on which species are present in the equilibrium. If neither sensitive cells nor lysogens are present, then the virulent phages will have no cells to infect and therefore they cannot invade. If sensitive cells or lysogens or both are present, as in Model 4 (E2 and E4) and Model 5 (E2, E5, and E7), then a virulent phage population with a high enough burst size (β_V) and adsorption rate (δ_V) will be able to invade. We can see this by considering the invasion eigenvalue for each of these equilibria. For the equilibria which include sensitive cells but no lysogens (i.e. Model 4, E2 and Model 5, E2), this eigenvalue is given by $\beta_V\delta_V\hat{S}-\omega$, while for the equilibria which include both sensitive cells and lysogens (i.e. Model 4, E4 and Model 5, E5 and E7), the eigenvalue is $\beta_V\delta_V(\hat{S}+\hat{L})-\omega$. Note that if the product $\beta_V\delta_V$ is sufficiently high then the presence of virulent phages will lead to the extinction of the available host cells and consequently the extinction of the phage population as well, as shown in Figure 2.5(A).

The ability of temperate phages and their lysogens to invade also depends on which species are present in the existing equilibrium. If sensitive cells are not present (as in Model 1 (E1), Model 2 (E1), Model 3 (E1 and E2), Model 4 (E1), and Model 5 (E1 and E3)) then the phages will have no potential host cells to infect. However, if the growth rate of the lysogens ($\psi_L(\hat{R})$) is greater than the combined rates of induction, segregation (i.e. the rate at which lysogens become sensitive cells again, as a result of losing their prophage), and outflow, then an invasion by lysogens is possible. In each of these equilibria, the invasion eigenvalue is given by $\psi_L(R_0)-i-\xi-\omega$. Thus we have obtained the new finding that the conditions for a successful invasion depend only on the characteristics of the lysogens (i.e. growth rate, induction rate, and segregation rate), and not on the characteristics of the phages (i.e. burst size and adsorption rate). The presence of the lysogens would in turn lead to sensitive cells and temperate

phages appearing in the environment via the processes of segregation and induction respectively. If sensitive cells are present in the initial equilibrium (as in Model 2 (E2), Model 3 (E3), Model 4 (E2 and E3), and Model 5 (E2, E4, and E6)), then characteristics of the phage population as well as the lysogen population will be relevant in determining whether an invasion is possible; thus, for these equilibria, there are two relevant invasion eigenvalues - one for the lysogens and one for the temperate phages - and in each case these are obtained from a 2×2 matrix of the form

$$\begin{pmatrix} \psi_L(\hat{R}) - \delta_V \hat{V} - i - \omega - \xi & p\delta_T \hat{S} \\ i\beta_T & \beta_T(1-p)\delta_T \hat{S} - \omega \end{pmatrix}$$

A high burst size and adsorption rate will improve the chances of a successful invasion by the phages (but as with virulent phages, there is a risk of the sensitive cells becoming extinct if the rate of phage infection is too high). If virulent phages are present in the initial equilibrium then this will make invasion by lysogens more difficult, since some of the lysogens will be infected and lysed by virulent phages.

The question of why temperance evolved as a characteristic of certain phages is unresolved, but models such as the ones analysed in this chapter can provide some clues, and also suggest directions for future investigations. The models can also indicate which conditions will favour populations of temperate phages over virulent ones.

Assuming that there is a plentiful supply of resources and sensitive cells present in the environment, the outcome of competition between temperate and virulent phage populations will depend on the parameter values, in particular: (i) the relative adsorption rates and burst sizes of the two populations; (ii) the probability of lysogeny and the induction rate of the temperate phages. Given an equilibrium of virulent phages and sensitive cells (Model 4, E3) the analysis showed that the conditions for a successful invasion by temperate phages and lysogens are more likely to be satisfied if the probability of lysogeny p and the induction rate i are both low.

In a lysogen the prophage provides the bacterial host with new genes. For example, when Stx phages form lysogens with *E. coli*, the host cell acquires new DNA, including the genes which code for Shiga toxins. Some of this additional DNA may have an influence on the fitness of the lysogen (Smith et al, 2007). For example, Shiga toxins are only released on induction and lysis (i.e. death) of a host cell, but this release of toxins may result in the creation of more favourable conditions for the remainder of the lysogen population. The release of Shiga toxins causes bleeding in the mammalian gut, thus providing a source of iron to surviving lysogens from decaying blood cells

(Canchaya et al, 2004).

Virulent phages run the risk of being too virulent and lysing the entire population of sensitive cells, so that the newly released phages cannot reproduce, and the phage population becomes extinct. Temperate phages do not risk extinction in this way, because even if all sensitive cells are infected by temperate phages, some of these will become lysogens which will preserve the phage DNA. Thus, phages may have evolved to be able to lysogenize their hosts as a method of surviving periods when the supply of sensitive cells is low. The level of resources present in the environment, which may vary over time, will also affect the sensitive cell population. Note that the models considered in this chapter assume a constant input resource concentration, and therefore do not consider the impact of resource variability on populations of phages and bacteria; both Stewart and Levin (1984) and Mittler (1996) show briefly how seasonal variations in resource levels may be incorporated into their population dynamical models, but there is much scope for future research in this area.

In this chapter we have considered population dynamical models of phages and bacteria. This work provides the basis for modelling the evolution of temperate phages in Chapter 3.

Chapter 3

Adaptive Dynamics of Temperate Phages

3.1 Introduction

Temperate bacteriophages (phages) select between two developmental pathways following adsorption to a host bacterial cell. These pathways are known as lysis and lysogeny. During lysis, many copies of the phage are produced and then released when the cell is lysed. If the lysogenic pathway is selected, the phage genome is inserted into the bacterial genome and replicated passively every time the cell divides. Following creation of a lysogen, a process known as induction may be initiated at a later time, leading to lysis of the host cell and the release of new phage particles. In the extensively studied temperate phage lambda, an increasingly well understood molecular switching mechanism selects between the two pathways, and can also initiate induction of a lysogen (Ptashne, 2004; Evans et al, 2007). For the purposes of this chapter the behaviour of the switch is characterized by two parameters: the probability of lysogeny (p) and the lysogen induction rate (i).

Using a chemostat model, Mittler (1996) investigated the outcome of pairwise competition between phage strains with different (fixed) values of i and p. In this model, strains with low values of both p and i were found to be strong competitors and generally able to invade when rare. It was speculated that this may be the reason why well-studied temperate phages such as phage lambda, Mu, and P1 have all evolved to have probabilities of lysogeny lower than 0.5 and induction rates of the order of 0.00001 per cell and generation (assuming that cells are not starved and are infected by a single phage) (Kourilsky, 1973; Howe and Bade, 1975; Rosner, 1972); in theory p could be anywhere between 0 and 1, and i could be any non-negative number. The aim of this chapter is to investigate the evolution of the parameters p and i.

The theory of Adaptive Dynamics (Geritz et al, 1998) provides a framework

for modelling the evolution of a single trait within a population. Initially there is a resident population of identical individuals at equilibrium, but small mutations can occur in this population. If a few mutants emerge, they may simply die out so that the previous equilibrium is restored; alternatively, their population may grow so that they eventually replace the existing resident population. Evolution thus proceeds via a series of small mutations. Evolutionary singularities play a central role, and they can be of various types corresponding to very different evolutionary outcomes. They can be attractors (commonly associated with the long-term emergence of intermediate trait values), repellors ('extreme' trait values) or branching points (dimorphisms/trait coexistence).

In the present chapter,the methods of Adaptive Dynamics are applied to the Mittler (1996) model. The aim is to determine which evolutionary outcomes are possible in this model, and to interpret these outcomes biologically. In common with applications in many other areas (e.g. Bowers and White (2002), de Mazancourt and Dieckmann (2004)), a constraint is introduced such that $i = f(p)$ for some function f. Some analytical results are derived which can be used to locate and classify the evolutionary singularities of the system, and we explore the importance of the shape of the function f in determining the number and nature of the singularities. The theoretical results obtained are illustrated with a number of examples.

3.2 A two-strain model

The chemostat model of host-phage interactions as described by Mittler (1996) consists of two phage strains (P_1 and P_2) and their associated host lysogens (L_1 and L_2 respectively). There is also a flow of sensitive bacteria (S) and resources (R) into the chemostat. Following adsorption of a P_1 phage to a sensitive bacterial cell, an L_1 lysogen may be formed, while adsorption of a P_2 phage may result in the formation of an L_2 lysogen. Strains 1 and 2 differ only in their probabilities of lysogeny (p_1 and p_2 respectively) and their induction rates (i_1 and i_2). The model is given below:

$$\frac{dR}{dt} = \omega(R_0 - R) - \epsilon r(S + L_1 + L_2)R/(R + k) \quad (3.2.1)$$

$$\frac{dS}{dt} = \omega(S_0 - S) + rSR/(R + k) + \xi(L_1 + L_2) - \delta SP_1 - \delta SP_2 \quad (3.2.2)$$

$$\frac{dL_1}{dt} = p_1\delta SP_1 + rL_1R/(R + k) - i_1L_1 - \xi L_1 - \omega L_1 \quad (3.2.3)$$

$$\frac{dL_2}{dt} = p_2\delta SP_2 + rL_2R/(R + k) - i_2L_2 - \xi L_2 - \omega L_2 \quad (3.2.4)$$

$$\frac{dP_1}{dt} = (1 - p_1)\beta\delta SP_1 + \beta i_1L_1 - \delta(L_1 + L_2)P_1 - \omega P_1 \quad (3.2.5)$$

$$\frac{dP_2}{dt} = (1 - p_2)\beta\delta SP_2 + \beta i_2L_2 - \delta(L_1 + L_2)P_2 - \omega P_2 \quad (3.2.6)$$

Here ω is the chemostat flow rate, and R_0 and S_0 are the concentrations of resource and susceptible bacteria in the input reservoir. Thus resources and susceptible bacteria enter the habitat at rates of ωR_0 and ωS_0 respectively. Similarly, all of the constituent species within the habitat are washed out at a rate proportional to ω. The growth rates of susceptible bacteria and lysogens are related to the availability of resources via the Monod function $rR/(R + k)$ (Monod, 1949), where r is the maximal growth rate and k is the resource concentration at which cells grow at half their maximal growth rate. The efficiency with which cells take up resources is measured by the parameter ϵ, so that resources are consumed at a rate of $\epsilon rR(S + L_1 + L_2)/(R + k)$. The parameter δ is associated with the rate at which free phages encounter and adsorb to bacterial cells. The probability that a phage of strain P_1 (P_2) will form a lysogen with its bacterial host is denoted p_1 (p_2), and i_1 (i_2) is the spontaneous induction rate for a lysogen of type L_1 (L_2). Those phages which do not form lysogens will enter the lytic cycle immediately following adsorption to a susceptible bacterial cell. Following lysis of an infected cell, the number of newly created phages is given by the burst size, β. The parameter ξ allows for the event of a lysogen losing its prophage and thus returning to its original state of a susceptible bacteria. The model assumes that lysogens are immune to further infection by either phage strain.

Now suppose that there is a resident population of strain 1 and its lysogen at equilibrium. Strain 2 and its lysogen will be able to invade when rare if the following condition is satisfied (Mittler, 1996; see Appendix A for a derivation):

$$Q(p_1, i_1)^2\gamma(p_1, i_1) + Q(p_1, i_1)i_2 - Q(p_1, i_1)\mu(p_1, i_1)p_2 > 0 \quad (3.2.7)$$

where

$$\begin{aligned}\gamma(p,i) &= P^*/\beta L^* \\ \mu(p,i) &= \delta S^* P^*/L^* \\ Q(p,i) &= (\beta p \delta S^* P^* - \beta i L^*)/P^*\end{aligned}$$

and S^*, L^*, and P^* are the equilibrium densities of S, L, and P for a resident phage with parameters p and i. It can be seen from (3.2.7) that the value of $Q(p_1, i_1)$ will be important in determining whether or not strain 2 can invade. If $Q(p_1, i_1)$ is positive then a strain with low p_2 and a high i_2 can invade, while if $Q(p_1, i_1)$ is negative then a strain with a high p_2 and a low i_2 can invade.

By setting the right hand side of Equation (3.2.5) equal to zero, and re-arranging, the expression for $Q(p, i)$ can be shown to be equivalent to:

$$Q(p,i) = \beta\delta S^* - \delta L^* - \omega$$

and so $Q(p, i)$ can be interpreted as the net rate at which the phage population would increase if the probability of lysogeny were zero.

We now summarise some observations regarding the function Q which were stated in Mittler (1996). Firstly, if $Q(p_1, i_1)$ and $Q(p_2, i_2)$ have opposite signs then both strains can invade when rare and the two strains will coexist. On the other hand, if $Q(p_1, i_1)$ and $Q(p_2, i_2)$ have the same sign then the strain with the lower value of $|Q|$ can invade when rare, while the strain with the greater value of $|Q|$ cannot invade when rare. Furthermore, if the resident has $Q = 0$ then invasion is not possible by any mutant strain; if the mutant has $Q = 0$ then it can invade any resident with $Q \neq 0$, but will not drive it to extinction. The results which we obtain using adaptive dynamics will shed further light on these observations.

3.3 The adaptive dynamics approach

The approach used by Mittler (1996) involves modelling the outcome of competition between two fixed phage strains, whereas the adaptive dynamics approach enables repeated mutation and selection to be modelled. We aim to investigate long-term evolutionary outcomes for temperate phages using this approach, in the context of an equitable environment.

We assume that there is a function f such that $i = f(p)$. This represents constraints in the system or trade-offs corresponding to cost-benefit dependencies (for general discussions see Bowers et al, 2005, de Mazancourt and Dieckmann, 2004, and Rueffler et al, 2004). Then, using (3.2.7), we obtain the following function:

$$s_{p_1}(p_2) = Q(p_1)^2\gamma(p_1) + Q(p_1)f(p_2) - Q(p_1)\mu(p_1)p_2 \tag{3.3.1}$$

We shall refer to $s_{p_1}(p_2)$ as the mutant's fitness function, since it is (by the argument of Appendix A) sign equivalent to the dominant eigenvalue of the invasion Jacobian. This eigenvalue is taken as the standard definition of fitness (Geritz et al, 1998), but any sign equivalent quantity is acceptable (e.g. Giafis, 2007).

Since $s_{p_1}(p_1) = 0$, we can re-write (3.3.1) as:

$$\begin{aligned} s_{p_1}(p_2) &= s_{p_1}(p_2) - s_{p_1}(p_1) \\ &= Q(p_1)\left[f(p_2) - f(p_1) - \mu(p_1)(p_2 - p_1)\right] \end{aligned} \tag{3.3.2}$$

From (3.3.2) we see that a cost-benefit interpretation of $i = f(p)$ suggests $f'(p) > 0$; otherwise both contributions in the second factor will have the same sign. The sign of $Q(p_1)$ plays a role here as discussed later.

3.3.1 Location of singularities

An evolutionary singularity p^* occurs at any point at which the partial derivative $\partial s_{p_1}(p_2)/\partial p_2$ evaluated at $p_1 = p_2 = p^*$ is equal to zero. At such a point, the partial derivative $\partial s_{p_1}(p_2)/\partial p_1$ will also be zero (Geritz et al, 1998). Differentiating (3.3.2) with respect to p_2 and setting this equal to zero, we have

$$Q(p^*)\left[f'(p^*) - \mu(p^*)\right] = 0 \tag{3.3.3}$$

and so there is a singularity at any point p^* where one of the following expressions holds:

$$Q(p^*) = 0 \tag{3.3.4}$$

or

$$f'(p^*) = \mu(p^*) \tag{3.3.5}$$

The expression $Q(p, i) = 0$ describes a straight line in (p, i) space (see Appendix B). Condition (3.3.4) indicates that there will be a singularity at any point of intersection between the trade-off function and the line $Q(p, i) = 0$. Condition (3.3.5) tells us that there will be a singularity at any point at which the gradient of the trade-off function is equal to the value of μ. These are new results which can be used to locate all the evolutionary singularities easily.

3.3.2 Classification of singularities

Having located the singularities, the next step is to classify each singularity as an attractor, a repellor, or a branching point. To do this we need to use the second order partial derivatives of the fitness function. Define a and b as follows:

$$a = \left.\frac{\partial^2 s_{p_1}(p_2)}{\partial p_1^2}\right|_{p_1=p_2=p^*}$$

$$b = \left.\frac{\partial^2 s_{p_1}(p_2)}{\partial p_2^2}\right|_{p_1=p_2=p^*}$$

By differentiating (3.3.2) twice with respect to p_2, we obtain the following expression for b:

$$b = Q(p^*)f''(p^*) \tag{3.3.6}$$

and by differentiating (3.3.2) twice with respect to p_1, we find

$$a = -Q(p^*)f''(p^*) - 2\left[\left.\frac{dQ(p)}{dp}\right|_{p=p^*}(f'(p^*) - \mu(p^*)) - \left.\frac{d\mu(p)}{dp}\right|_{p=p^*}Q(p^*)\right] \tag{3.3.7}$$

and this expression can be simplified using either (3.3.4) or (3.3.5) as appropriate. For a singularity which satisfies (3.3.4), we have

$$a = -2\left[\left.\frac{dQ(p)}{dp}\right|_{p=p^*}(f'(p^*) - \mu(p^*))\right] \tag{3.3.8}$$

while for a singularity which satisfies (3.3.5), we have

$$\begin{aligned} a &= Q(p^*)\left(2\left.\frac{d\mu(p)}{dp}\right|_{p=p^*} - f''(p^*)\right) \\ &= -b + 2\left.\frac{d\mu(p)}{dp}\right|_{p=p^*}Q(p^*) \end{aligned} \tag{3.3.9}$$

Now, a singularity p^* is evolutionarily stable (ES, or by common usage ESS) if $b < 0$ at p^*, and this means that no nearby mutant can invade. The singularity p^*

is convergence-stable (CS) if $a - b > 0$, and this means that a nearby mutant can be invaded by mutants which are even closer to the singularity (Geritz et al. 1998).

The above results and definitions provide us with the tools we need in order to classify any singularity which may arise, as described below.

Singularities with $Q = 0$

Suppose that p^*satisfies (3.3.4) but not (3.3.5). In this case $b = Q(p^*)f''(p^*) = 0$, and so p^* is marginally ESS. It turns out that p^* must also be CS. To see this note that p^* will be CS if $a > 0$ (since b is zero). There are two cases to consider: (i) $f'(p^*) < \mu_0$ and (ii) $f'(p^*) > \mu_0$, where μ_0 is the gradient of the line $Q = 0$ in (p, i) space. The two cases are dealt with below.

To begin with, note that Q is positive below and negative above the line $Q = 0$ in (p, i) space (see Appendix B). If $f'(p^*) < \mu_0$, then we have $Q(p^* - \epsilon, f(p^* - \epsilon)) < 0$, $Q(p^*, f(p^*))=0$, and $Q(p^* + \epsilon, f(p^* + \epsilon)) > 0$, for small $\epsilon > 0$. Therefore $\left.\frac{dQ(p)}{dp}\right|_{p=p^*}$ is positive, and so $a = -2\left[\left.\frac{dQ(p)}{dp}\right|_{p=p^*}(f'(p^*) - \mu_0))\right] > 0$. A similar argument shows that if $f'(p^*) > \mu_0$ then $\left.\frac{dQ(p)}{dp}\right|_{p=p^*}$ must be negative and hence $a > 0$ and p^* is CS as claimed.

Thus if $Q(p^*) = 0$ and $f'(p^*) \neq \mu_0$, then p^* is a marginally ESS attractor.

Singularities with $Q \neq 0$

Now suppose we have a singularity p^* which satisfies (3.3.5) but not (3.3.4). Using (3.3.6), this singularity will be ESS if and only if $Q(p^*)$ and $f''(p^*)$ have opposite signs. Using (3.3.9), we need to find $\left.\frac{d\mu(p)}{dp}\right|_{p=p^*}$ in order to determine the value of a; it turns out that this partial derivative must always be zero (see Appendix C), and therefore $a = -b$.

Since $a = -b$, a singularity of this type must either be (i) both ESS and CS, or (ii) neither ESS nor CS (note that branching points, which are CS but not ESS, are not possible in the current setting). Thus, using (3.3.6), there are four possible cases:

$$Q(p^*) < 0, f''(p^*) > 0 \implies p^* \text{ is an attractor (ESS, CS)} \quad (3.3.10)$$

$$Q(p^*) < 0, f''(p^*) < 0 \implies p^* \text{ is a repellor (not ESS, not CS)} \quad (3.3.11)$$

$$Q(p^*) > 0, f''(p^*) > 0 \implies p^* \text{ is a repellor (not ESS, not CS)} \quad (3.3.12)$$

$$Q(p^*) > 0, f''(p^*) < 0 \implies p^* \text{ is an attractor (ESS, CS)} \quad (3.3.13)$$

Note (see Equation (3.3.2)) that if $Q > 0$ then an increase in i is a benefit and an increase in p is a cost; on the other hand, if $Q < 0$ then an increase in i is a cost while

an increase in p is a benefit. Therefore the above conditions can be re-written as:

$$f \text{ decceleratingly costly} \implies p^* \text{ is a repellor (not ESS, not CS)}$$
$$f \text{ acceleratingly costly} \implies p^* \text{ is an attractor (ESS, CS)}$$

It can also be shown (see Appendix C) that for any singularity p^* which satisfies (3.3.5), we must have that

$$\left.\frac{dQ}{dp}\right|_{p=p^*} = 0$$

Thus, the value of Q is either locally maximised or locally minimised at p^*.

Singularities which satisfy both criteria

Now suppose we have a singularity which satisfies both (3.3.5) and (3.3.4). In this case a and b will be zero, and the singularity will be on the borderline of both the ES and the CS conditions.

3.4 Some examples

Here we present four examples which illustrate how the use of different trade-off curves can result in different numbers and types of singularities. Figure 3.1 shows some contours of the function Q for our chosen set of parameter values, and in particular shows the location of the line $Q = 0$. In order for the relationship $i = f(p)$ to represent a trade-off, f must be an increasing function of p (as discussed in Section 3.3). The general form of the trade-off functions used is as follows (White et al, 2006):

$$f(p) = i_{max} - \frac{(i_{max} - i_{min})(1 - \frac{p - p_{min}}{p_{max} - p_{min}})}{(1 + \frac{\alpha(p - p_{min})}{p_{max} - p_{min}})} \tag{3.4.1}$$

The value of the parameter α determines the curvature of the trade-off function. The value of α is taken to lie in the interval $(-1, \infty)$. If α lies in $(0, \infty)$ then the trade-off is acceleratingly costly. If α lies in (-1,0) then the trade-off is deceleratingly costly.

We use pairwise invasibility plots (PIPs) (Geritz et al, 1998) to illustrate the examples. These show the sign of the mutant's fitness for all possible combinations of p_1 and p_2. The mutant's fitness along the leading diagonal is always zero, because the resident population is at equilibrium and mutant and invader are identical. Evolutionary singularities occur at any point of intersection between the leading diagonal and another line along which the mutant's fitness is zero, while the pattern of signs around a singularity determines the nature of the singularity (Geritz et al, 1998).

For each example below we use a PIP and a plot of the line $Q = 0$ and the trade-off function to illustrate the way that the singularities shown in the PIP correspond to different points along the trade-off function. We also show the results of simulating the mutation-selection process in a multi-strain model, to show how the resident strategy evolves either towards an attractor or away from a repellor (Miller et al, 2005; White and Bowers, 2005; Bowers et al, 2005).

3.4.1 An attractor

For this and the remaining examples, i is constrained to be an increasing function of p (White et al, 2006):

$$f(p) = i_{max} - \frac{(i_{max} - i_{min})(1 - \frac{p - p_{min}}{p_{max} - p_{min}})}{(1 + \frac{\alpha(p - p_{min})}{p_{max} - p_{min}})} \tag{3.4.2}$$

The PIP (Figure 3.2(A)) shows that there is a singularity near $p = 0.6$. The pattern of signs around the singularity (minus signs above and below, plus signs to the left and right) indicates that it is an attractor.

Figure 3.2(B) shows the trade off function and the $Q = 0$ line in (p, i) space. There is no point of intersection between the two lines, and so there are no solutions to (3.3.4). The point p^* on the trade-off curve at which (3.3.5) is satisfied (i.e. the slope of the trade-off curve is equal to the value of the function μ) corresponds to the singularity identified in the PIP. Solving (3.3.5) numerically yields a value of $p^* = 0.597$. The tangent to the trade-off curve at $(p^*, f(p^*))$ is also shown in the Figure.

The results of a dynamical simulation for this scenario are shown in Figure 3.2(C). Starting with an initial resident strain with a value of p around 0.2, evolution proceeds via small mutations towards the attractor p^*.

Both the PIP-based approach and the dynamical simulations corroborate the algebraic theory of Section 3.3. Since numerical evaluation gives $Q(p^*) < 0$ and $f''(p^*) > 0$, Statement (3.3.10) indicates that p^* is indeed an attractor.

3.4.2 A repellor

The PIP (Figure 3.3(A)) shows that there is a singularity near $p = 0.24$. This time, the pattern of signs around the singularity (plus signs above and below, minus signs to the left and right) indicates that it is a repellor.

Figure 3.3(B) shows the trade off function and the $Q = 0$ line in (p, i) space. There is no point of intersection between the two lines, and so there are no solutions to (3.3.4). Solving (3.3.5) numerically yields a value of $p^* = 0.237$. The tangent to the trade-off curve at $(p^*, f(p^*))$ is also shown in the Figure.

The dynamical simulation illustrated in Figure 3.3(C) shows evolution directed away from the singularity p^* and towards the extreme value $p = 0.1$.

Since evaluation gives $Q(p^*) < 0$ and $f''(p^*) < 0$, Statement (3.3.11) confirms that p^* is a repellor.

3.4.3 Multiple singularities (I)

The PIP in Figure 3.4(A) shows three singularities, which we will refer to as p_1^*, p_2^*, and p_3^* (where $p_1^* < p_2^* < p_3^*$). The central singularity p_2^* (around $p = 0.73$) is a repellor, while p_1^* and p_3^* are marginally ESS attractors.

Figure 3.4(B) shows the trade off function and the $Q = 0$ line in (p, i) space. There are two points of intersection between the two lines, and so we expect to find two solutions to (3.3.4). Solving (3.3.4) numerically yields values of $p_1^* = 0.531$ and $p_3^* = 0.854$. We can also solve (3.3.5) numerically to find $p_2^* = 0.730$.

A dynamical simulation for this scenario is shown in Figure 3.4(C). Starting with an initial resident strain with a value of p close to the repellor p_2^*, evolution proceeds via small mutations away from the repellor and towards the lower attractor p_1^*.

For p_2^* we have $Q > 0$ and $f'' > 0$, and so (3.3.11) confirms that p_2^* is a repellor.

3.4.4 Multiple singularities (II)

The example shown in Figure 3.5 is similar to the previous example except that the curvature of the trade-off function has been changed from concave to convex. There are still a single repellor ($p_2^* = 0.652$) and two marginally ESS attractors ($p_1^* = 0.532$ and $p_3^* = 0.842$).

This example and the previous one illustrate the point that if the trade-off function intersects the line $Q = 0$ at two distinct points - p_a and p_b, say (with $p_a < p_b$) - then there must be a point p_c (where $p_a < p_c < p_b$) corresponding to an evolutionary repellor.

For p_2^* we have $Q < 0$ and $f'' < 0$, and so (3.3.11) confirms that p_2^* is a repellor.

3.5 Discussion

We have applied the methods of Adaptive Dynamics to the chemostat model of Mittler (1996). This approach has enabled us to develop and extend Mittler's work, and in particular to model the continuous evolution of temperate phage strains via small mutations.

We have shown that the location and nature of the evolutionary singularities depends on the shape of the function f (which relates the parameters i and p) and also

on the position of f relative to the straight line $Q = 0$. Marginal attractor singularities occur at points of intersection between f and the $Q = 0$ line. Singularities also occur at points along f at which f' is equal to the value of the function μ; at a singularity of this type, the value of $|Q|$ is locally maximised or minimised.

We have established that, in contrast to other studies in adaptive dynamics (e.g. Boots and Haraguchi (1999), White and Bowers (2005), Miller et al (2005)), evolutionary branching does not occur in the present setting. It would be instructive to carry out experimental work into the occurence of branching in real populations of temperate phages.

The gradient of the $Q = 0$ line is equal to the value of the function μ and is therefore always positive (as shown in Appendix B). However, any change in the non-evolving parameter values (e.g. the input concentrations of resources or sensitive bacteria) which alters the equilibrium levels of the populations will also alter the $Q = 0$ gradient, and possibly the nature of any singularities. For example, a repellor at which the value of Q is initially positive will become an attractor if there is a change in the parameter values which causes the slope of $Q = 0$ to decrease sufficiently; i.e. the singularity now appears on the other side of the $Q = 0$ line, so that its Q value is negative. Therefore the choice of parameter values is particularly important in cases where singularities occur close to the $Q = 0$ line.

Provided that i is an increasing function of p, then it is possible for f to intersect the line $Q = 0$ at two seperate points, and these will correspond to marginal ESS attractors. When this happens, there will always be a repellor in between the two attractors, as in Figures 3.5 and 3.6.

As mentioned in the introduction, phage lambda and other well-studied temperate phages have evolved to have values of i and p at the lower end of the ranges of possible values. In the adaptive dynamics framework, this could occur as a result of evolution away from a repellor (as in Figure 3.4). Phages with low values of i and p are likely to perform better than other phages when the environment is subject to variation, since they will be able to survive lean periods (via lysogenic infections) but also to compete strongly (via lysis) when resources and sensitive bacteria are plentiful (see Mittler (1996) for a discussion of this point).

By assuming that $f' > 0$, we have been able to interpret $i = f(p)$ in terms of a cost-benefit relationship in which the function f represents a trade-off. If we allow an interpretation in which, while f represents a constraint, changes in i and p are such that $f' < 0$, then our results change. In this case there will be a marginally ESS attractor at the (single) point of intersection between f and the line $Q = 0$ (if such a point exists). However, no other singularities are possible: the contours $Q = x$ in (p, i) space are straight lines with a positive gradient (as shown in Appendix B), and therefore if f has

a negative slope there will be no point on f whose tangent coincides with a contour of Q, and therefore no point at which $|Q|$ is either locally maximised or locally minimised. An example of this type of scenario is shown in Figure 3.6.

We have shown (Appendix A) that whereas a temperate resident phage can be invaded by a virulent mutant (depending on the sign of Q_1), a virulent resident can not be invaded by a temperate mutant, in the present setting. This raises the question of why temperate phages emerged in the first place (assuming that they have evolved from virulent phages). The role of environmental fluctuation is likely to form part of the answer to this. Population models which include an environmental fluctuation term have been discussed by Stewart and Levin (1984) and Mittler (1996). In the present chapter we have considered a constant input of resources and sensitive bacteria to the chemostat, but it would be interesting to study models of phage evolution in the context of a fluctuating environment.

3.6 Appendix A: The fitness function

Here we present an outline of the method used to derive the fitness function $s_{p_1}(p_2)$.

Let R^*, S^*, L_1^*, and P_1^* be the equilibrium values of R, S, L_1, and P_1 calculated from equations (3.2.1), (3.2.2), (3.2.3), and (3.2.5), with $L_2 = P_2 = 0$. To see what will happen if a small number of mutant type 2 phages and lysogens emerge, we can consider the linearized system

$$\begin{aligned}
\frac{dL_2}{dt} &= [rR^*/(R^*+k) - i_2 - \xi - \omega]L_2 + [p_2\delta S^*]P_2 \\
\frac{dP_2}{dt} &= [\beta i_2]L_2 + [\beta(1-p_2)\delta S^* - \delta L_1^* - \omega]P_2
\end{aligned}$$

Now we assume that p_2 and i_2 are both greater than zero. Strain 2 and its lysogen can invade when rare if the above system has at least one positive eigenvalue. The eigenvalues are the solutions of

$$(a-\lambda)(d-\lambda) - bc = 0,$$

where $a = rR^*/(R^*+k) - i_2 - \xi - \omega$, $b = p_2\delta S^*$, $c = \beta i_2$, and $d = \beta(1-p_2)\delta S^* - \delta L_1^* - \omega$. There will be a positive eigenvalue if either $ad < bc$ or $(a+d) > 0$, or both. In fact, it is only necessary to consider the condition $ad < bc$, since it can be shown that it is not possible for both a and d to be positive (see Mittler, 1996); if one of them is positive and the other is negative then then there will certainly be an positive eigenvalue, because $ad < bc$. If both a and d are negative then $a + d < 0$, and so there will only be a

positive eigenvalue if $ad < bc$ holds. Thus, checking the condition $ad < bc$ covers all possibilites.

It is straightforward to show that the condition $ad < bc$ is equivalent to

$$Q(p_1, i_1)^2\gamma(p_1, i_1) + Q(p_1, i_1)i_2 - Q(p_1, i_1)\mu(p_1, i_1)p_2 > 0$$

where $\gamma(p, i) = P^*/\beta L^*$; $\mu(p, i) = \delta S^* P^*/L^*$; and $Q(p, i) = (\beta p \delta S^* P^* - \beta i L^*)/P^*$ (Mittler, 1996).

In the special case of a virulent mutant, i.e. $p_2 = i_2 = 0$, then there are no L_2 lysogens and there is a single invasion eigenvalue $\lambda = \beta\delta S^* - \delta L_1^* - \omega = Q(p_1, i_1)$. Therefore a resident strain can be invaded by a virulent mutant if $Q(p_1, i_1) > 0$; on the other hand, if $Q(p_1, i_1) < 0$ then a virulent mutant can not invade.

In the special case where the resident phage is virulent, i.e. $p_1 = i_1 = 0$, then $Q(p_1, i_1) = 0$ and so the fitness of an invading mutant (i.e. $Q(p_1, i_1)^2\gamma(p_1, i_1) + Q(p_1, i_1)i_2 - Q(p_1, i_1)\mu(p_1, i_1)p_2$) will be zero for any values of p_2 and i_2. Therefore no mutant phage can invade.

3.7 Appendix B: The Q function

Here we show that given a real number x, the line $Q(p,i) = x$ (if it exists) is linear in (p,i) space. Setting the right hand sides of equations (3.2.1), (3.2.2), (3.2.3), and (3.2.5) all equal to zero (with $P_2 = L_2 = 0$), and using the relationship $Q(p,i) = x$, we obtain:

$$\begin{aligned}
0 &= \omega(R_0 - R^*) - \epsilon r(S^* + L_1^*)R^*/(R^* + k) \\
0 &= \omega(S_0 - S^*) - rS^*R^*/(R^* + k) + \xi L_1^* - \delta S^* P_1^* \\
0 &= x + \frac{\beta r L_1 R}{P_1(R+k)} - \frac{\beta\xi L_1}{P_1} - \frac{\beta\omega L_1}{P_1} \\
0 &= -x + \beta\delta S - \delta L_1 - \omega
\end{aligned}$$

Since p and i do not appear in the above equations, the values of R^*, S^*, L_1^*, and P_1^* are constant along the line $Q(p,i) = x$.

Since $Q(p,i) = (\beta p_1 \delta P_1^* S^* - \beta i_1 L_1^*)/P_1^*$, the line $Q(p,i) = x$ must be a straight line through the origin with gradient $\delta P_1^* S^*/L_1^*$ and intercept $-xP_1/(\beta L_1)$ (where R^*, S^*, L_1^*, and P_1^* are obtained from the four equations above). Note that the gradient is equal to the value of the function μ, and that all points along the line $Q(p,i) = x$ must have the same value of μ.

To show that $Q(p,i)$ is positive for all points below the line $Q(p,i) = 0$, we can consider the single point $(p,0)$, where $0 < p < 1$. At this point, we have $Q = (\beta p \delta S^* P_1^*)/P_1^* > 0$.

To show that $Q(p,i)$ is negative for all points above the line $Q(p,i) = 0$, we can consider the single point $(0,i)$, where $0 < i < 1$. At this point, we have $Q = -\beta i_1 L_1^*/P_1^* < 0$.

3.8 Appendix C: Derivatives of μ and Q at p^*

In this section, we assume that p^* is a singularity which satisfies Equation (3.3.5) of the text.

(i) Differentiating μ:

To find the derivative of μ at p^*, we begin by setting the right hand sides of Equations (3.2.1), (3.2.2), (3.2.3), and (3.2.5) all equal to zero (with $P_2 = L_2 = 0$ and $i = f(p)$), to obtain four equations of the form:

$$\begin{aligned} f_1(R, S, L, P, p) &= 0 \\ f_2(R, S, L, P, p) &= 0 \\ f_3(R, S, L, P, p) &= 0 \\ f_4(R, S, L, P, p) &= 0 \end{aligned}$$

and now we can write

$$\begin{aligned} \frac{\partial f_1}{\partial R}R' + \frac{\partial f_1}{\partial S}S' + \frac{\partial f_1}{\partial L}L' + \frac{\partial f_1}{\partial P}P' + \frac{\partial f_1}{\partial p} &= 0 \\ \frac{\partial f_2}{\partial R}R' + \frac{\partial f_2}{\partial S}S' + \frac{\partial f_2}{\partial L}L' + \frac{\partial f_2}{\partial P}P' + \frac{\partial f_2}{\partial p} &= 0 \\ \frac{\partial f_3}{\partial R}R' + \frac{\partial f_3}{\partial S}S' + \frac{\partial f_3}{\partial L}L' + \frac{\partial f_3}{\partial P}P' + \frac{\partial f_3}{\partial p} &= 0 \\ \frac{\partial f_4}{\partial R}R' + \frac{\partial f_4}{\partial S}S' + \frac{\partial f_4}{\partial L}L' + \frac{\partial f_4}{\partial P}P' + \frac{\partial f_4}{\partial p} &= 0. \end{aligned}$$

Thus

$$\begin{pmatrix} \frac{\partial f_1}{\partial R} & \frac{\partial f_1}{\partial S} & \frac{\partial f_1}{\partial L} & \frac{\partial f_1}{\partial P} \\ \frac{\partial f_2}{\partial R} & \frac{\partial f_2}{\partial S} & \frac{\partial f_2}{\partial L} & \frac{\partial f_2}{\partial P} \\ \frac{\partial f_3}{\partial R} & \frac{\partial f_3}{\partial S} & \frac{\partial f_3}{\partial L} & \frac{\partial f_3}{\partial P} \\ \frac{\partial f_4}{\partial R} & \frac{\partial f_4}{\partial S} & \frac{\partial f_4}{\partial L} & \frac{\partial f_4}{\partial P} \end{pmatrix} \begin{pmatrix} R' \\ S' \\ L' \\ P' \end{pmatrix} = \begin{pmatrix} \frac{\partial f_1}{\partial p} \\ \frac{\partial f_2}{\partial p} \\ \frac{\partial f_3}{\partial p} \\ \frac{\partial f_4}{\partial p} \end{pmatrix} = \begin{pmatrix} 0 \\ 0 \\ \delta SP - f'L \\ -\beta\delta SP + \beta f'L \end{pmatrix}$$

The vector on the right hand side of the above expression apparently has two non-zero elements. However, for a singularity which satisfies Equation (3.3.5) of the text, these entries vanish and we are left with an equation of the form

$$JX = 0$$

and X = (0 0 0 0) will be the only solution of this equation, provided that J is invertible. To see that J is indeed invertible, remember that we are assuming that the equilibrium (R^*, S^*, L^*, P^*) is stable. The Jacobian matrix used to determine stability is the same as the matrix J. Therefore the determinant of J must be non-zero, and hence J is invertible.

Thus, we have shown that

$$(R',\ S',\ L',\ P') = (0,\ 0,\ 0,\ 0) \qquad \text{(C1)}$$

at p^*. But $\mu = \delta SP/L$, so we must also have that $\mu' = 0$.

(ii) Differentiating Q:

Differentiating Q with respect to p, and using (C1) above and Equation (3.3.5) of the text, we find that

$$\left.\frac{dQ}{dp}\right|_{p=p^*} = 0.$$

Thus the value of $|Q|$ is either locally maximized or locally minimized at p^*. The second order derivative of Q at p^* will determine which of these possibilities is the case, but the expression for this quantity involves the second order derivatives of S, L, and P (with respect to p), for which we have not been able to obtain analytical expressions.

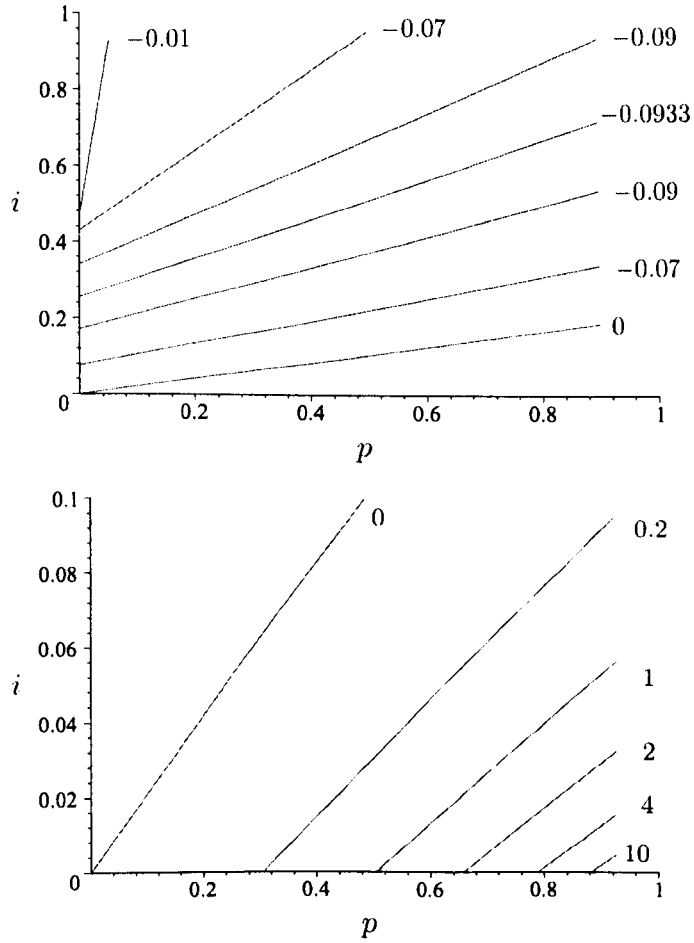

Figure 3.1: Contour plots for the function Q. Each contour is labelled with its respective Q value. The contours are all straight lines, and the gradient of each line is equal to the value of the function μ along that line. Parameter values: $R_0 = 100$, $S_0 = 2 \times 10^8$, $\delta = 10^{-9}$, $\beta = 100$, $\xi = 0.0001$, $r = 0.7$, $k = 4.0$, $\epsilon = 5 \times 10^{-7}$, $\omega = 0.2$.

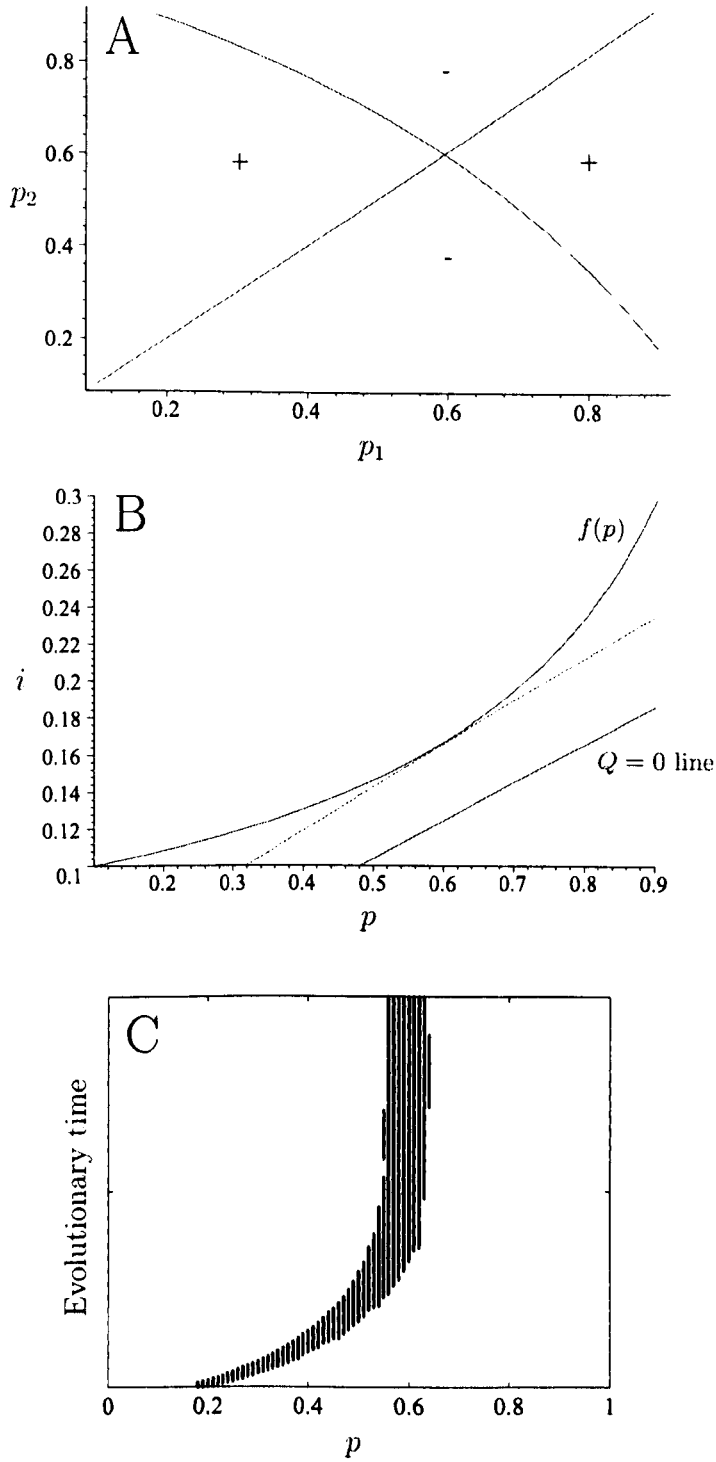

Figure 3.2: An attractor singularity (A) PIP showing the attractor at $p = 0.6$. (B) Plot of trade-off curve and the line $Q = 0$ line. The tangent to the trade-off curve at the singularity is also shown. (C) Dynamical simulation. Parameter values: $\alpha = -0.7$, other parameters as in Figure 3.1.

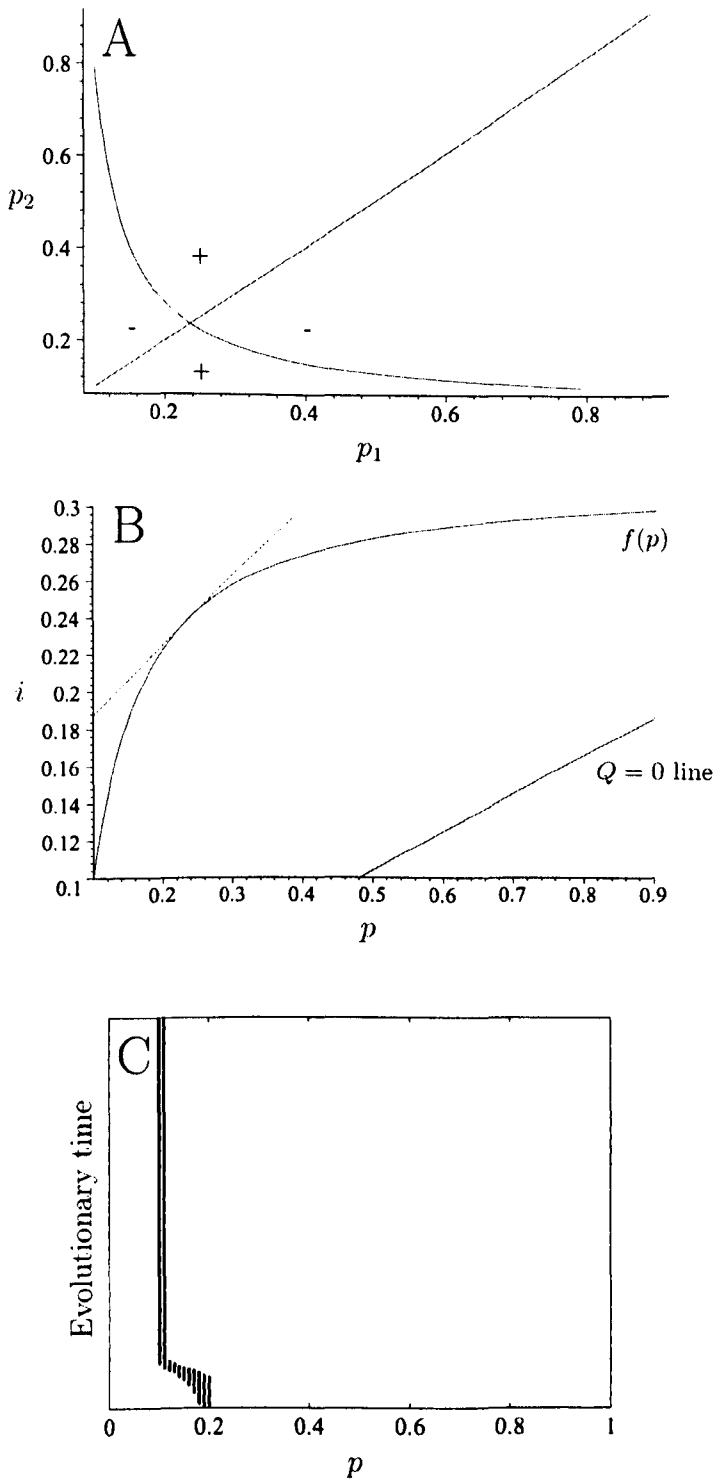

Figure 3.3: A repellor singularity. (A) PIP showing the repellor at $p = 0.24$. (B) Plot of trade-off curve and the line $Q = 0$ line. The tangent to the trade-off curve at the singularity is also shown. (C) Dynamical simulation. Parameter values: $\alpha = 10$, other parameters as in Figure 3.1.

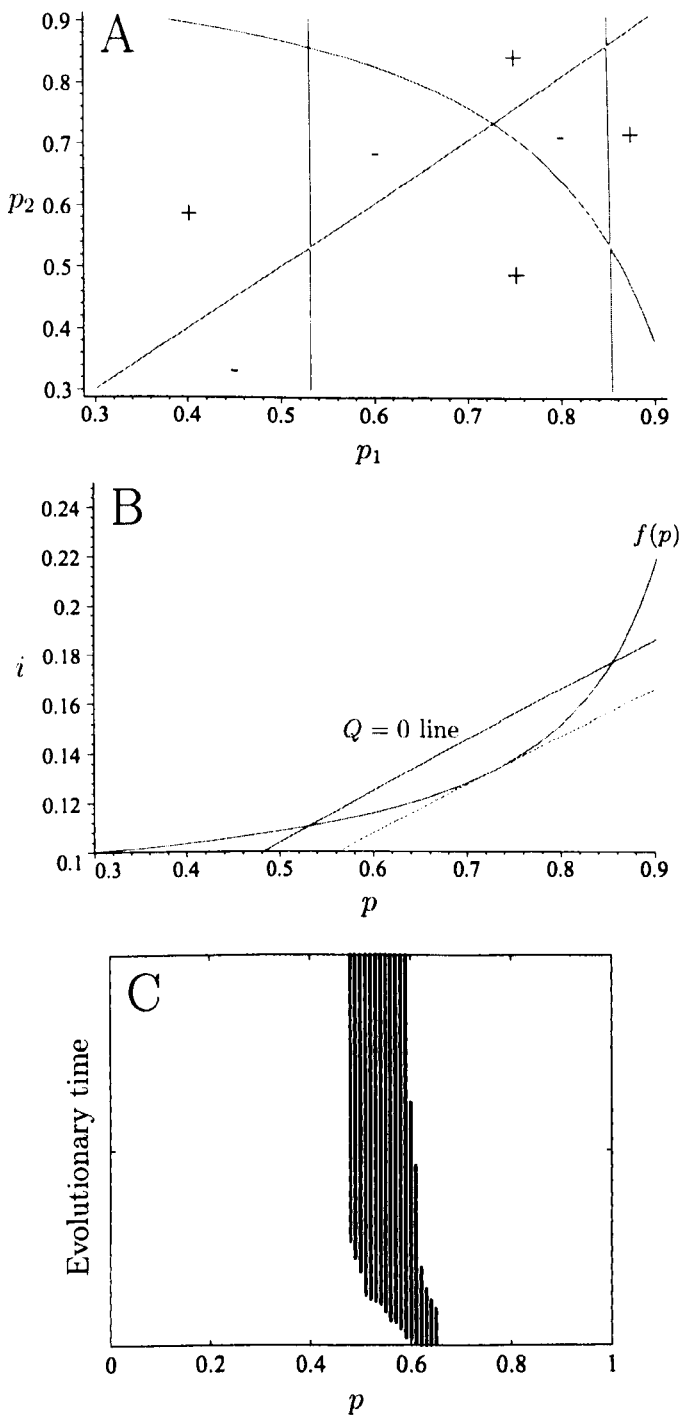

Figure 3.4: Multiple singularities (I). (A) PIP showing a repellor at $p = 0.73$, and two marginally ESS attractors (at $p = 0.53$ and $p = 0.85$). (B) Plot of trade-off curve and the line $Q = 0$ line. The tangent to the trade-off curve at the repellor singularity is also shown. (C) Dynamical simulation. Parameter values: $\alpha = -0.85$, other parameters as in Figure 3.1.

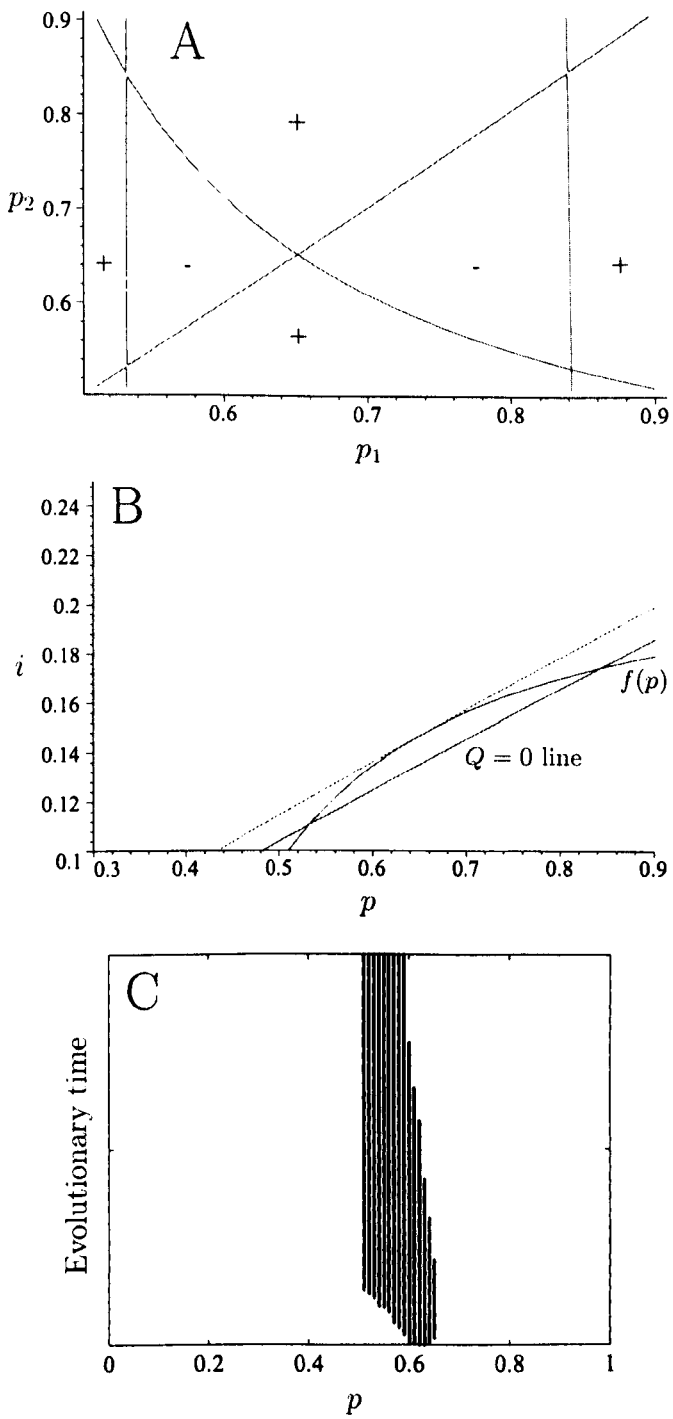

Figure 3.5: Multiple singularities (II). (A) PIP showing a repellor at $p = 0.65$, and two marginally ESS attractors (at 0.53 and 0.84). (B) Plot of trade-off curve and the line $Q = 0$ line. The tangent to the trade-off curve at the repellor singularity is also shown. (C) Dynamical simulation. Parameter values: $\alpha = 1.5$, other parameters as in Figure 3.1.

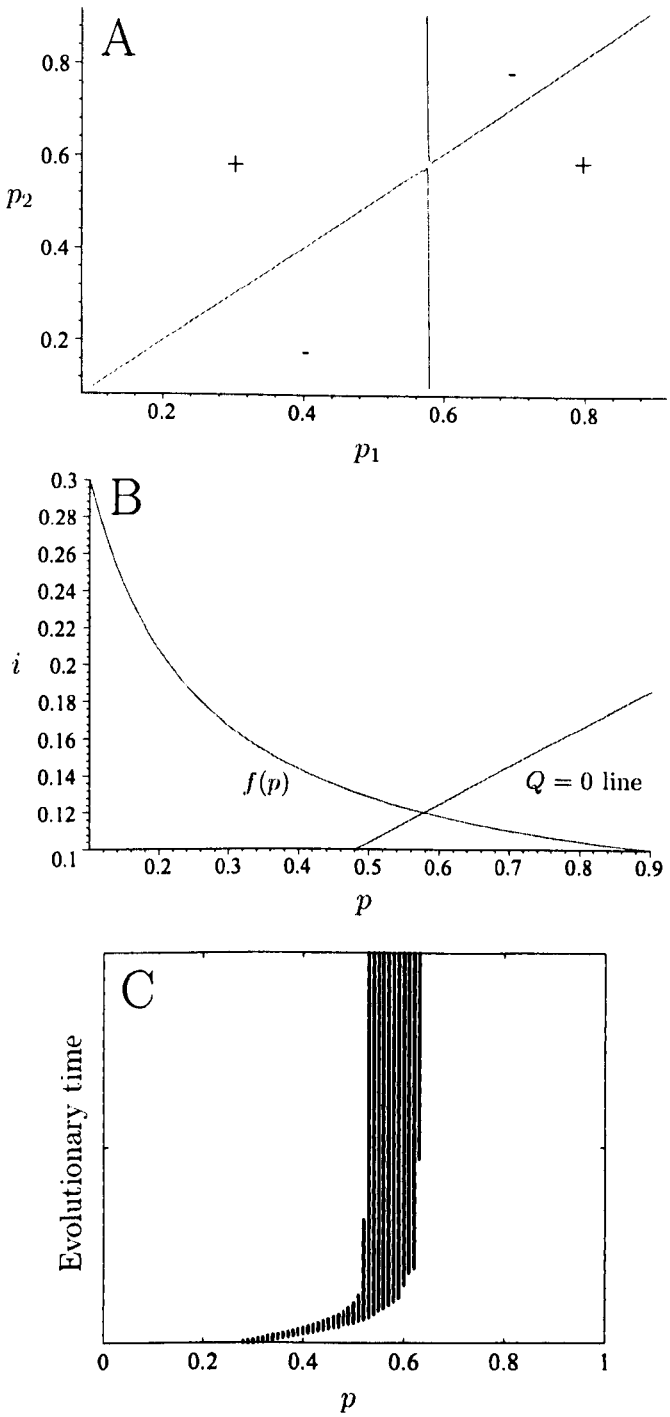

Figure 3.6: Constraining i to be a decreasing function of p. (A) PIP showing a marginally ESS attractor at $p = 0.58$. (B) Plot of trade-off curve and the line $Q = 0$ line. (C) Dynamical simulation. Parameter values: $\alpha = 5$, other parameters as in Figure 3.1.

Chapter 4

Modelling the Stability of Stx Lysogens

4.1 Introduction

Like all lambdoid phages, Stx phages are temperate - following adsorption to an *E. coli* cell, they are capable of both lytic and lysogenic reproduction. During lytic reproduction, multiple copies of the infecting virus are constructed, and then released - together with toxin molecules - through bacterial lysis (cell burst). Lysogenic reproduction is the mechanism by which the phage DNA (or prophage) becomes incorporated into the bacterial genome, and is then replicated passively during the *E. coli* replication cycle. A lysogen may later enter the lytic cycle through a process known as 'induction'.

In lambdoid phages, a molecular switching mechanism governs the selection of either the lytic or lysogenic pathway, and also determines the rate at which lysogens undergo induction. Lambda prophages are generally very stable, with an intrinsic induction rate of the order of 10^{-7} per cell per generation (Aurell et al., 2002; Little et al., 1999). However when the survival of the bacterial host is threatened by adverse environmental conditions, such as through starvation or exposure to ultra-violet light, the rate of lambda prophage induction is known to increase (Ptashne, 2004). It has been shown that the lysogens of the Stx phages 933W and H19B induce more readily than lambdoid phages which do not encode Stx toxin, with intrinsic induction rates of 1.4 x 10^{-4} and 5 x 10^{-5} respectively (Livny and Friedman, 2004). Such Stx lysogens will induce at a lower dosage of 'inducer' (e.g. UV light) compared with lambda lysogens, and this phenomenon is unlikely to be directly caused by the presence of the Stx toxin genes themselves since they are not involved in the switching mechanism. Therefore 933W and H19B have been described as having 'hair-trigger' switches (Livny and Friedman, 2004), a phrase used to convey the order of magnitude difference in induction sensitivity between these lambdoid Stx phages and the reference bacteriophage

lambda.

In the genome of an Stx phage, the *stx* gene is located downstream of the lysis genes (Unkmeir and Schmidt, 2000). Stx lysogens release Shiga toxins only when the bacterial cell is lysed, either following the initial infection event or following induction of a lysogen. Thus the factors regulating the lysis-lysogeny switch play an important role in the regulation of Shiga-toxin production and release (Tyler et al., 2004). Using an approach based on the methods of Ackers et al. (1982) and Shea and Ackers (1985), Santillan and Mackey (2004) developed a mathematical model which addresses the high level of stability of lambda lysogens. Various differences between the physical components of lambda and Stx switches have been reported in the literature (e.g. Koudelka et al., 2004; Tyler et al., 2004). The aim of this chapter is to contribute to the understanding of the sensitivity of the molecular switch by investigating the impacts of known differences in the molecular binding affinities and structure of Stx and lambda phages on switch dynamics and lysogen stability. The findings of this Chapter were published in Evans et al. (2007).

4.2 Modelling the switch

In lambda lysogens, the concentrations of two regulatory proteins, CI and Cro, determine whether the lysogenic state is maintained or the lytic cycle is initiated. The protein CI represses induction and lysis, as described below, and is therefore referred to as 'the repressor'. The CI and Cro proteins regulate the expression of two genes, *cI* and *cro*, in a feedback mechanism determined by the structure of the genome region associated with the switch (Figure 4.1). The O_R region of the genome is situated between the genes *cI* and *cro*, which code for CI and Cro respectively, and contains the three binding sites O_R1, O_R2, and O_R3. Molecules of CI and Cro in their dimerized form (denoted CI_2 and Cro_2) bind to these sites and in doing so regulate the expression of the two genes. If a CI_2 molecule is bound to O_R1 or O_R2 then an RNA polymerase ($RNAP$) molecule cannot bind to the *cro* promoter P_R, and so transcription of *cro* is blocked. Similarly, if a CI_2 or Cro_2 molecule is bound to O_R3 then transcription of *cI* is blocked.

The typical molecular configuration at the right operator (see Figure 4.1) in a stable lambda lysogen is that O_R1 and O_R2 are both occupied by CI_2 repressor molecules, while O_R3 is unbound (Ptashne, 2004). In this configuration, transcription of *cro* is 'off' but transcription of *cI* is 'on'. The bound repressor molecules continually dissociate from the operator sites, but are replaced by other nearby repressors. The lysogenic state is maintained as long as the concentration of repressor molecules is such that there will always be sufficient nearby repressor molecules to bind to O_R1 and O_R2

when these sites become vacant. If the repressor concentration falls, transcription is initiated by $RNAP$ binding at the promoter site P_R during a transient period when O_R1 and O_R2 are unbound. Transcription of *cro* ultimately leads to lysis of the cell and the release of new phage particles.

An important feature of the regulation of the switch is cooperative binding between repressor dimers. If a CI_2 molecule is bound to O_R1 then the probability of a CI_2 molecule binding to O_R2 is increased, i.e. the presence of the CI_2 molecule at O_R1 has the effect of increasing the binding affinity between CI_2 and O_R2.

A simple mathematical model of the lambda switch was presented by Ackers et al (1982). The model is based around the three binding sites at the right operator. Repressor dimers bind to these sites with probabilities determined by the binding affinites of the system. Dissociation of repressor dimers, and association of repressor monomers is also allowed for. The binding affinites were calculated from the results of earlier experimental work (Johnson et al, 1979). At any given time, each binding site is either unoccupied or bound by a repressor dimer. Thus there are 8 possible binding configurations. The results of the model indicated that cooperative binding between repressor molecules at O_R1 and O_R2 plays an important role in maintaining the lysogenic state, and also in allowing lysogens to be easily induced when the repressor concentration falls.

The static model of Ackers et al (1982) was later used as the basis for a dynamical model which also included Cro dimers and monomers, the enzyme $RNAP$, and the two promoters P_R and P_{RM} (Shea and Ackers, 1985). In this model, at any given time a binding site may either be unbound or bound by a dimer (CI_2 or Cro_2). Similarly, a promoter may be unbound or bound by an $RNAP$ molecule. There are now a total of 40 possible binding configurations (bearing in mind that certain configurations are excluded, e.g. O_R3 and P_{RM} cannot both be occupied simultaneously).

Using a model based on the work of Shea and Ackers (1985), Reinitz and Vaisnys (1990) explored whether or not the observed behaviour of the lambda switch could be accounted for by existing knowledge of the regulatory mechanisms. It was found that there were inconsistencies between observations and the theory. In particular, the level of P_R repression predicted by the model would not be sufficient to maintain the lysogenic state. This implied that an important component of regulatory activity was missing from the model.

It has been proposed (Dodd et al, 2001) that repressor molecules bound to the left operator of phage lambda contribute to the stability of lambda lysogens. The left operator region O_L contains three binding sites: O_L1, O_L2, and O_L3. Dimers of CI and Cro can bind to the left operator binding sites. Experimental evidence due to Dodd et al (2001) and Ptashne and Gann (2000) indicates that repressor molecules bound

at the left and right operators can interact cooperatively to form a stable complex, as illustrated in Figure 4.1.

The model of Santillan and Mackey (2004) extends the Shea and Ackers (1985) model to include the three binding sites of O_L, and cooperative interactions between repressor dimers at the left and right operators are allowed for. This model is presented below, since it provides the basis for my own modelling work. This is followed by a description of the method used to extend the model in order to model Stx lysogen stability.

4.2.1 The lambda model

The delay differential equation model of Santillan and Mackey (2004) captures the biochemical processes that govern the lambda molecular switch. It includes the right and left operators, the promoters P_R and P_{RM}, the enzyme $RNAP$, and the proteins CI and Cro in their monomer and dimer forms. The equations are:

$$\begin{aligned}
\frac{d[M_{cI}]}{dt} &= k^q_{cI}[O_R]f^q_{RM}([CI_2]_{\tau_M}, [Cro_2]_{\tau_M}) + k^s_{cI}[O_R]f^s_{RM}([CI_2]_{\tau_M}, [Cro_2]_{\tau_M}) \\
&\quad - (\gamma_M + \mu)[M_{cI}] \qquad (4.2.1)\\
\frac{d[M_{cro}]}{dt} &= k_{cro}[O_R]f_R([CI_2]_{\tau_M}, [Cro_2]_{\tau_M}) - (\gamma_M + \mu)[M_{cro}] \qquad (4.2.2)\\
\frac{d[CI_T]}{dt} &= \rho_{cI}[M_{cI}]_{\tau_{cI}} - (\gamma_{cI} + \mu)[CI_T] \qquad (4.2.3)\\
\frac{d[Cro_T]}{dt} &= \rho_{cro}[M_{cro}]_{\tau_{cro}} - (\gamma_{cro} + \mu)[Cro_T] \qquad (4.2.4)
\end{aligned}$$

where $[M_{cI}]$ and $[M_{cro}]$ are the concentration of cI and cro mRNA molecules respectively, and $[CI_T]$ and $[Cro_T]$ denote the total concentration of CI and Cro monomers respectively (here the total number of monomers means the number of free monomers plus twice the number of dimers). A quasi-steady-state assumption is used to determine the protein dimer concentrations in terms of the total monomer concentrations (Santillan and Mackey, 2004). The other symbols which appear in the above equations are defined in Tables 4.1 and 4.2.

In this model there are 1200 possible molecular configurations altogether, and for each state i there is an associated binding energy E_i which is the amount of energy which would be required to disassemble the configuration (the formula for calculating binding energies in phage lambda is a specific case of the formula presented in Section 4.2.3). Once the energy of each state has been determined, the probability of each state is calculated with the technique used by Ackers et al. (1982) and Shea and Ackers (1985):

$$P_i = \frac{exp(-E_i/RT)[CI_2]^{\alpha_i}[Cro_2]^{\beta_i}[RNAP]^{\delta_i}}{Z} \tag{4.2.5}$$

where R is the ideal gas constant and T is the absolute temperature (taken to be 37°C). The partition function Z is given by

$$Z = \sum_i exp(-E_i/RT)[CI_2]^{\alpha_i}[Cro_2]^{\beta_i}[RNAP]^{\delta_i} \tag{4.2.6}$$

where α_i, β_i, and δ_i are, respectively, the numbers of CI_2, Cro_2, and $RNAP$ molecules bound to the complex in the i-th state.

The quantities P_i are used to calculate the f functions. The probability that P_R is bound by an $RNAP$ molecule, f_R, may be calculated by summing the probabilities of all the states in which P_R is bound by an $RNAP$ molecule. Similarly, f^q_{RM} can be calculated by summing the probabilities of all the states in which both (i) P_{RM} is bound by an $RNAP$ molecule and (ii) O_R2 is bound by a CI_2 dimer. Finally, f^s_{RM} is calculated as the sum of the probabilities of all the states in which (i) P_{RM} is bound by an $RNAP$ molecule and (ii) O_R2 is not bound by a CI_2 dimer.

4.2.2 Properties of the model

The model predicts that, for a given set of parameter values, there will either be one or three equilibrium points. For low values of the CI degradation rate (γ_{cI}) there will generally be a single stable equilibrium corresponding to lysogeny (i.e. the repressor concentration will be relatively high and the Cro concentration will be relatively low at this point). If γ_{cI} is increased sufficiently, two additional equilibria will appear via a saddle node bifurcation, one of which is stable and corresponds to lysis (low repressor concentration and high Cro concentration) while the other is unstable. If γ_{cI} is increased even further, then the unstable and lysogenic equilibria will collide and annihilate each other, leaving only the stable lytic equilibrium.

The steady-states of this model of CI and Cro concentrations are the points of intersection between two curves, $\Phi = 0$ and $\Theta = 0$, where Φ and Θ are defined as follows (Santillan and Mackey, 2004):

$$\begin{aligned}\Phi([CI_T],[Cro_T],\gamma_{cI}) &= \frac{\rho_{cI}}{\gamma_M+\mu}[O_R](k^q_{cI}f^q_{RM} + k^s_{cI}f^s_{RM}) \\ &\quad - (\gamma_{cI}+\mu)[CI_T]\end{aligned} \tag{4.2.7}$$

and

$$\Theta([CI_T],[Cro_T]) = \frac{\rho_{cro}}{\gamma_M + \mu}[O_R]k_{cro}f_R - (\gamma_{cro} + \mu)[Cro_T] \tag{4.2.8}$$

The symbols which appear in the above equations are defined in Tables 4.1 and 4.2.

The equation $\Theta([CI_T],[Cro_T]) = 0$ determines a single curve in $([CI_T],[Cro_T])$ space, whereas the equation $\Phi([CI_T],[Cro_T],\gamma_{cI}) = 0$ determines a family of curves in the same space (one for each value of γ_{cI}, the degradation rate of CI). Since exogenous (exposure to ultra-violet light) and endogenous (starvation) factors influence γ_{cI}, it is included as an argument of the function Φ so that the behaviour of the system under different degradation rates can be explored.

4.2.3 Generalization of the model

For the purposes of this chapter, the main modelling concerns relate to the functions f^q_{RM}, f^s_{RM}, and f_R, which use the energies of the molecular binding states to calculate the probabilities of $RNAP$ molecules binding to the promoters P_{RM} and P_R. The formula for calculating these energies is different for Stx phage compared to lambda, owing to structural differences between their switch mechanisms. The formula, generalized from Santillan and Mackey (2004), for calculating the binding energy of each state i is given by:

$$\begin{aligned}
E_i &= \sum_{Y=CI_2,Cro_2} \sum_{\nu=1}^{\nu_L} \Delta G^Y_{O_{L^\nu}} \Gamma^Y_{O_{L^\nu}}(i) \\
&+ \sum_{Y=CI_2,Cro_2} \sum_{\nu=1}^{\nu_R} \Delta G^Y_{O_{R^\nu}} \Gamma^Y_{O_{R^\nu}}(i) \\
&+ \sum_{Y=CI_2,Cro_2} \sum_{\nu=1}^{\nu_L-1} \Delta G^Y_{O_{L^{\nu\nu+1}}} \Gamma^Y_{O_{L^\nu}}(i)\Gamma^Y_{O_{L^{\nu+1}}}(i) \\
&+ \sum_{Y=CI_2,Cro_2} \sum_{\nu=1}^{\nu_R-1} \Delta G^Y_{O_{R^{\nu\nu+1}}} \Gamma^Y_{O_{R^\nu}}(i)\Gamma^Y_{O_{R^{\nu+1}}}(i) \\
&+ \sum_{X=R,L} \Delta G^{Cro_2}_{O_{X^{123}}} \Gamma^{Cro_2}_{O_{X^1}}(i)\Gamma^{Cro_2}_{O_{X^2}}(i)\Gamma^{Cro_2}_{O_{X^3}}(i) \\
&+ \sum_{\nu=1}^{min(\nu_L,\nu_R)} \Delta G_{RL} \Gamma^{CI_2}_{O_{R^\nu}}(i)\Gamma^{CI_2}_{O_{L^\nu}}(i) \\
&+ \sum_{X=RM,R,L} \Delta G^{RNAP}_{P_X} \Gamma^{RNAP}_{P_X}(i)
\end{aligned} \tag{4.2.9}$$

where

$$\Gamma_X^Y(i) = \begin{cases} 1 & \text{if the binding site or promoter } X \text{ exists, and molecule } Y \\ & \text{is bound to } X \text{ (in state } i) \\ 0 & \text{otherwise} \end{cases}$$

In the above formula, ν_L and ν_R denote the number of binding sites at the left and right operators respectively. The terms $\Delta G_{P_X}^{RNAP}$ $(X = RM, R, L)$ represent the binding energy of a $RNAP$ molecule bound to the promoter P_X. The terms $\Delta G_{O_{X^\nu}}^{Y}$ $(X = R, L)$ represent the binding energy of a molecule of Y to the operator site O_{X^ν}. The terms $\Delta G_{O_{X^{\nu\nu+1}}}^{Y}$ represent the interaction energy between two Y molecules bound to the operator sites O_{X^ν} and $O_{X^{\nu\nu+1}}$. The terms $\Delta G_{O_{X123}}^{Cro_2}$ represent the interaction energy between 3 Cro_2 molecules bound to O_X1, O_X2, and O_X3. This notation is made more explicit in Table 4.3, which contains a list of the binding energies used in the model. All of these energies have been determined experimentally for phage lambda (Santillan and Mackey, 2004). The interaction energy between a CI_2 bound to $O_R\nu$ and a CI_2 bound to $O_L\nu$ (denoted by ΔG_{RL}) is also included in the model, although this quantity has not yet been measured experimentally and must therefore be estimated.

4.3 Phage scenarios

There are known differences between the switches of certain Stx phages and phage lambda. The analysis in this chapter compares the stability of phage lambda lysogens with four different Stx phage "scenarios" (Stx 1, Stx 2, Stx 3, and Stx 4) as shown in Table 4.4. The scenarios are obtained by varying the number of operator sites in the left and right operators, and by varying the value of the parameter $\Delta G_{O_R2}^{CI_2}$.

For phage lambda we have $\nu_R = 3$ and $\nu_L = 3$, while for the Stx phage 933W we have $\nu_R = 3$ but $\nu_L = 2$ (Tyler et al., 2004). So for Stx 1, ν_L is set equal to 2, so that the effect on lysogen stability of removing O_L3 can be examined.

It has been speculated that O_R3 does not function as an active binding site in some Stx phages (H. Allison, personal communication). For Stx 2 ν_L, ν_R are set equal to 3 and 2 respectively to see the effect of removing O_R3 in isolation, and then for Stx 3 both operator sites are absent (i.e. $\nu_L = 2$, $\nu_R = 2$) to see the combined effect of removing both operator sites.

The 933W phage is also known to have different relative binding affinities at the O_L and O_R operators, compared to phage lambda (Koudelka et al., 2004). In particular in most lambdoid phages, cooperative binding between repressors at O_R1 and O_R2 enables repressor molecules to bind to these two sites at almost identical concentrations. However, in 933W a 3- to 4-fold higher concentration is needed for repressor to bind to O_R2 compared to O_R1 (Koudelka et al., 2004). Thus Stx 4 has

been subdivided into 4 scenarios ((i), (ii), (iii), (iv)). In Stx 4(i), the value of $\Delta G^{CI_2}_{O_R2}$ is set equal to the value for phage lambda (i.e. -10.5 kcal /M), while in Stx (ii), (iii), and (iv) the absolute value of this parameter is progressively lowered, to reflect the weaker binding affinity in 933W. In order to model the known structure of 933W as closely as possible, the O_L3 site is removed from the model for Stx 4.

For each scenario, Equation (3) is used (with the appropriate values of ν_L and ν_R) to calculate the binding energies of each possible molecular configuration. In the absence of experimentally determined parameter values for Stx phage, the parameter values used are those given in Santillan and Mackey (2004) for phage lambda, except where otherwise indicated.

4.4 Results

4.4.1 Stx Phage scenarios 1, 2, and 3

Figure 4.2 shows the curves $\Theta = 0$ and $\Phi = 0$ for both lambda and Stx 1. Both phages have a steady state corresponding to lysogeny (shown in C and F), but notice that the concentration of CI_T at the lysogenic equilibrium is greater in Stx1 than in lambda. Figure 4.2E reveals that the removal of O_L3 in Stx 1 has introduced two additional steady-states, one of which is stable and corresponds to lysis. However, the overall effect of the absence of O_L3 on the stability of the lysogenic equilibrium is small. This is not surprising because although CI_2 molecules bound at O_L3 and O_R3 interact cooperatively (with binding affinity ΔG_{RL}) and thus increase the strength with which they are bound to their respective binding sites, it is usually the case that in a lambda lysogen the O_R3 site is unbound (Ptashne, 2004), in which case this cooperative interaction is not a factor in lysogen stability.

With $\gamma_{cI} = 0$, the phages lambda, Stx 2, and Stx 3 are all lysogenically monostable, but for other values of γ_{cI} these phages may exhibit different properties. Figure 4.3 shows the curves $\Theta = 0$ and $\Phi = 0$ for lambda, Stx 2, and Stx 3 when γ_{cI} is set to 0.061 min^{-1}; Stx 2 is monostable with a single lysogenic equilibrium (B and E), while lambda is clearly bistable. This indicates that the lack of an O_R3 binding site in Stx 2 enhances the stability of its lysogens. Stx 3 is bistable for this value of γ_{cI}, but only just, and comparison of Figures B and C shows that the presence or absence of the O_L3 site has only a minor impact on the stability properties of the system.

The finding that the absence of O_R3 in Stx 2 greatly increases lysogen stability is not surprising, because in phage lambda a CI_2 molecule can bind to O_R3 in order to repress the *cI* gene and prevent the repressor concentration from becoming too high. A large excess of CI_2 molecules would reduce the sensitivity of the lysogen to changes in endogenous and exogenous environmental factors, since a high γ_{cI} degradation rate

would then be needed in order to flip the switch from lysogenic to lytic growth. If O_R3 is missing, then no matter how high the concentration of CI_2 becomes, CI production will not be switched off and so the switch sensitivity to environmental factors will be reduced.

4.4.2 Stx Phage scenario 4

A more detailed analysis is presented for Stx 4, which is designed to represent the structure (lack of a third O_L binding site) and the binding affinities (reatively weak binding between repressor and O_R2) of 933W. We begin looking at the stability structure of the system by examining the solutions to the equilibrium equations. Numerical measures of the stability of the lysogenic equilibria are then presented for different values of γ_{cI}, and compare the results for Stx 4 and lambda.

Figure 4.4 shows the solutions of the equilibrium equations (with $\gamma_{cI} = 0$) for lambda, Stx 4(i), and Stx 4(iii) (cf Table 4.4). The graphs in A and B show that there is very little difference between the solutions for lambda and Stx 4(i), although Stx 4(i) is actually bistable while lambda is lysogenically monostable. On the other hand, Stx 4(iii) is clearly bistable. The three graphs indicate that while the absence of the O_L3 site in Stx 4(i) does not make much difference, the weaker binding affinity between repressor and O_R2 in Stx 4(iii) has a significant impact on the stability structure of the system.

Figure 4.5 shows projections in $([CI_T], [Cro_T])$ space for lambda and Stx 4(iii), with γ_{cI}=0.20 min^{-1}, for different initial protein concentrations. These projections are obtained by numerically solving the delay differential equations comprising the model. The graphs illustrate that while lambda is bistable at this value of γ_{cI}, Stx 4(iii) is lytically monostable. So it is clear that a lower value of γ_{cI} is needed to eliminate the lysogenic equilibrium in Stx 4(iii) than in lambda. This further illustrates the lower lysogen stability of Stx 4(iii) compared to lambda.

The way in which the values of $\Delta G^{CI_2}_{O_R2}$ and γ_{cI} determine the stability structure of Stx 4 are illustrated in the bifurcation diagram in Figure 4.6. For the range of $\Delta G^{CI_2}_{O_R2}$ values considered, there is no region of lysogenic monostability at all, and as the absolute value of this parameter decreases the minimum value of γ_{cI} required to eliminate the lysogenic equilibrium decreases, implying that lysogen stability also decreases.

So far only the presence or absence of lytic and lysogenic equilibria has been considered. The stability of the lysogenic equilibria were examined by determining the leading eigenvalues, and also by numerical determination of the concentration of Cro and the likelihood of repression of the promoter P_R. Use of these three methods lent robustness to the conclusions drawn from the results. The first of these is a

standard mathematical method for stability analysis, and the second and third allow biological interpretation of the dynamics of the system. The quantity P_R-repression is the probability, given the concentrations of CI_T and Cro_T, that transcription of the *cro* gene is blocked; a lower value of P_R-repression means that induction of the lytic cycle is more likely to occur. The three methods are illustrated in Figure 4.7.

The graphs in Figure 4.7 show that the three methods of measuring lysogen stability all indicate that in general lysogen stability decreases as γ_{cI} increases. It is also clear that the lysogens of Stx 4(iv), which has the lowest absolute value of $\Delta G^{CI_2}_{O_R2}$, are generally the least stable for a given value of γ_{cI}. Lysogen stability increases as $\Delta G^{CI_2}_{O_R2}$ is increased, and there is almost no difference between the stability of Stx 4(i) and lambda lysogens (which have the same value of $\Delta G^{CI_2}_{O_R2}$, i.e. -10.5 kcal / M).

However, the eigenvalue graph in Figure 4.7B reveals an interesting prediction of the model, namely that the stability of Stx 4 and lambda lysogens as measured by the leading eigenvalue initially increases as γ_{cI} is increased from zero up to the value of γ_{cro} (0.016 min^{-1}). The eigenvalue then remains roughly constant (at a value of around $-(\mu + \gamma_{cro})$, i.e. -0.036) as γ_{cI} increases further, until eventually the leading eigenvalue begins to approach zero. The initial increase in stability may enable the phage to bide its time before responding to worsening environmental conditions. A small increase in γ_{cI} may mean that conditions for survival of bacteria are poor, and therefore lysis of a host cell could endanger the bacterial population. Hence an increase in lysogen stability may be prudent for small increases in γ_{cI}, with initiation of the lytic cycle only occurring once it is clear that the host cell is in severe peril.

When the eigenvalues are calculated for the ordinary differential equation model obtained by setting τ_{cI} and τ_{cro} equal to zero (data not shown), it is found that these are almost identical to the delay model eigenvalues, both for lambda and the four Stx scenarios. This indicates that these delays do not significantly affect lysogen stability; it also allows us to discuss the above behaviour of the leading eigenvalue using the model without delay.

For this model, the diagonal elements of the Jacobian are: $-(\gamma_M + \mu) = -0.14$, $-(\gamma_M + \mu) = -0.14$, $-(\gamma_{cI} + \mu) = -0.02 + \gamma_{cI}$, and $-(\gamma_{cro} + \mu) = -0.036$. Many of the non-diagonal elements are exactly zero; moreover, the other elements are also often sufficiently small that it is possible to regard the eigenvalues as perturbations of the above diagonal elements. Thus for $\gamma_{cI} = 0$, the dominant eigenvalue is a perturbation of $-\mu$: as γ_{cI} increases, the eigenvalue close to $-(\gamma_{cI} + \mu)$ remains dominant until it becomes more negative than $-(\gamma_{cro} + \mu)$ which then dominates. Subsequently non-diagonal elements of the Jacobian approach this element in size and the dominant eigenvalue approaches zero. This final procedure begins consistently earlier as we move through the scenarios from lambda/Stx4(i) to Stx4(iv).

4.5 Discussion

The Stx phages 933W and H19B have been described as having 'hair-trigger' switches, because of their greater propensity for lysogen induction compared to phage lambda. It has been speculated that one of the reasons for this in 933W is the lower binding energy between O_R2 and repressor, since this results in tighter regulation of the repressor gene (Koudelka et al., 2004), i.e. lower levels of repressor concentration in Stx lysogens. The results presented in this chapter support this view, and indicate that a lower binding affinity between repressor molecules and the O_R2 binding site will result in a reduction of lysogen stability.

The relatively rapid rise in the observed prevalence of Stx genes since their initial discovery in 1982 could be due in part to the hair-trigger nature of the molecular switch and the relative instability of Stx lysogens. Thus, the lysogenic state in which the phages are benignly replicated in conjunction with the rest of the bacterial genome is less abundant and the switch to lysis more frequent, resulting in propagation and dissemination of Stx phages amongst host populations. Rounds of integration into bacterial genomes and subsequent induction to the lytic cycle would dramatically increase the opportunities for genetic recombination, including the acquisition and spread of genes that promote the ability of the bacterial host to colonise the intestine (Dziva et al. 2004). Furthermore, the switch is also involved in immunity to multiple phage infection, and it may be that the hair-trigger switch also promotes multiple infections (Allison et al., 2003) providing the opportunity for genetic recombination within single bacterial cells, which would contribute further to the evolution of the heterogeneity that has been documented in Stx phages.

While it is known that the strength of the binding affinity between O_R2 and repressor is relatively low in 933W, the numerical values of the binding affinities between binding sites and regulatory proteins have not been experimentally measured for any Stx phage. Obtaining these values would enable a more accurate comparison of lambda and Stx lysogen stability. Knowledge of the Stx binding affinities would also help to establish whether the relative strengths of the binding affinities are the main cause of lower Stx lysogen stability, or whether other factors have a significant impact as well.

Lysogens of phage lambda are immune to superinfection by other lambda phages, and a single lysogen encodes only one prophage. However, lysogens of the Stx phage $\Phi 24_B$ are not immune to superinfection by this phage, and the existence of multiple lysogens (i.e. lysogens whose genomes encode more than one prophage) of this phage has been demonstrated; it is speculated that the presence of multiple *stx* genes may lead to greater toxin production and virulence (Fogg et al, 2007). Phage $\Phi 24_B$ encodes a gene which is similar to the anti-repressor gene of the phage P22; if the

corresponding gene product is indeed a functional anti-repressor in $\Phi 24_B$ lysogens, then it is likely to play a role in enabling superinfection of lysogens (Fogg et al, 2007). The presence of an anti-repressor protein may also reduce the stability of single and multiple lysogens by inactivating molecules of the CI repressor and so raising the probability of *cro* being expressed. However, the mechanism by which this protein operates is not yet known. The extent to which other Stx phages are immune to superinfection, and the implications of superinfection immunity for Stx lysogen stability and toxin release, are important areas for future research.

While there are many instances amongst bacterial pathogens in which disease-causing traits have originated from bacteriophage infection (for example *Vibrio cholerae* (Waldor et al., 1996) and *Neisseria meningitidis* (Bille et al., 2005), and see Allison (2007) for a review), shigatoxigenic *E. coli* are the only pathogens in which virulence has been demonstrated to be associated with the phage induction cycle. There are nevertheless many pathogenicity phenomena which are unexplained, and given the widespread distribution of lysogenic phages amongst bacterial pathogens, it seems likely that concomitant switching on of the phage lytic cycle and the expression of genes involved in promotion of disease is not restricted to the well-studied shigatoxigenic *E. coli* strains.

In this chapter it has been shown how the Santillan and Mackey (2004) phage lambda model can be extended to deal with different phage characteristics. The approach used here may thus provide the basis for future modelling of temperate phages, as more is discovered about the characteristics of different phage strains - such as the ability to form stable complexes as in phage lambda, and the magnitude of the binding energies involved in such complexes.

Symbol	Description
CI, Cro	Regulatory proteins
cI, cro	The genes which code for CI and Cro respectively
M_{cI}, M_{cro}	mRNA transcripts of cI and cro respectively
P_{RM}	The promoter for cI
P_R	The promoter for cro
O_R	The right operator
O_R1, O_R2, O_R3	The binding sites at the right operator
O_L	The left operator
O_L1, O_L2, O_L3	The binding sites at the left operator
f^s_{RM}	Probability for a RNAP molecule to be bound to P_{RM} without a CI_2 molecule bound to O_R2
f^q_{RM}	Probability for a RNAP molecule to be bound to P_{RM} with a CI_2 molecule bound to O_R2
f_R	Probability for a RNAP molecule to be bound to P_R
$\Theta = 0, \Phi = 0$	Model equilibrium equations

Table 4.1: Symbols used in the model representation of the switch.

Parameter	Description	Estimated value
ρ_{cI}	CI translation initiation rate	0.09 min^{-1}
ρ_{cro}	Cro translation initiation rate	3.2 min^{-1}
γ_M	Common degradation rate of M_{cI} and M_{cro}	0.12 min^{-1}
μ	Bacterial growth rate	2.0×10^{-2} min^{-1}
k_{cI}^{s}	Transcription initiation rate at P_{RM} without a CI_2 molecule bound to O_R2	0.35 min^{-1}
k_{cI}^{q}	Transcription initiation rate at P_{RM} with a CI_2 molecule bound to O_R2	4.29 min^{-1}
k_{cro}	Transcription initiation rate at P_R	2.76 min^{-1}
τ_{cI}	Time delay owing to CI translation	0.24 min
τ_{cro}	Time delay owing to Cro translation	6.6×10^{-2} min

Table 4.2: Description of parameters with estimated values for phage lambda (source: Santillan and Mackey, 2004).

Binding energy	Estimated value		Binding energy	Estimated value
$\Delta G_{O_R1}^{CI_2}$	-12.5 kcal / mol		$\Delta G_{O_L1}^{CI_2}$	-11.5 kcal / mol
$\Delta G_{O_R2}^{CI_2}$	-10.5 kcal / mol		$\Delta G_{O_L2}^{CI_2}$	-9.7 kcal / mol
$\Delta G_{O_R3}^{CI_2}$	-9.5 kcal / mol		$\Delta G_{O_L3}^{CI_2}$	-9.7 kcal / mol
$\Delta G_{O_R12}^{CI_2}$	-2.7 kcal / mol		$\Delta G_{O_L12}^{CI_2}$	-2.7 kcal / mol
$\Delta G_{O_R23}^{CI_2}$	-2.9 kcal / mol		$\Delta G_{O_L23}^{CI_2}$	-2.9 kcal / mol
$\Delta G_{O_R1}^{Cro_2}$	-12.0 kcal / mol		$\Delta G_{O_L1}^{Cro_2}$	-12.0 kcal / mol
$\Delta G_{O_R2}^{Cro_2}$	-10.8 kcal / mol		$\Delta G_{O_L2}^{Cro_2}$	-10.8 kcal / mol
$\Delta G_{O_R3}^{Cro_2}$	-13.4 kcal / mol		$\Delta G_{O_L3}^{Cro_2}$	-13.4 kcal / mol
$\Delta G_{O_R12}^{Cro_2}$	-1.0 kcal / mol		$\Delta G_{O_L12}^{Cro_2}$	-1.0 kcal / mol
$\Delta G_{O_R23}^{Cro_2}$	-0.6 kcal / mol		$\Delta G_{O_L23}^{Cro_2}$	-0.6 kcal / mol
$\Delta G_{O_R123}^{Cro_2}$	-0.9 kcal / mol		$\Delta G_{O_L123}^{Cro_2}$	-0.9 kcal / mol
$\Delta G_{P_R}^{RNAP}$	-12.5 kcal / mol		P_L^{RNAP}	-11.3 kcal / mol
$\Delta G_{P_{RM}}^{RNAP}$	-11.5 kcal / mol		ΔG_{RL}	-3.1 kcal / mol

Table 4.3: Table of binding energies with estimated values for phage lambda (source: Santillan and Mackey, 2004).

Phage scenario	Number of left operator binding sites, ν_L	Number of right operator binding sites, ν_R	Binding energy of CI_2 to O_R2, $\Delta G^{CI_2}_{O_R2}$ (kcal / Mol)	Total number of molecular binding states
Lambda	3	3	-10.5	1200
Stx 1	2	3	-10.5	400
Stx 2	3	2	-10.5	600
Stx 3	2	2	-10.5	200
Stx 4	2	3	(i) -10.5 (ii) -10 (iii) -9 (iv) -8	400

Table 4.4: The lambda and Stx phage scenarios. Stx phages differ from lambda either in the numbers of binding sites in the left and right operator regions (O_L and O_R), or in the strength of the binding energy between CI_2 molecules and the second binding site in O_R, or both. Note that Stx 1 and Stx 4(i) are actually identical, but are treated as separate in order to make the analysis in the text clearer.

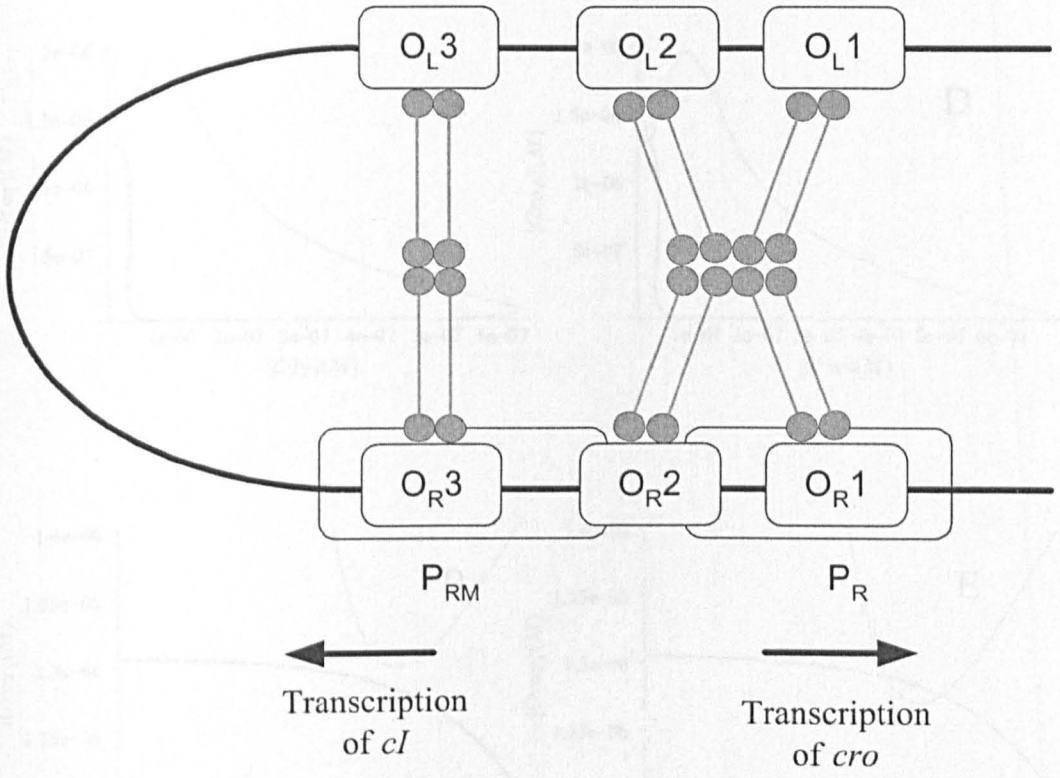

Figure 4.1: The region of lambda DNA which comprises the molecular switch between lysis and lysogeny. It includes the left and right operators, which are regions of DNA which can regulate gene transcription. There are three binding sites at the right operator (O_R1, O_R2, and O_R3) and another three binding sites at the left operator (O_L1, O_L2, and O_L3). The promoters for the genes *cI* and *cro* are labelled P_{RM} and P_R respectively. Repressor molecules are shown bound at all six operator sites. The diagram shows how adjacent repressor molecules interact cooperatively, so as to increase the stability of the molecular configuration. In the configuration shown, transcription of both *cI* and *cro* is blocked. (After Ptashne, 2004).

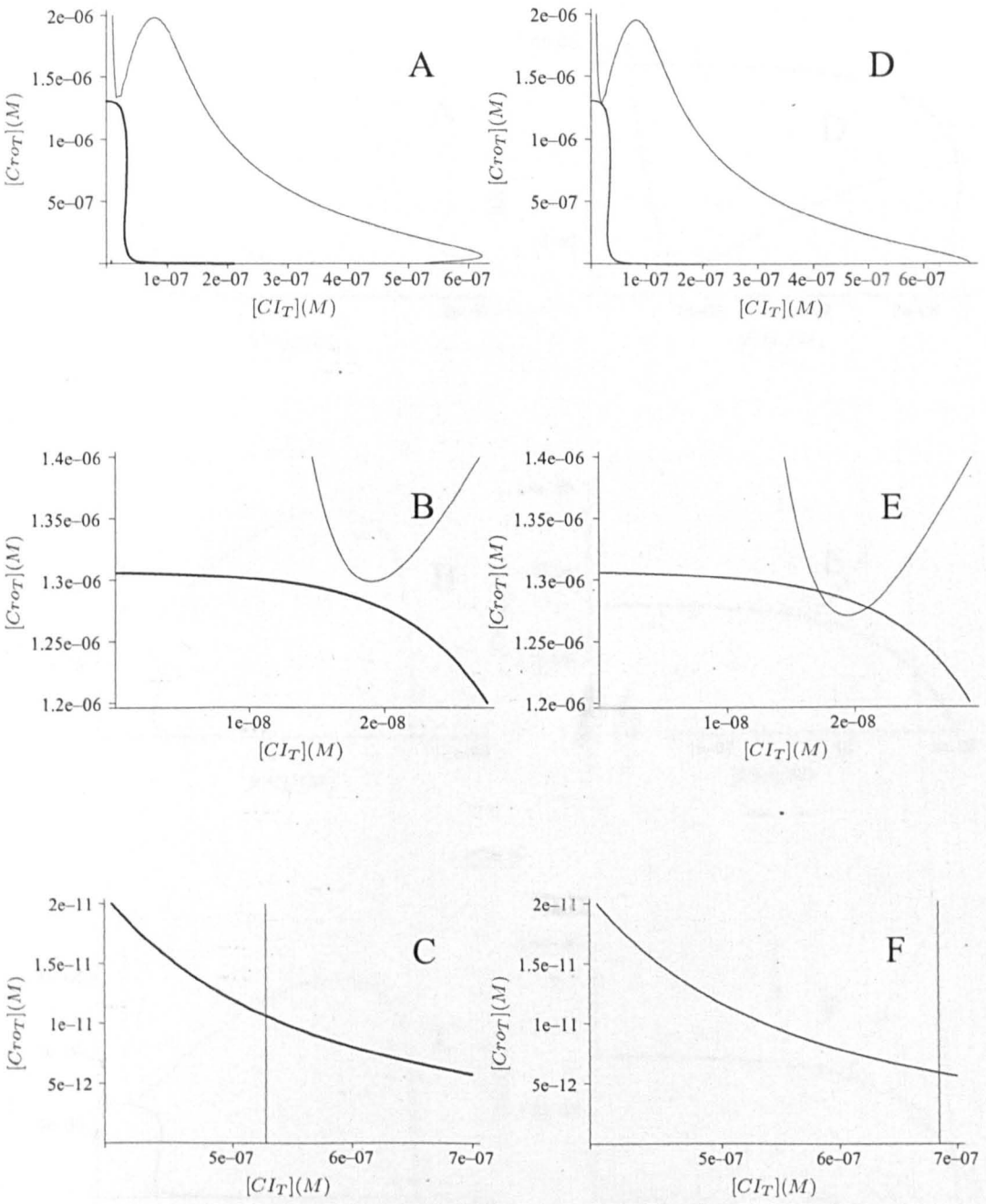

Figure 4.2: Plots of the equilibrium equations $\Theta = 0$ (thick black line) and $\Phi = 0$ (with γ_{cI}=0 min^{-1}) for lambda (A, B, and C) and Stx 1 (D, E, and F). The graphs in B, C, E, and F show close ups of the regions where the curves intersect. These points of intersection correspond to the steady states of the models.

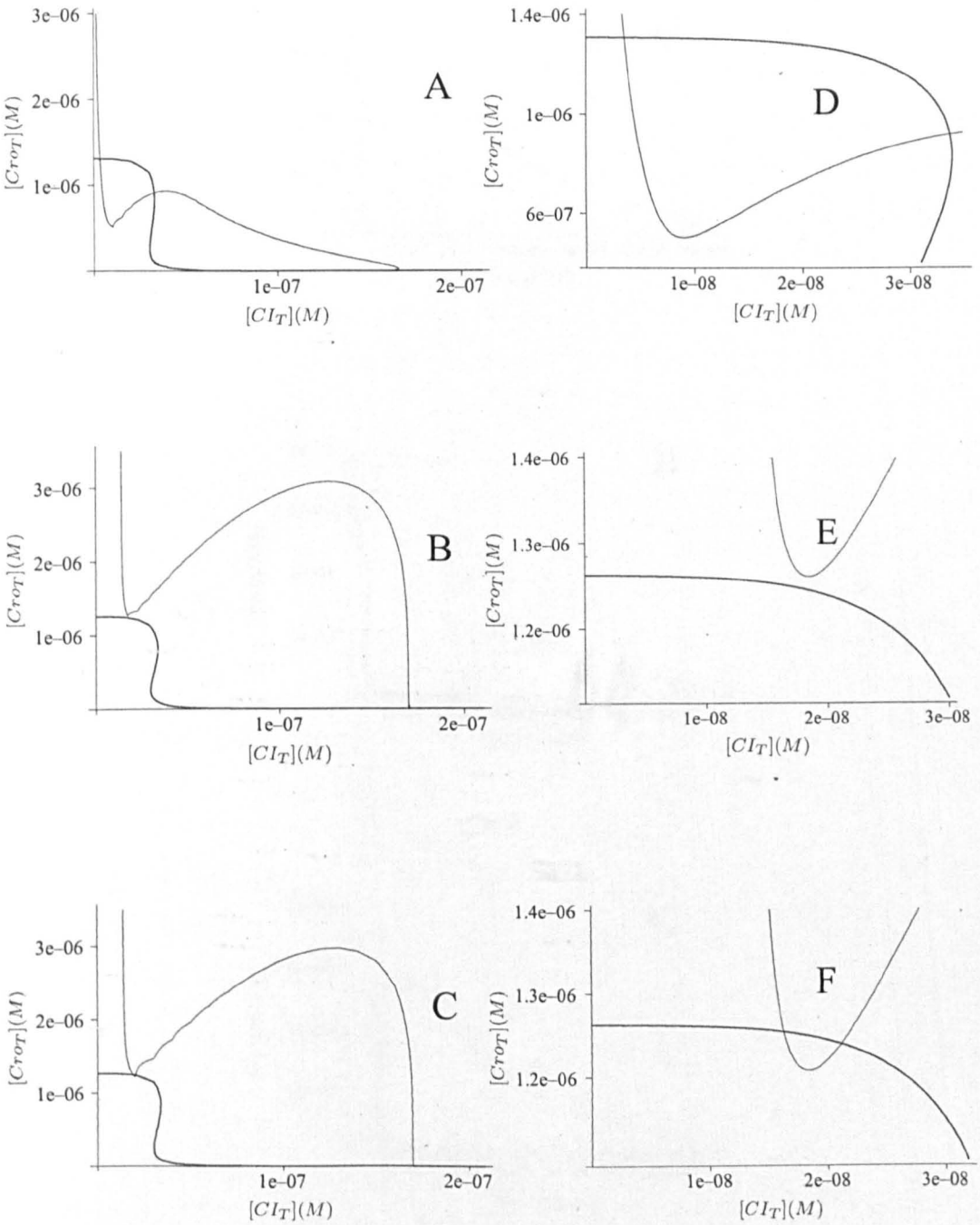

Figure 4.3: Plots of the equilibrium equations $\Theta = 0$ (thick black line) and $\Phi = 0$ (with γ_{cI}=0.061 min^{-1}) for lambda (A), Stx 2 (B), and Stx 3 (C). The graphs in D, E, and F show close-ups of the regions where the lytic and unstable equilibria first appear via a saddle node bifurcation

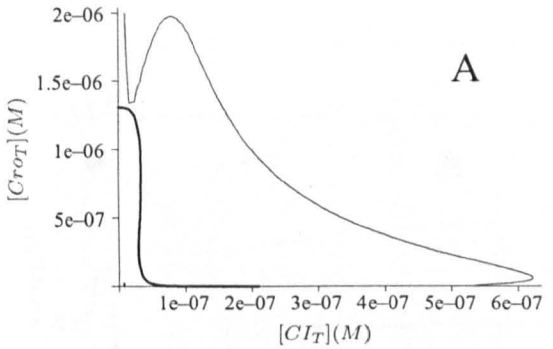

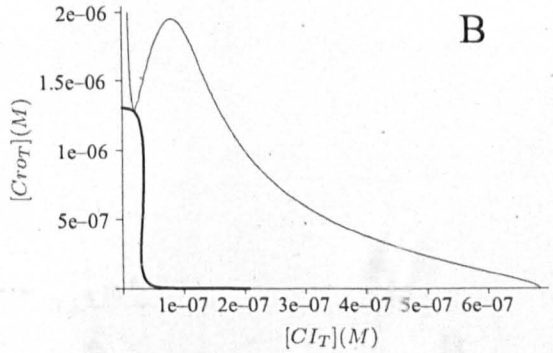

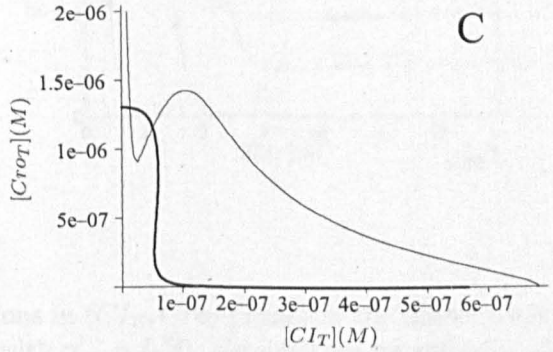

Figure 4.4: Plots of the equilibrium equations $\Theta = 0$ (thick black line) and $\Phi = 0$ (with γ_{cI}=0 min^{-1}) for lambda (A), Stx 4(i) (B), and Stx 4(iii) (C).

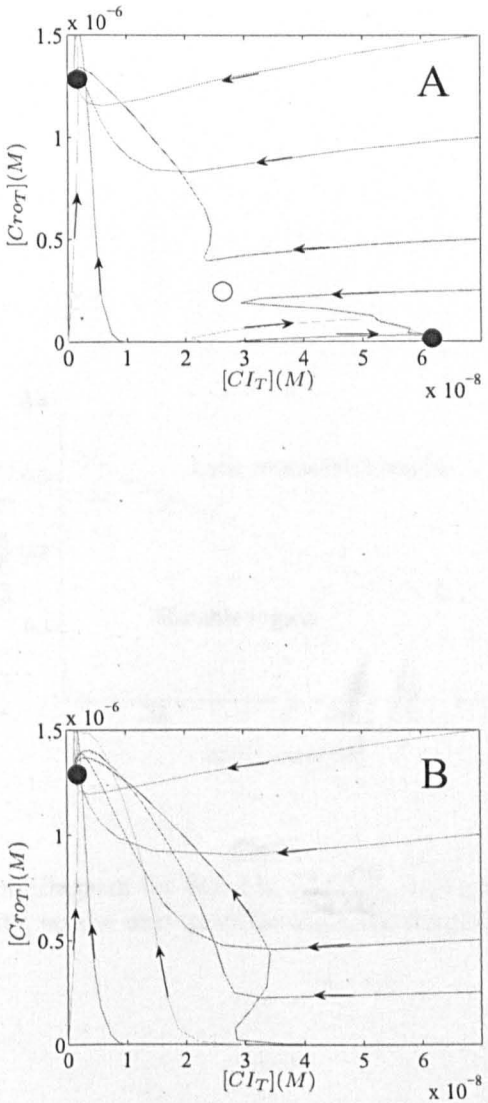

Figure 4.5: Projections in (CI_T, Cro_T) space of the model trajectories for lambda (A) and Stx 4(iii) (B), with $\gamma_{cI} = 0.20$, obtained by numerically solving the model delay differential equations. Filled circles indicate stable equilibria, while the empty circle in A represents an unstable equilibrium.

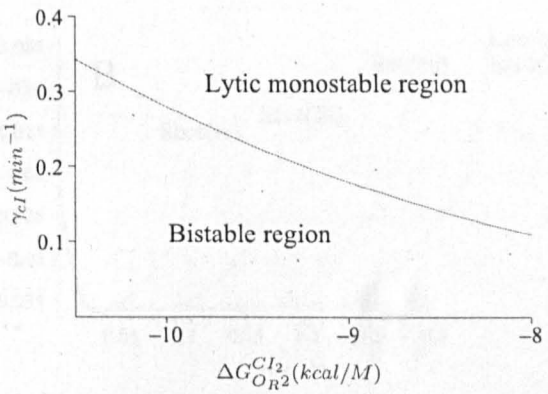

Figure 4.6: Bifurcation diagram for Stx 4 in $(\Delta G_{O_R2}^{CI_2}, \gamma_{cI})$ space. There is no region of lysogenic monostability, so the only possible stability structures are bistability or lytic monostability.

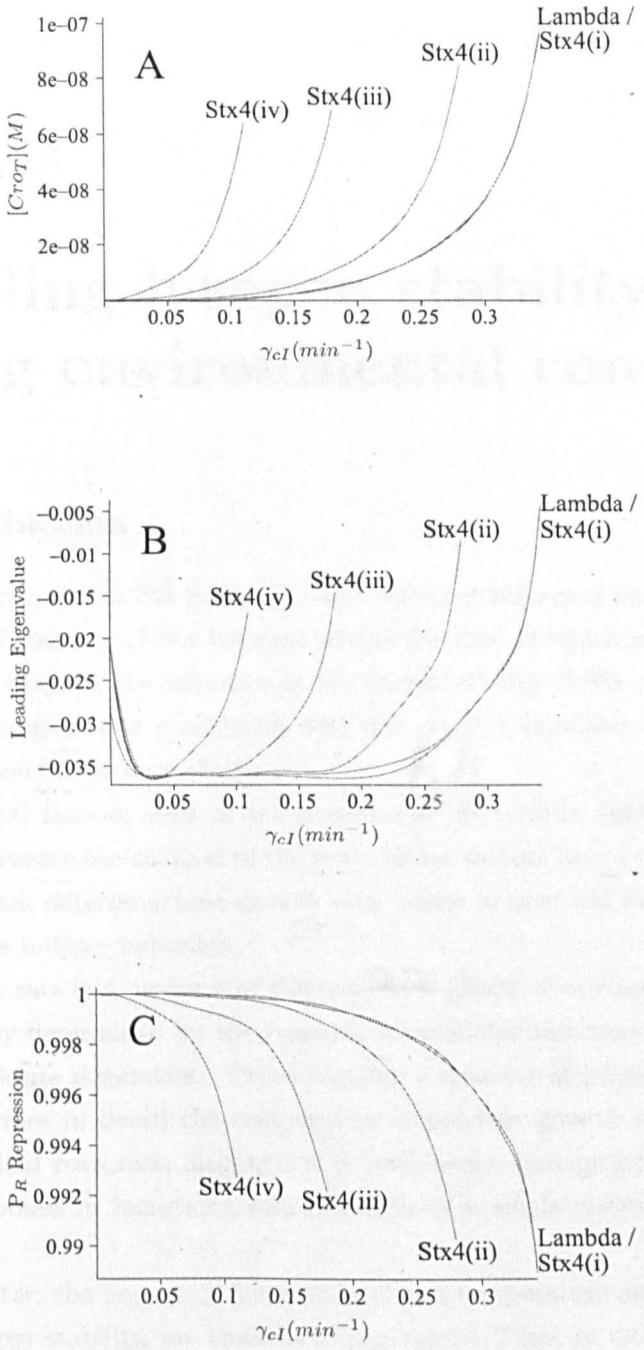

Figure 4.7: Graphs showing three numerical measures of the stability of lysogenic equilibria: (A) Concentration of Cro_T; (B) Leading eigenvalue; and (C) P_R repression.

Chapter 5

Modelling lysogen stability under varying environmental conditions

5.1 Introduction

During induction of an Stx lysogen, toxins will be synthesized and released. Therefore, the level of stability of Stx lysogens affects the rate at which toxins are released. In the previous chapter, the influence of the characteristics of Stx phages on the stability of their lysogens was considered, and this chapter examines the effect of some environmental conditions on stability.

Environmental factors, such as the presence of ultra-violet light (Ptashne, 2004), may directly influence the survival of the host. Other factors have an impact on molecular processes that determine host growth rate, which in turn will influence the rate at which prophages initiate induction.

Host growth rate is a measure of the combined effects of environmental influences and is inherently determined by the response to available resources (nutrients) which may be temperature dependent. There remains a sparcity of published experimental data that describes in detail the temperature dependent growth responses of phage hosts to individual resources; although it is well known that growth rate exhibits an asymptotic response to increasing concentration of a single resource (Monod, 1949; Powell, 1967).

In this chapter, the impact of nutrient level and temperature on host growth rate, and hence lysogen stability, are considered seperately. Thus, in modelling the impact of environmental conditions on lysogen stability, the approach taken is to consider (a) variable resource concentration (nutrient) at constant temperature, and (b) variable temperature at a constant resouce level.

The Santillan and Mackey (2004) model (Chapter 4) is used to explore the effects of temperature and resources on lysogen stability. This model includes a term which

represents the concentration of operator sites, O_R, and this depends on the number of genome equivalents present in the cell. The average number of genome equivalents per cell, $\bar{G}$, is dependent on the nutrient level present in the environment (Bremer and Dennis, 1996). Note that $\bar{G}$ is essentially unaffected by changes in temperature (Bremer and Dennis, 1996), and the reasons for this will be addressed later on. Changes in temperature and nutrient level also affect the calculation of the probabilities of different binding configurations at the molecular switch, as described in Section 5.1.1.

In Section 5.2 we present a variation of the proof of a formula due to Powell (1956) which can be used to determine the age distribution of bacterial cells in batch culture. This formula was used by Cooper and Helmstetter (1968) to obtain an expression for the average number of genome equivalents per cell $\bar{G}$ for different host growth rates, and hence different nutrient levels; few details were provided by these authors, and so we provide a summary of the important steps of the derivation.

The stability of lysogens containing multiple prophages is also considered in this chapter. It has been shown that the Stx phage $\Phi 24_B$ is able to form multiple lysogens with its host (Allison et al, 2003); the presence of multiple Stx lysogens may increase the rate at which toxins are released into the environment, leading to increased virulence (Fogg et al, 2007).

5.1.1 The modelling approach

One of the most widely studied strains of *E. coli* is strain B (Schneider et al, 2002). The strain known as *E. coli* B/r is a mutant of *E. coli* B which is resistant to ultra-violet light (Adler and Haskins, 1960). Bremer and Dennis (1996) presented data on the amounts of DNA, RNA and protein molecules present in the *E. coli* strain B/r at different nutrient levels and also at different temperatures. These data can be incorporated into the Santillan and Mackey (2004) model of lysogen stability, to examine the effect that changes in nutrient levels and temperature can have on lysogen stability, as described below. The model in question is a delay differential equation (DDE) model. However, since it was found in Chapter 4 that the ordinary differential equation (ODE) version of the model (obtained by replacing the delayed variables with their non-delayed counterparts) produced almost identical eigenvalues to the DDE model at every equilibrium considered, here we restrict our attention to the ODE version in order to simplify the process of calculating eigenvalues. The ODE model is given below:

$$\frac{d[M_{cI}]}{dt} = k^q_{cI}[O_R]f^q_{RM}([CI_2],[Cro_2]) + k^s_{cI}[O_R]f^s_{RM}([CI_2],[Cro_2]) - (\gamma_M + \mu)[M_{cI}] \quad (5.1.1)$$

$$\frac{d[M_{cro}]}{dt} = k_{cro}[O_R]f_R([CI_2],[Cro_2]) - (\gamma_M + \mu)[M_{cro}] \quad (5.1.2)$$

$$\frac{d[CI_T]}{dt} = \rho_{cI}[M_{cI}] - (\gamma_{cI} + \mu)[CI_T] \quad (5.1.3)$$

$$\frac{d[Cro_T]}{dt} = \rho_{cro}[M_{cro}] - (\gamma_{cro} + \mu)[Cro_T] \quad (5.1.4)$$

An explanation of the terms in the above model can be found in Section 4.2.1.

The adjustments which must be made to the model depend on whether changes in nutrient level or temperature are being modelled. The nutrient level data is presented in Table 5.1. The numbers 1 (lowest) to 5 (highest) are used as proxies to indicate nutrient level, since the actual levels are not included in the published data. The function shown in Figure 5.1 (a) is used as a hypothetical relationship between nutrient level and *E. coli* growth rate. Note that the growth rate (μ), the average number of genome equivalents per cell ($\bar{G}$), and the amount of active RNAP in each cell all increase as the nutrient level increases (with the temperature held constant at 37 °C).

Thus, for variations in the nutrient level, the model parameters which are affected are the quantities μ and $[O_R]$ (which can be obtained from $\bar{G}$, since the number of operator regions is assumed to be equal to number of genome equivalents per cell), and also the functions f^q_{RM}, f^s_{RM}, and f_R (see Section 4.2.1 for a description of these functions). The three functions are affected because of the change in $[RNAP]$.

The temperature data is given in Table 5.2. This data was obtained for *E. coli* in a "glucose minimal medium" (Bremer and Dennis, 1996); for modelling purposes it is assumed that this corresponds to the lowest nutrient level (level 1) in Table 5.1. As the temperature is increased from 20 °C to 40 °C (with the nutrient level held constant at a non-limiting level), the growth rate increases. However, the replication patterns are identical at different temperatures (Bremer and Dennis, 1996), i.e. the ratios C/τ and D/τ remain constant as the temperature changes. Thus the average number of genome equivalents per cell $\bar{G}$ (as given by (5.2.9)), and hence the value of $[O_R]$, do not change with temperature. This contrasts with the nutrient level data, where the replication pattern is altered when the nutrient level increases.

So for variations in temperature, the terms affected are μ and the functions f^q_{RM}, f^s_{RM}, and f_R. The three functions are affected because of the change in absolute temperature, T. The values of the parameters $\bar{G}$, and $RNAP$ are assumed to be fixed at the values given in Table 5.1 for nutrient level 1.

Other model parameters which are not mentioned above are assumed to be constant

Parameter	Symbol	Units	1	2	3	4	5
Growth rate	μ	min^{-1}	0.007	0.012	0.017	0.023	0.029
Doubling time	τ	min	100	60	40	30	24
C period	C	min	67	50	45	43	42
D period	D	min	30	27	25	24	23
DNA/cell	$\bar{G}$	genome equiv./cell	1.6	1.8	2.3	3.0	3.8
Active RNAP/cell	$RNAP$	RNAP/cell	205	503	992	1929	3298

Table 5.1: Parameter values for *E. coli* B/r at different nutrient levels. There are 5 nutrient levels, labelled 1 (lowest) to 5 (highest). The values of $\bar{G}$ are obtained using equation (5.2.9) in the text. Source: Bremer and Dennis (1996).

Parameter	Symbol	Units	20 °C	25 °C	30 °C	35 °C	40 °C
Growth rate	μ	min^{-1}	0.00475	0.00754	0.0106	0.0137	0.0157

Table 5.2: Growth rates of *E. coli* B/r at different temperatures. Source: Bremer and Dennis (1996).

with respect to nutrient level and temperature. Parameters which do not feature in Tables 5.1 and 5.2 are assumed to be fixed at the values given by Santillan and Mackey (2004). In particular, it is assumed that the rates of transcription and translation are unaffected by changes in nutrient level and temperature. In reality it is likely that there would be an impact on these rates, and hence on the time delays due to transcription and translation. However, in the previous chapter it was found that the location and stability of the equilibria were not sensitive to changes in these time delays (by comparing the eigenvalues from the DDE and ODE versions of the model, which were found to be almost identical), and so in this sense the assumption is justified.

5.2 Derivation of the average number of genome equivalents per cell

The term "batch culture" is used to describe a bacterial population growing in a closed system. There is an initial supply of nutrients which is not replenished, and so the population will reach its maximum level when a nutrient which is needed for growth is exhausted, i.e. becomes growth-limiting. Powell (1956) showed that the spread of ages within a population of bacteria in batch culture is determined by the frequency function ϕ, given by:

$$\begin{aligned}\phi(a) &= 2\nu e^{-\nu a} \qquad (a < A)\\ &= 0 \qquad\qquad (a > A)\end{aligned}$$

where a represents age, A is the age at which cells divide (a fixed constant), and $\nu = \ln 2/A$. The above function can be derived (in a somewhat novel way) as follows.

Let $N(a,t)$ be the number of cells aged a at time t, and let $N_T(t)$ be the total number of cells at time t. We have

$$N(0,0)da = N_T(0)\phi(0)da$$

When the cells reach age a $(a < A)$, we have

$$N(a,a)da = N(0,0)da = N_T(0)\phi(0)da$$

and

$$\phi(a) = \frac{N(a,a)}{N_T(a)} = \frac{N_T(0)\phi(0)}{N_T(a)}$$

The bacterial population grows exponentially, i.e. $N_T(t) = N_T(0)e^{\nu t}$, so we can write

$$\phi(a) = \frac{N_T(0)\phi(0)da}{N_T(0)e^{\nu a}da} = \phi(0)e^{-\nu a} \qquad a \leq A \tag{5.2.1}$$

Since $\int_0^\infty \phi(a)da = \int_0^A \phi(a)da = 1$, the above expression implies that

$$\phi(0)\int_0^A e^{-\nu a}da = 1$$

and so

$$\frac{\phi(0)}{\nu}(1 - e^{-\nu A}) = 1 \tag{5.2.2}$$

Note that the population growth rate is equal to $\nu N_T(t)$, and therefore

$$\begin{aligned}\nu N_T(t) &= N(A,t)\\ &= N_T(t)\phi(A)\\ &= N_T(t)\phi(0)e^{-\nu A}\end{aligned}$$

Hence

$$\nu = \phi(0)e^{-\nu A} \tag{5.2.3}$$

From (5.2.2) and (5.2.3), we have

$$\begin{aligned} e^{\nu A}(1 - e^{-\nu A}) &= 1 \\ \Longrightarrow\ e^{\nu A} - 1 &= 1 \\ \Longrightarrow\ e^{\nu A} &= 2 \end{aligned}$$

This states firstly that $\nu = \frac{1}{A}\ln 2$, and secondly that $2\nu = \phi(0)$ (using (5.2.3)). Incorporating both of these relationships into (5.2.1) yields

$$\begin{aligned} \phi(a) &= \nu 2^{1-\frac{a}{A}} \\ &= \frac{1}{A}(\ln 2)2^{1-\frac{a}{A}} \end{aligned}$$

If A=1 then the age distribution function reduces to

$$\phi(a) = (\ln 2)\, 2^{1-a} \qquad (0 \leq a \leq 1) \tag{5.2.4}$$

Note that $\int_0^1 \phi(a)\, da = 1$. The average number of genome equivalents per cell can now be calculated as

$$\bar{G} = \int_0^1 \phi(a) G(a)\, da \tag{5.2.5}$$

where G is a function defined such that $G(a)$ gives the number of genome equivalents in a cell whose age is a. Cooper and Helmstetter (1968) obtained an expression for G by dividing the bacterial division cycle into n intervals, such that within each interval the number of replication points operating is constant, and hence the rate of DNA synthesis is constant. Then the number of genome equivalents at age a is given by:

$$\begin{aligned} G(a) &= F_1 k a + G(0) && 0 \leq a \leq a_1 \\ &= F_2 k a + a_1 k(F_1 - F_2) + G(0) && a_1 \leq a \leq a_2 \\ &= F_3 k a + a_1 k(F_1 - F_2) + a_2 k(F_2 - F_3) + G(0) && a_2 \leq a \leq a_3 \\ &= F_n k a + k \sum_{i=1}^{n-1} a_i k(F_i - F_{i+1}) + G(0) && a_{n-1} \leq a \leq a_n \end{aligned}$$

where a_i is the age of the cell at the end of the i^{th} interval, k is the rate of DNA synthesis per replication point, and F_i is the number of replication points in the i^{th} interval.

First note that putting $a = 1$ in (5.2.6), and replacing $G(1)$ with $2G(0)$, yields

$$G(0) = F_n k + k \sum_{i=1}^{n-1} a_i (F_i - F_{i+1}) \tag{5.2.6}$$

Now, substituting (5.2.4) and (5.2.6) into (5.2.5), we obtain:

$$\begin{aligned} \bar{G} &= 2\ln 2 \left[k \sum_{i=1}^{n} F_i \int_{a_{i-1}}^{a_i} 2^{-a} a \, da \right. \\ &+ k \sum_{j=2}^{n} \sum_{i=1}^{j-1} a_i (F_i - F_{i+1}) \int_{a_{i-1}}^{a_i} 2^{-a} da \\ &+ \left. \int_0^{a_n} 2^{-a} G(0) da \right] \end{aligned} \tag{5.2.7}$$

The integrals in the first line of the above expression may be evaluated using integration by parts. For an integer i, where $1 \leq i \leq n$, we have:

$$\int_{a_{i-1}}^{a_i} 2^{-a} a \, da = \frac{1}{\ln 2} \left(a_{i-1} 2^{-a_{i-1}} - a_i 2^{-a_i} \right) + \frac{1}{(\ln 2)^2} \left(2^{-a_{i-1}} - 2^{-a_i} \right)$$

The integrals in the second line of (5.2.7) are evaluated using simple integration to give:

$$\int_{a_{i-1}}^{a_i} 2^{-a} da = \frac{1}{\ln 2} \left(2^{-a_{i-1}} - 2^{-a_i} \right)$$

Evaluating the integral in the third line of (5.2.7) (with $a_n = 1$), and using (5.2.6), we obtain:

$$\begin{aligned} \int_0^1 2^{-a} G(0) da &= \frac{G(0)}{2\ln 2} \\ &= \frac{F_n k + k \sum_{i=1}^{n-1} a_i (F_i - F_{i+1})}{2\ln 2} \end{aligned}$$

After evaluating the above integrals, we find that all of the terms from the second and third lines of (5.2.7) cancel out. Most, but not all, of the terms from the first line also cancel, and we are left with:

$$\bar{G} = \frac{k}{\ln 2}\left[2F_1 - F_n + \sum_1^{n-1} 2^{(1-a_i)}(F_{i+1} - F_i)\right] \tag{5.2.8}$$

For $n = 3$, it is possible to re-write $\bar{G}$ in terms of C, D and τ (Cooper and Helmstetter, 1968), where τ is the population doubling time, C is the time required to replicate the chromosome, and D is the time period between termination of a round of replication and the following cell division. Let x be the number of cell divisions which occur during a round of replication plus 1. The ages a_1 and a_2 divide the division cycle into 3 intervals, and represent either initiation or termination of a round of replication. If a_1 corresponds to initiation then a_2 corresponds to termination, and vice versa; which of these is the case depends on the particular pattern of replication. The age of a cell at the time of replication intiation is $(\tau - D)/\tau$, and the age of a cell at replication termination is $[x\tau - (C + D)]/\tau$. So, for example, if a_1 occurs at the end of a round of replication then we must have $a_1 = [x\tau - (C + D)]/\tau$. In this case a_2 must occur at the initiation of replication, and therefore $a_2 = (\tau - D)/\tau$. Cooper and Helmstetter considered a number of different replication patterns with n=3; they found by substituting for a_1 and a_2 in (5.2.8), and using the appropriate values of F_1, F_2 and F_3, that the following expression was obtained in each case:

$$\bar{G} = \frac{\tau}{C\ln 2}\left[2^{(C+D)/\tau} - 2^{D/\tau}\right] \tag{5.2.9}$$

The above expression was used by Bremer and Dennis (1996) to calculate the value of $\bar{G}$ in relation to nutrient level.

5.3 Results and Discussion

5.3.1 Varying the nutrient level: phage lambda

At each nutrient level examined, if the value of γ_{cI} is low (i.e. within the range $0 < \gamma_{cI} < 0.1$) then the values of $\partial f_R/\partial[CI_T]$ and $\partial f_R/\partial[Cro_T]$ are very small (at the lysogenic equilibrium). If we assume that they are zero, then the Jacobian at the lysogenic equilibrium has the following form:

$$J = \begin{pmatrix} -\gamma_M - \mu & 0 & [O_R](k^q_{cI}w^* + k^s_{cI}x^*) & [O_R](k^q_{cI}y^* + k^s_{cI}z^*) \\ 0 & -\gamma_M - \mu & 0 & 0 \\ \nu_{cI} & 0 & -\gamma_{cI} - \mu & 0 \\ 0 & \nu_{cro} & 0 & -\gamma_{cro} - \mu \end{pmatrix}$$

where

$$
\begin{aligned}
w^* &= \left.\frac{\partial f^q_{RM}}{\partial [CI_T]}\right|_{[CI_T]=[CI_T]^*,[Cro_T]=[Cro_T]^*} \\
x^* &= \left.\frac{\partial f^s_{RM}}{\partial [CI_T]}\right|_{[CI_T]=[CI_T]^*,[Cro_T]=[Cro_T]^*} \\
y^* &= \left.\frac{\partial f^q_{RM}}{\partial [Cro_T]}\right|_{[CI_T]=[CI_T]^*,[Cro_T]=[Cro_T]^*} \\
z^* &= \left.\frac{\partial f^s_{RM}}{\partial [Cro_T]}\right|_{[CI_T]=[CI_T]^*,[Cro_T]=[Cro_T]^*}
\end{aligned}
$$

The eigenvalues of the above matrix are given by:

$$(-\gamma_M - \mu) \tag{5.3.1}$$

$$(\ \gamma_{cro}\ \ \mu) \tag{5.3.2}$$

$$-\mu - \frac{\gamma_{cI}}{2} - \frac{\gamma_M}{2} \pm \frac{\sqrt{\gamma^2_{cI} - 2\gamma_{cI}\gamma_M + \gamma^2_M + 4[O_R]\nu_{cI}(k^q_{cI}w^* + k^s_{cI}x^*)}}{2} \tag{5.3.3}$$

Note that y^* and z^* do not appear in these expressions. For $\gamma_{cI} = 0$, the leading eigenvalue is given by Equation 5.3.3 (with the square root term added rather than subtracted) for all nutrient levels. At each nutrient level, the value of this eigenvalue depends only on μ and the quantity $[O_R](k^q_{cI}w^* + k^s_{cI}x^*)$ (all the other parameter values are fixed with respect to nutrient level). As the nutrient level increases there is not much variation in the latter quantity, and so there is a steady increase in stability which is mainly due to the increase in μ. The increase in stability is illustrated by the $\gamma_{cI} = 0$ curve in Figure 5.1 (b).

For both $\gamma_{cI} = 0.05$ and $\gamma_{cI} = 0.10$, the leading eigenvalue is given by $(-\gamma_{cro} - \mu)$. So at higher nutrient levels, and hence higher growth rates, there is a greater degree of stability, as shown in Figure 5.1 (b) (note that the leading eigenvalue plots for $\gamma_{cI} = 0.05$ and $\gamma_{cI} = 0.10$ overlap).

For higher values of γ_{cI} (i.e. $\gamma_{cI} > 0.1$) the values of $\partial f_R/\partial CI_T$ and $\partial f_R/\partial Cro_T$ at the lysogenic equilibrium are not negligible. Therefore the eigenvalue expressions derived above, no longer apply. As shown in Figure 5.1 (b), there is an initial decrease in stability as the nutrient level is increased. Once the nutrient level passes increases beyond a certain point (i.e. nutrient level 6, in the case of $\gamma_{cI} = 0.37$), the stability begins to increase slightly. On the basis of numerical experiments, this behaviour can be explained in terms of two factors. An increase in nutrient level and hence growth rate tends to increase lysogen stability, as in the low γ_{cI} cases. On the other hand, as the nutrient level increases the derivatives of the functions f^q_{RM}, f^s_{RM}, and f_R

with respect to CI_T and Cro_T also change. In particular, on the basis of numerical experiments (results not shown), there was an increase in the absolute value of $\frac{\partial f_R}{\partial CI_T}$ as μ increased, and this tends to reduce stability; changes in the values of the other partial derivatives were found to have a much lower impact on stability. Whether there is an increase or decrease in stability when moving from one nutrient level to another is largely determined by which of the two factors dominates. At the higher nutrient levels, the effect of higher growth rate dominates, and so there is an increase in stability.

In order to illustrate the behaviour of the eigenvalues more clearly, Figure 5.2 illustrates all four eigenvalues for phage lambda over the five nutrient levels, for different values of γ_{cI}. Notice that the eigenvalue$(-\gamma_{cro} - \mu)$ is the leading eigenvalue for $0 < \gamma_{cI} < 0.30$.

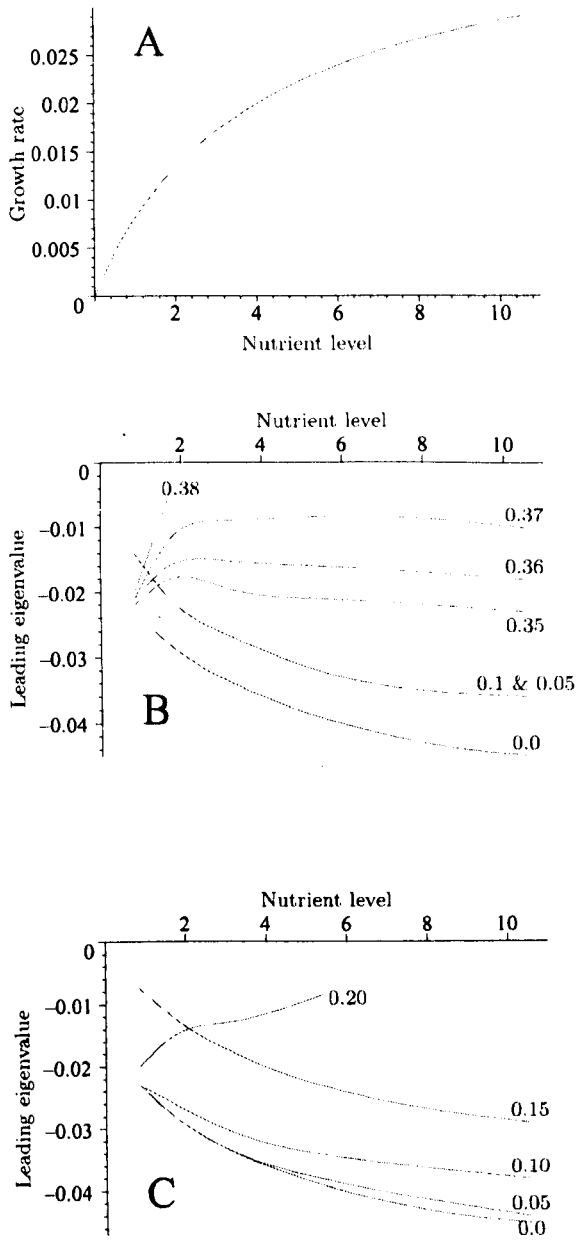

Figure 5.1: Modelling changes in lysogen stability in response to changes in the nutrient level. (a) The example relationship between nutrient level and *E. coli* growth rate which has been adopted for modelling purposes. (b) Leading eigenvalues of the lysogenic equilibrium versus nutrient level (phage lambda). (c) Leading eigenvalues of the lysogenic equilibrium versus nutrient level (Stx3). The curves are labelled with the appropriate value of γ_{cI}.

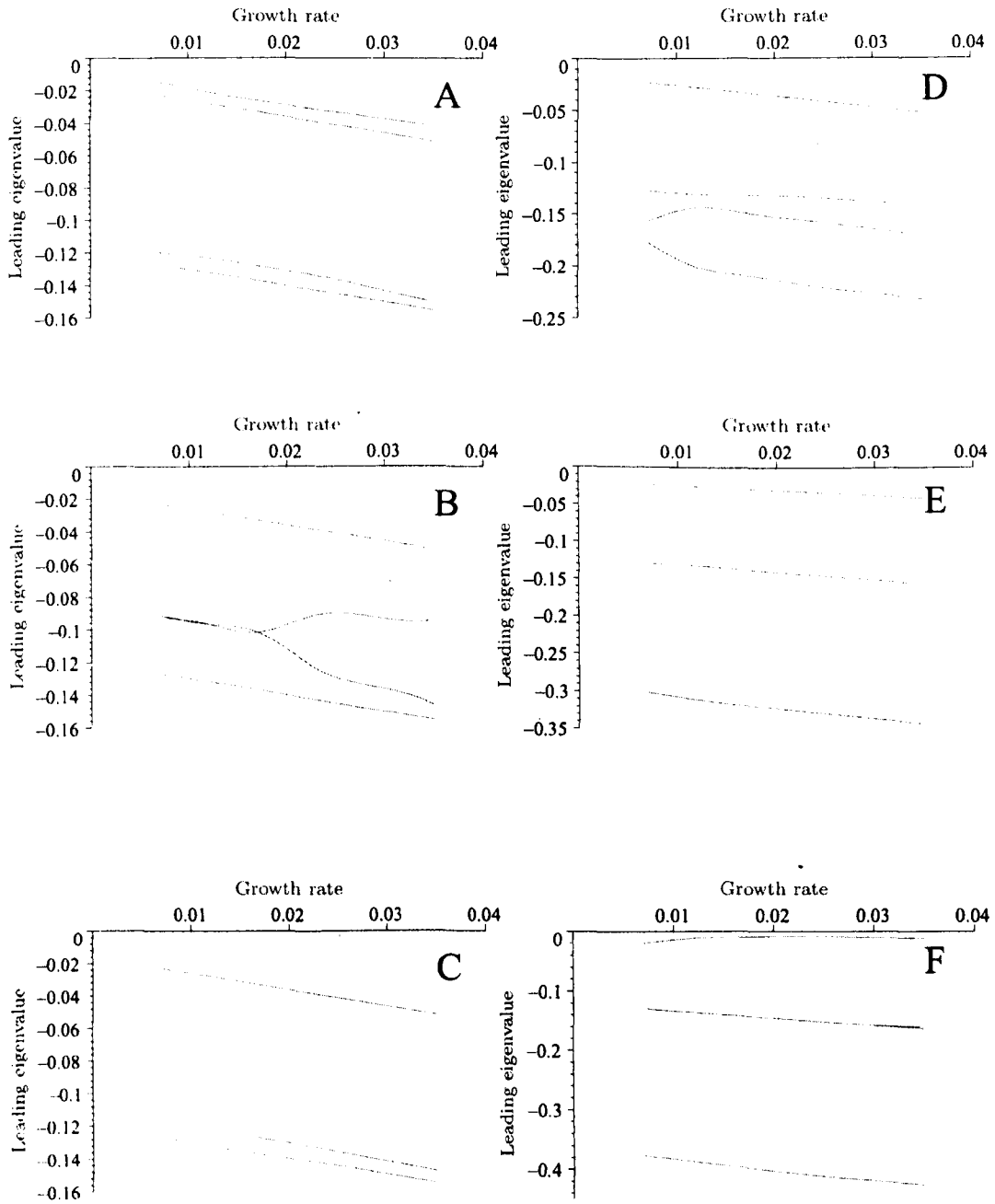

Figure 5.2: Plots of the four eigenvalues of the lysogenic equilibrium against *E. coli* growth rate for different values of the CI degradation rate, γ_{cI} (phage lambda only). (a) $\gamma_{cI} = 0.0$. (b) $\gamma_{cI} = 0.05$. (c) $\gamma_{cI} = 0.10$. (d) $\gamma_{cI} = 0.20$. (e) $\gamma_{cI} = 0.30$. (f) $\gamma_{cI} = 0.37$.

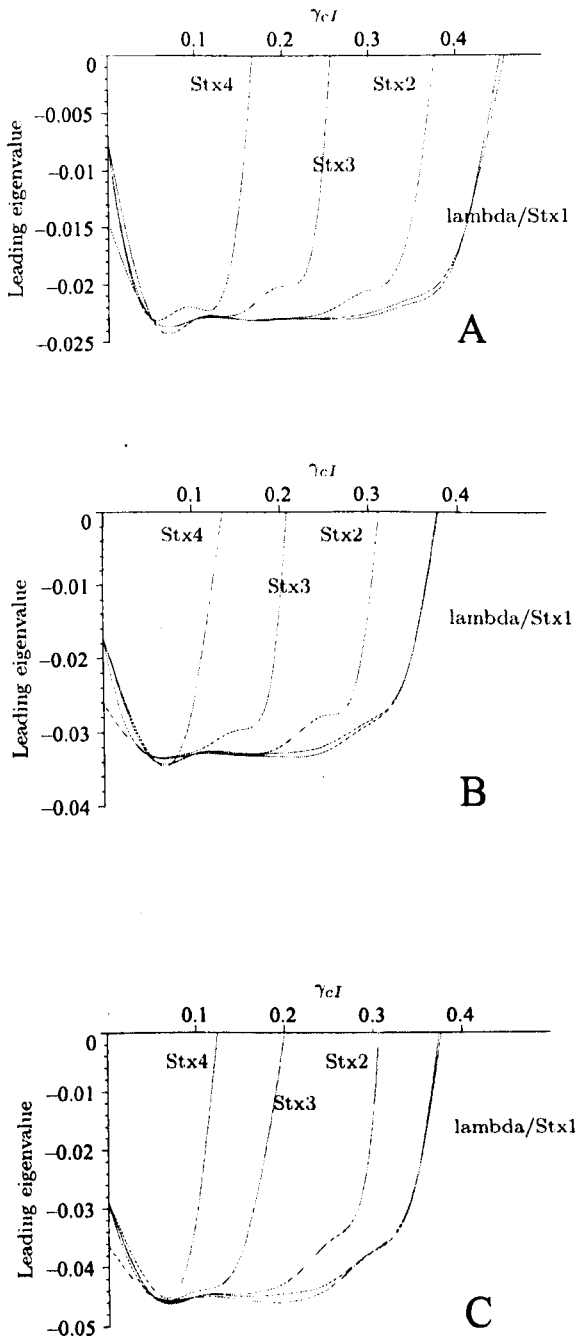

Figure 5.3: Plots of the leading eigenvalue of the lysogenic equilibrium against γ_{cI} for phage lambda and the four Stx scenarios, at three different nutrient levels (a) Low nutrient level. (b) Medium nutrient level. (c) High nutrient level.

5.3.2 Varying the nutrient level: comparison of Stx scenarios and lambda

Figure 5.1 shows that over the range $0 \leq \gamma_{cI} \leq 0.10$, the stability of lysogens of lambda and Stx3 are very similar. However, for higher values of γ_{cI} the stability of Stx3 lysogens are clearly lower than those of lambda.

Figure 5.3 compares the stability of lysogens of lambda and the four Stx scenarios at three different nutrient levels (corresponding to the first (low), third (medium) and fifth (high) nutrient levels considered by Bremer and Dennis (1996)), and at each level the pattern is the same. As γ_{cI} is increased from zero, the stability of all five lysogen types increases until a maximum level of stability is reached (corresponding to the $(-\gamma_{cro} - \mu)$ eigenvalue). A small increase in γ_{cI} is sufficient to reduce the stability of Stx4 lysogens (as a different eigenvalue becomes dominant), and further increases in γ_{cI} lead to reduced stability of lysogens of Stx2, followed by those of Stx3, and finally Stx4 and lambda (whose stability curves almost overlap). Although this pattern is observed for each of the three nutrient levels considered, notice that for the medium nutrient level lysogen stability begins to decrease at lower values of γ_{cI} compared to the low nutrient level, so that (for example) if $\gamma_{cI} = 0.40$ then with a low nutrient level there are no lysogenic equilbria, but with a medium nutrient level there is still a lysogenic equilibrium for Stx4. There is very little difference between the stability curves for the medium and high nutrient levels.

5.3.3 Varying the temperature: phage lambda

Bremer and Dennis (1996) provide data for five temperatures: 20 °C, 25 °C, 30 °C, 35 °C, and 40 °C. The eigenvalue formulae (5.3.1)-(5.3.1) apply here (for low values of γ_{cI}), but notice that the value of $[O_R]$ does not change with temperature (as we are assuming that the macromolecular composition of the cell is independent of temperature). Also in this case the calculation of the f functions depends on temperature, since the expressions for these functions involve an absolute temperature term, T. The Bremer and Dennis (1996) data show that as temperature increases, the *E.coli* growth rate μ increases. Figure 5.4 (b) shows how lysogen stability changes with growth rate for different values of γ_{cI}.

For $\gamma_{cI} = 0$ the leading eigenvalue is given by (5.3.3), while for $\gamma_{cI} = 0.05$ and $\gamma_{cI} = 0.1$ the leading eigenvalue is given by (5.3.2). In all three cases, an increase in μ resulting from an increase in temperature causes lysogen stability to increase.

A different pattern of stability is observed for higher values of γ_{cI}. For example, with $\gamma_{cI} = 0.35$ the stability increases as temperature increases from 20 to 30; but as μ increases from 30 to 35, there is a fairly sharp decrease in stability. For high values

of γ_{cl}, there are two opposing factors to consider. As the temperature is increased, the increase in the growth rate tends to increase stability, while the changes in the derivatives of the functions f^q_{RM}, f^s_{RM}, and f_R tend to reduce stability. At lower temperatures the effect of the growth rate dominates, resulting in increased stability, while at higher temperatures the changes in the derivatives dominate. Unlike the nutrient level case, all four partial derivatives contribute to the lowered stability. Figure 5.5 shows plots of all four eigenvalues for different values of γ_{cl}.

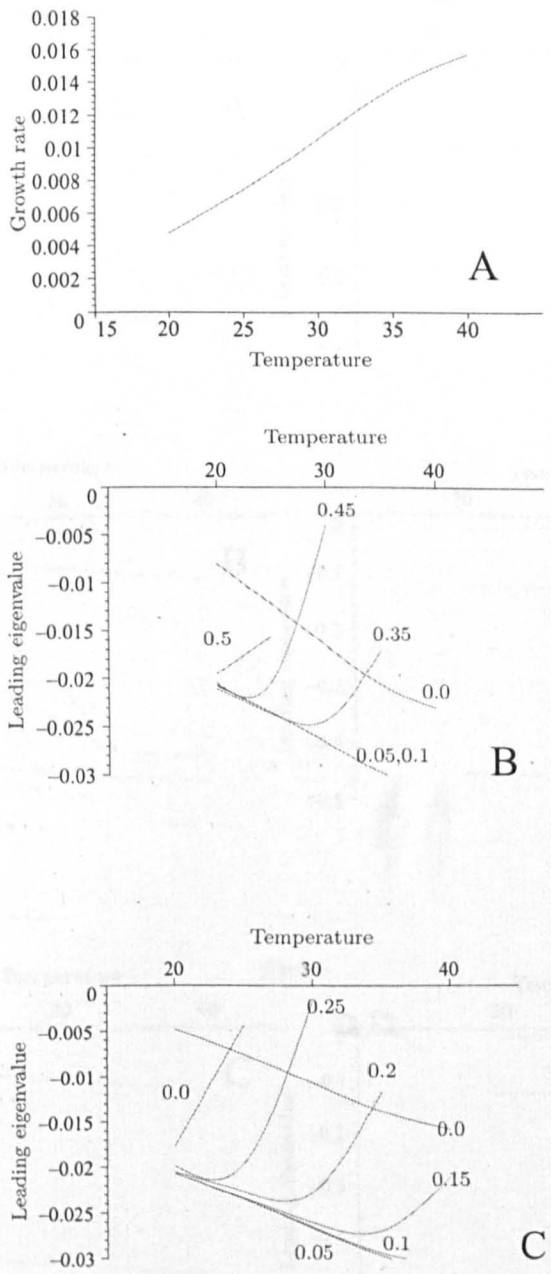

Figure 5.4: Modelling changes in lysogen stability in response to changes in temperature. (a) The relationship between temperature and *E. coli* growth rate reported by Bremer and Dennis (1996). (b) Leading eigenvalue of the lysogenic equilibrium versus temperature (phage lambda). (c) Leading eigenvalue of the lysogenic equilibrium versus temperature (Stx3).

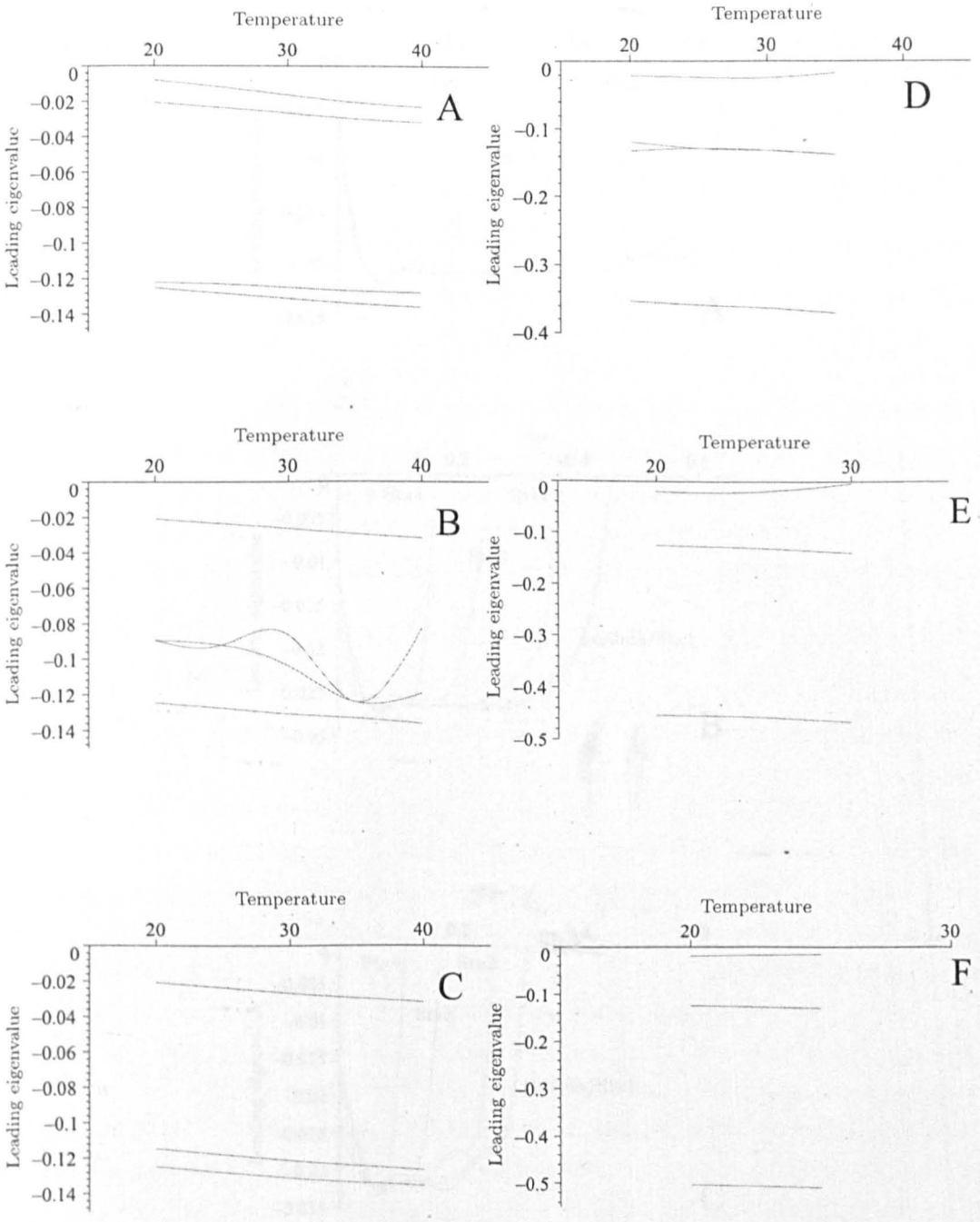

Figure 5.5: Plots of the four eigenvalues of the lysogenic equilibrium against temperature for different values of the CI degradation rate, γ_{cI} (phage lambda only). (a) $\gamma_{cI} = 0.0$. (b) $\gamma_{cI} = 0.05$. (c) $\gamma_{cI} = 0.10$. (d) $\gamma_{cI} = 0.35$. (e) $\gamma_{cI} = 0.45$. (f) $\gamma_{cI} = 0.50$.

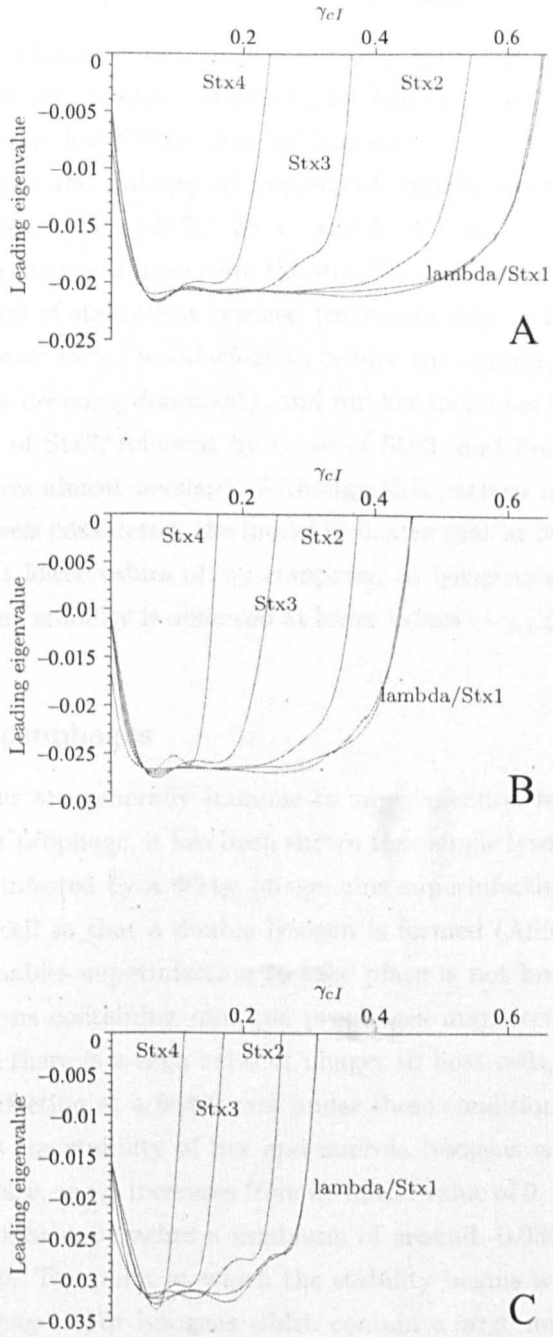

Figure 5.6: Plots of the leading eigenvalue of the lysogenic equilibrium against γ_{cI} for phage lambda and the four Stx scenarios, at three different temperatures. (a) 20 °C. (b) 30 °C. (c) 40 °C.

5.3.4 Varying the temperature: comparison of Stx scenarios and lambda

Figure 5.4 shows that over the range $0 \leq \gamma_{cI} \leq 0.10$, the stability of lysogens of lambda and Stx3 are very similar. However, for higher values of γ_{cI} the stability of Stx3 lysogens are clearly lower than those of lambda.

Figure 5.6 compares the stability of lysogens of lambda and the four Stx scenarios at three different temperatures (20 °C, 30 °C, and 40 °C), and at each level the pattern is the same. As γ_{cI} is increased from zero, the stability of all five lysogen types increases until a maximum level of stability is reached (corresponding to the $(-\gamma_{cro} - \mu)$ eigenvalue). A small increase in γ_{cI} is sufficient to reduce the stability of Stx4 lysogens (as a different eigenvalue becomes dominant), and further increases in γ_{cI} lead to reduced stability of lysogens of Stx2, followed by those of Stx3, and finally Stx4 and lambda (whose stability curves almost overlap). Although this pattern is observed for each of the three nutrient levels considered, the model indicates that at 30 °C, lysogen stability begins to decrease at lower values of γ_{cI} compared to lysogens at 20 °C. Similarly at 40 °C, reduced lysogen stability is observed at lower values of γ_{cI} (compared to lysogens at 30 °C).

5.3.5 Multiple prophages

Although lysogens are generally immune to superinfection by phages of the same strain as the resident prophage, it has been shown that single lysogens of the Stx phage $\Phi 24_B$ may be superinfected by a $\Phi 24_B$ phage; this superinfecting phage may in turn lysogenize the host cell so that a double lysogen is formed (Allison et al, 2003). The mechanism which enables superinfection to take place is not known at present (Fogg et al, 2007). Lysogens containing multiple prophages may occur more frequently in environments where there is a high ratio of phages to host cells, since single lysogens will undergo superinfection at a faster rate under these conditions.

Figure 5.7 shows the stability of Stx and lambda lysogens which contain multiple prophages. In each case, as γ_{cI} increases from its initial value of 0, the leading eigenvalue at the lysogenic equilibrium reaches a minimum of around -0.036 and then eventually begins to approach 0. The point at which the stability begins to decrease depends on the number of prophages. For lysogens which contain a large number of prophages, a large increase in γ_{cI} (from its initial value of 0) must occur before the lysogen stability begins to decrease. This indicates that the presence of multiple prophages helps to stabilize the lysogen.

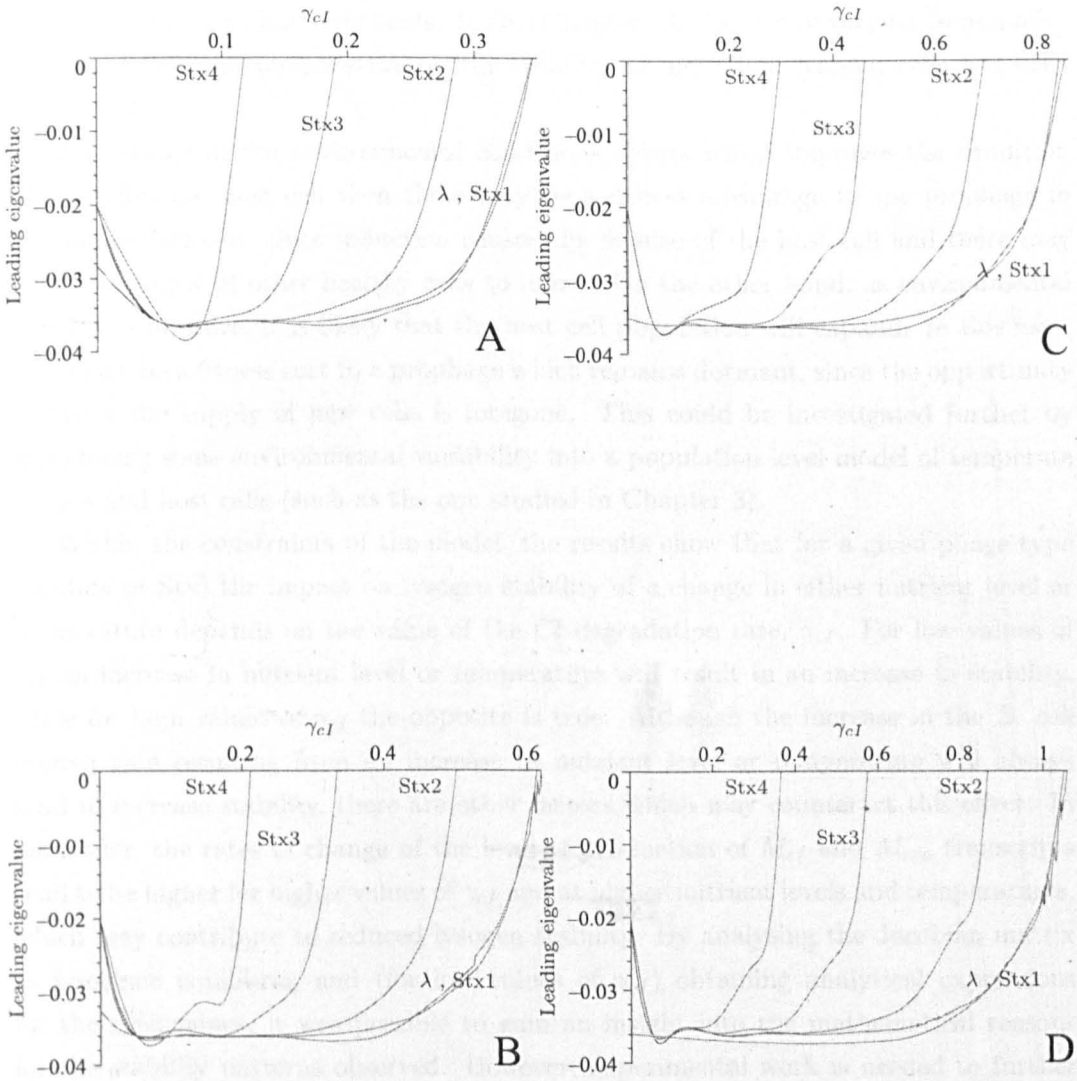

Figure 5.7: Plots of the leading eigenvalue of the lysogenic equilibrium against γ_{cI} for phage lambda and the four Stx scenarios. (a) 1 prophage per lysogen. (b) 2 prophages per lysogen. (c) 3 prophages per lysogen. (d) 4 prophages per lysogen.

5.3.6 Concluding remarks

Since Stx lysogens can only release toxins on lysis of the host cell, it is important to understand the environmental factors which influence the rates at which Stx prophages initiate lysis of their bacterial hosts. In this Chapter, the impact of varying (seperately) nutrient levels and temperature on the stability of individual lysogen cells has been considered.

If a change in the environmental conditions occurs which improves the condition of an individual host cell then there may be a fitness advantage to the prophage in remaining dormant, since induction causes the demise of the host cell and there may not be a supply of other healthy cells to infect. On the other hand, as environmental conditions improve, it is likely that the host cell population will expand. In this case, there may be a fitness cost to a prophage which remains dormant, since the opportunity to infect the supply of new cells is foregone. This could be investigated further by introducing some environmental variability into a population level model of temperate phages and host cells (such as the one studied in Chapter 3).

Within the constraints of the model, the results show that for a given phage type (lambda or Stx) the impact on lysogen stability of a change in either nutrient level or temperature depends on the value of the CI degradation rate, γ_{cI}. For low values of γ_{cI} an increase in nutrient level or temperature will result in an increase in stability, while for high values of γ_{cI} the opposite is true. Although the increase in the *E. coli* growth rate resulting from an increase in nutrient level or temperature will always tend to increase stability, there are other factors which may counteract this effect. In particular, the rates of change of the level of production of M_{cI} and M_{cro} transcripts tend to be higher for higher values of γ_{cI} and at higher nutrient levels and temperatures, which may contribute to reduced lysogen stability. By analysing the Jacobian matrix at lysogenic equilibria, and (for low values of γ_{cI}) obtaining analytical expressions for the eigenvalues, it was possible to gain an insight into the mathematical reasons for the stability patterns observed. However, experimental work is needed to further investigate the biological implications of these results.

One assumption which is implicit in the modelling approach used is that the value of γ_{cI} is not dependent on either temperature or nutrient level, and this assumption is reasonable over ranges of temperatures and nutrient levels which do not threaten the survival of the host. However, at extreme temperatures or very low resource levels, there is likely to be a significant impact on γ_{cI}, and so a different approach would be needed in these cases.

The different values of γ_{cI} considered in this Chapter are assumed to arise from an external factor such as ultra-violet light. It is likely that the presence of ultra-violet

light would influence other model parameters as well, such as rates of transcription and translation. Further experimental is needed to determine the extent of such influences.

In this Chapter, it has also been shown that lysogens containing multiple prophages are more stable than single prophage lysogens. If multiple prophage lysogens comprise a large proportion of the total lysogen population, this may indicate that there is a shortage of susceptible host cells, and so there is likely be a fitness advantage associated with lower rates of induction. Lower induction rates imply lower levels of toxin release by multiple Stx lysogens, but this effect may be balanced out to some extent if multiple Stx lysogens are capable of synthesizing a higher number of toxin molecules during induction than single lysogens (Fogg et al, 2007)

To summarize, there is a dearth of experimental evidence regarding the influence of environmental conditions on lysogen stability. However, by making use of the available data concerning the *E. coli* growth rate and chemical composition at different nutrient levels and temperatures, this Chapter represents a first step in assessing the impact of the environment on the stability of Stx lysogens, and hence on levels of toxin release and virulence. Future work could involve investigating the effects of temperature and nutrient level on the levels of toxin release by populations of Stx lysogens. Another question to be considered is whether lysogens of different Stx phages respond differently to changes in the environment.

Chapter 6

Stochastic modelling of the intial decision between lysis and lysogeny in Stx phages

6.1 Introduction

As discussed in Chapter 4, an infection of an *E. coli* cell by one or more Stx phages will only lead to the release of Shiga toxins on lysis of the host cell. In the previous Chapter, the stability of Stx lysogens was considered via a deterministic mathematical model. Here, the initial decision between lysis and lysogeny in Stx infections, and the implications for the rate of toxin release, will be considered within a stochastic framework.

During a phage infection, the times at which events such as gene expression and translation occur depend partly on random factors such as the erratic motion of molecules within the cell. Unlike the deterministic modelling approach, the stochastic framework enables the random nature of the lysis-lysogeny decision to be modelled. Furthermore it provides a more natural setting for modelling small amounts of substances, since the quantities of interest are discrete numbers of molecules rather than continuous concentrations.

Arkin *et al* (1998) presented a stochastic model based on the known regulatory mechanisms (described below) which control the lysis-lysogeny switch in phage lambda (Herskowitz and Hagen, 1980; Ptashne, 1992). This is a highly complex model, involving five genes and their respective protein products, and therefore running the model requires a large amount of computing resources. In this Chapter a similar model is developed, in which certain simplifying assumptions are used in order to reduce the computational workload. This model is then adapted to enable Stx phage characteristics to be modelled.

A single run of the model corresponds to one complete cell cycle, and the results

are the numbers of each type of molecular entity over this time period. The outcome of each run is either lysis or lysogeny, and so the probability of lysogeny for a particular phage can be estimated by carrying out a large number of runs and calculating the proportion of lysogenic outcomes.

It would have been desirable to carry out many more runs of the model, and to investigate more Stx scenarios, than are presented here. However, limitations imposed by computer resources and time have meant that the results in this Chapter represent a preliminary investigation rather than a full analysis.

6.2 The lambda lysis-lysogeny switch

Here a description is provided of the biological processes which featured in the Arkin *et al* (1998) model, and a summary of the results which were obtained.

The model includes the proteins CI, Cro, N, CII, CIII, and their respective genes *cI*, *cro*, *n*, *cII*, and *cIII*. Monomers of CI and Cro can dimerize to form CI_2 and Cro_2 molecules. Figure 6.1 illustrates the various operator sites, promoters and terminators and the sequence of positions of these regulatory regions on the lambda genome. At the start of an infection there are no protein molecules present, but subsequently gene expression and the resulting mRNA transcripts translated into protein molecules. The simulation proceeds until the end of the cell cycle (35 minutes) is reached; at this time, it is the number of CI_2 and Cro_2 molecules which indicates whether lysis or lysogeny has taken place. If there are more CI_2 molecules than Cro_2 molecules, then the outcome of the infection is lysogeny, otherwise the outcome is lysis.

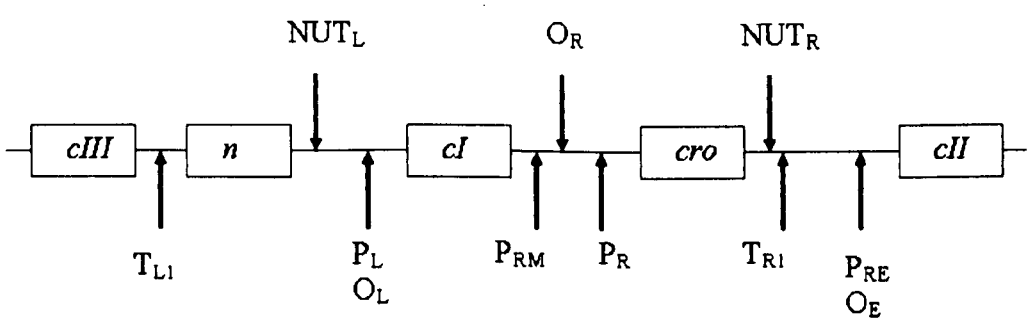

Figure 6.1: The region of lambda DNA which comprises the molecular switch between lysis and lysogeny. After Ptashne (1986).

Immediately after phage infection of a host bacterial cell, host RNAP molecules bind and begin transcription at P_L and P_R. The resulting mRNA transcripts are terminated when the RNAP molecule reaches the end of the genes *n* (in the case of

leftward transcription) and *cro* (in the case of rightward transcription). The transcripts are translated by host ribosomes into molecules of the regulatory proteins N and Cro.

The protein n acts as an anti-terminator. In the absence of the protein n, transcription is terminated once the RNAP molecule encounters the terminators T_{L1} and T_{R1} at the end of the n and *cro* genes respectively. However, as the concentration of n increases, molecules of n may act to anti-terminate RNAP at the NUT_L and NUT_R sites. When this happens, the RNAP molecule is able to continue moving along the DNA molecule beyond the terminators and thus to transcribe the additional genes *cII* and *cIII*.

The CII protein is vulnerable to attack by a bacterial protease known as HflB (Cheng et al. 1988), and it is proposed that a second protease also acts to degrade CII (Kihara et al. 1997); in Arkin et al (1998) these two proteases are labelled P1 and P2. The function of the protein CIII is to bind to molecules of P1 and P2 so as to protect CII from degradation.

The *cI* gene has two promoters, P_{RM} and P_{RE}. The P_{RM} promoter has three binding sites: O_R1, O_R2, and O_R3, while P_{RE} has a single binding site, O_E. In the early stages of the infection a Cro_2 dimer binds to O_R3, and this is sufficient to prevent transcription of *cI* from P_{RM}. Transcription of *cI* from P_{RE} can only proceed when a molecule of CII binds to O_E.

The level of activity of the protein CII largely determines whether or not lysogeny occurs. If there is a sufficient level of CII, then a CII molecule may activate the *cI* promoter P_{RE}. A CI_2 dimer can then bind to the operators O_L and O_R, and thereby promote the expression of *cI* from P_{RM} while turning off the promoters of all other genes. Thus, if CII is highly active the *cro* gene will be repressed and the phage will form a lysogen with its host. On the other hand, if production of CII is low then P_{RE} will not be activated; thus, there will not be sufficient production of CI to repress *cro*, and so production of Cro will be unchecked and the host cell will be lysed.

In Arkin *et al* (1998) a cell was considered to become committed to lysogeny if $[CI_2]>[Cro_2]$ at the end of the 35-minute cell cycle, and thus the probability of lysogeny was estimated by running a stochastic simulation of the above model (using the Gillespie algorithm, described below) many times, and calculating the proportion of runs which satisfied this condition. Arkin *et al* (1998) calculated the probability of lysogeny for phage lambda at different multiplicities of infection (MOI) and found that as MOI increases, the probability of lysogeny also increases, this being in agreement with previous experimental work by Kourilsky (1973). With their chosen parameter set (which was derived from published values in the literature), it was found that with MOI=1 the probability of lysogeny was approximately zero, while the probability of lysogeny approaches 1 as MOI is increased above 10.

6.3 The stochastic modelling framework

In order to model the processes described above, a large number of chemical reactions of different types must be considered. In a chemical reaction, the molecules react together to produce the product molecules. The number of reactant molecules determines the *order* of the reaction, e.g. 1st order (a single reactant), 2nd order (two reactants) etc. For example, a second order reaction with a single product may be written as:

$$R_1 + R_2 \longrightarrow S$$

The frequency with which this reaction occurs depends on the concentrations of R_1 and R_2 and a parameter known as the rate constant, k. Thus, in a differential equation model, the rate at which the concentration of S increases is given by

$$\frac{d[S]}{dt} = k[R_1][R_2]$$

where the notation $[X]$ means the concentration of substance X.

However, a continuous deterministic model described by differential equations is not appropriate for every situation. For example, small numbers of reactant molecules and infrequent reaction events can generally be handled better by a discrete stochastic model. In this type of model the quantities of interest are the numbers of molecules of the substances (rather than their concentrations), and the times at which reaction events occur are randomly generated from a chosen probability distribution.

The Gillespie algorithm (Gillespie 1976, 1977) is a stochastic simulation which proceeds by determining the time at which the next reaction event occurs, and the identity of this reaction (from a list of n possible reactions). The state of the system (i.e. the number of molecules of each substance) is then updated according to which reaction has occurred. This process is repeated until the simulated system time t reaches a certain value t_{max}.

At each iteration of the algorithm, it is necessary to calculate the reaction propensity of each reaction. For example, the propensity of the reaction

$$R_1 + R_2 \longrightarrow S$$

is given by cr_1r_2, where r_1 and r_2 are the numbers of molecules of R_1 and R_2 respectively, and c is the stochastic rate constant for this reaction.

Suppose that the latest reaction event occurred at time t. The length of time T until the next reaction event is calculated as an exponential random variable with parameter $1/\sum_{i=1}^{n} h_i$, so that

$$P(T \leq t) = 1 - \exp(-t \sum_{i=1}^{n} h_i) \qquad t \geq 0$$

where h_i is the propensity of the i^{th} reaction.

The identity of the reaction which occurs at time $t + T$ is determined by dividing the interval [0,1] into n sub-interval, where the widths of the sub-intervals are given by $h_i / \sum_{i=1}^{n} h_i$ $(i = 1..n)$. A uniform random number U is then generated in [0,1], and if U falls in the i^{th} sub-interval, then reaction i is selected.

There are situations where the time to the next reaction event is not exponentially distributed. For example, if the reactions are taking place within a growing cell then the increasing volume affects the frequency with which molecules collide and hence react with each other. Also, if a particular event consists of a series of exponentially distributed time steps, then this may be modelled by a single random number from a gamma distribution; an example of such an event is transcription of a gene, in which the RNAP enzyme moves from one end of the gene to the other in a series of steps from one nucleotide to the next. The Gibson-Bruck algorithm (Gibson and Bruck, 2000) is equivalent to the Gillespie algorithm, but it is formulated in such a way that it is easier to incorporate non-exponentially distributed reaction times.

Following Gibson and Bruck (2000), the simulation algorithm used to generate the results in this Chapter divides the set of all possible reactions into 3 classes: (i) gamma ; (ii) exponential; and (iii) second order. These are described below.

6.3.1 The gamma class of reactions

Movement of an RNAP enzyme along a DNA molecule and movement of a ribosome along an mRNA transcript are both modelled using a gamma distribution. This is possible because both these types of events consist of a series of steps. For example, suppose an RNAP enzyme binds to the promoter of a gene whose length is M nucleotides. Transcription of this gene involves movement of the enzyme from the promoter (call this position 0 on the DNA) to the terminator (position M on the DNA), which can be represented as:

$$\text{RNAP.DNA}_0 \longrightarrow \text{RNAP.DNA}_M$$

This event can be divided into M steps of the following form:

$$\text{RNAP.DNA}_n \longrightarrow \text{RNAP.DNA}_{n+1}$$

where $0 < n < M - 1$. The time at which the next single-nucleotide step occurs can be modelled as an exponential random variable, and so the overall time it takes for the enzyme to transcribe the gene is the sum of M exponential random numbers. Using the result from probability theory that a sum of independent identically distributed exponential random variables has a gamma distribution (Leon-Garcia, 1994), it is only necessary to generate a single gamma random variable to simulate transcription of the gene, rather than M exponential random variables. Given that genes may be several hundred nucleotides long, this approach greatly increases the speed of the simulation process. Some accuracy is lost however, since it must now be implicitly assumed that the movement of an enzyme molecule (or ribosome) proceeds unhindered at all times, whereas in reality there may be occasions when an enzyme has to wait for another enzyme molecule ahead of it to move out of the way.

6.3.2 The exponential class of reactions

Of the remaining reactions, those which are of 1st order may be modelled as having exponential firing times (second order reactions, which are influenced by changes in volume resulting from cellular growth, must be handled seperately). These 1st order reactions include degradation and dissociation. Degradation is the process by which a protein such as CI is lost to the system:

$$\text{CI} \longrightarrow \phi$$

and dissociation is where a protein dimer separates to form two monomers, e.g.:

$$\text{Cro}_2 \longrightarrow \text{Cro} + \text{Cro}$$

6.3.3 The second order class of reactions

Second order reactions involve two molecules colliding together and reacting to form new molecules. Since the reactions are taking place in a growing cell, the increasing volume affects the rate at which molecules collide. Allowing for increasing volume means that the distribution of firing times for second order reactions is not exponential. At time t, the variable

$$R = V(t)[U^{-c/a_i - 1}]/c \tag{6.3.1}$$

Phage scenario	Binding energy of Cl_2 to O_R2, $\Delta G^{Cl_2}_{O_R2}$ (kcal / Mol)
Lambda	-10.1
Stx 1	-8
Stx 2	-7

Table 6.1: The lambda and Stx phage scenarios.

has the correct distribution for a second order reaction (Gibson and Bruck, 2000), where: $V(t)$ is the cell volume at time t; U is a Uniform [0,1] random variable; c is the cellular growth rate; and a_i is the propensity for reaction i.

An example of this type of reaction is dimerization, where two protein monomers join together to form a dimer, e.g.:

$$Cro + Cro \longrightarrow Cro_2$$

6.4 The model

A Matlab (The MathWorks, Inc.) algorithm was written to model the lysis-lysogeny decision in phage lambda and in two Stx scenarios. As discussed in previous Chapters, the value of the binding energy $\Delta G^{Cl_2}_{O_R2}$ in the Stx phage 933W is lower than in phage lambda (Koudelka et al, 2004). Thus Stx scenarios were constructed by varying the value of this constant, as shown in Table 6.1. Following Arkin et al (1998), the multiplicity of infection (i.e. the number of infecting phages per host cell) was set equal to 6.

An outline of the algorithm used is given below, and an illustration is provided in Figure 6.2.

(1) Initialize the system.

(a) Let T be the system time; set T=0.

(b) Let V_0 be the initial volume of the cell; set $V_0 = 1$.

(c) Let X be the system state. This is a vector which stores the current number of molecules for each chemical species in the model. Set X equal to its initial value, X_0.

(d) The gamma class:

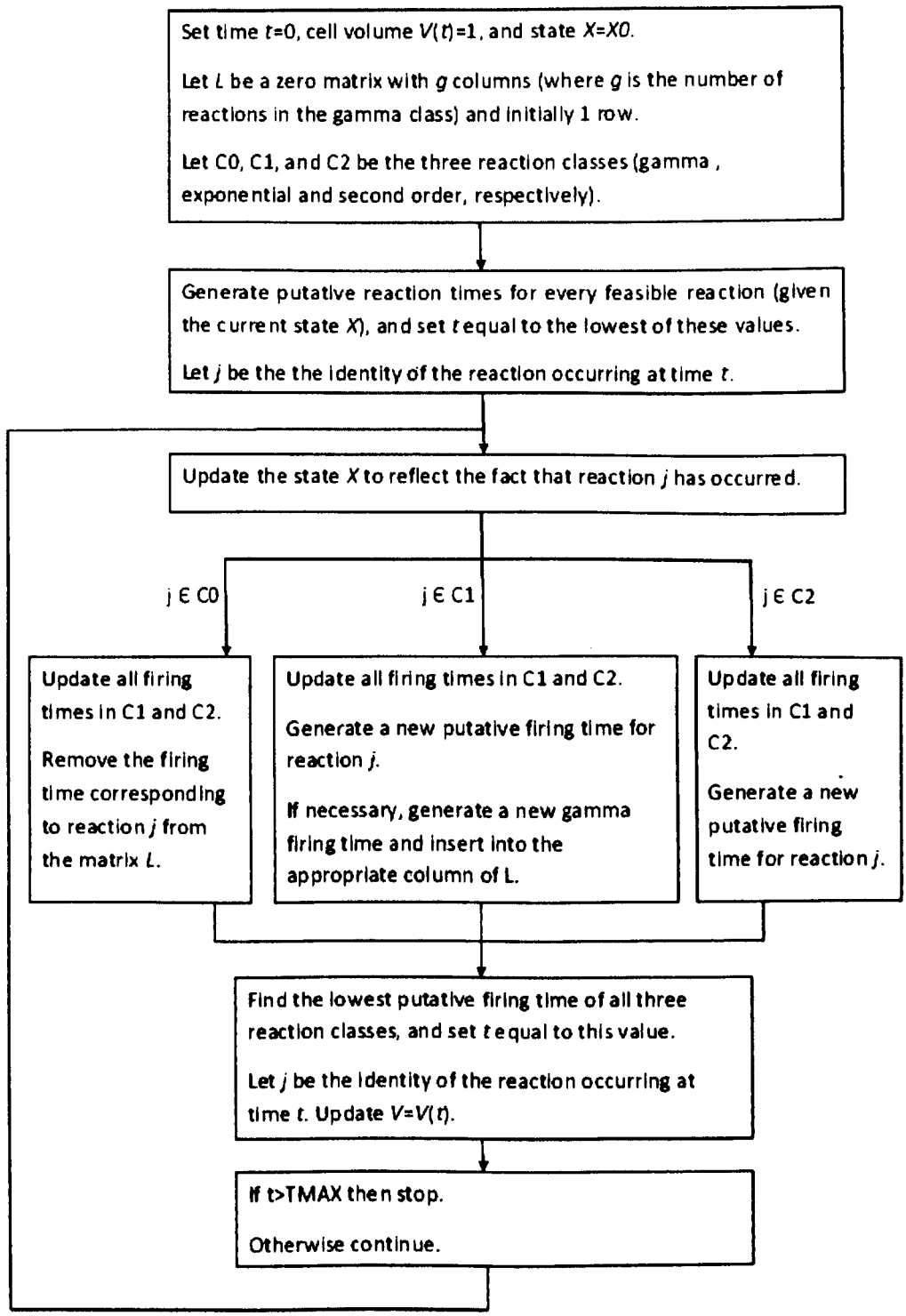

Figure 6.2: The model algorithm. (The notation $j \in C0$, for example, means that reaction j is a member of the gamma class, C0).

There are 20 reactions in the gamma class, 15 of which correspond to the movement of RNAP along a DNA molecule; the remaining 5 reactions correspond to movement of a ribosome along an mRNA transcript, i.e. translation.

Let L be a matrix with 20 columns and (initially) 1 row. This matrix will contain the firing times of the reactions in this class. Since the first reaction which occurs cannot be in the gamma class, set every entry of L equal to ∞. Let t0=∞ be the putative time at which the next gamma reaction fires.

(e) The exponential class:

There are 52 reactions in the exponential class. Reactions in which an RNAP molecules bind to promoters on a DNA molecule, and reactions in which ribosomes bind to mRNA transcripts, are included in this class.

For each exponential reaction i ($1 \leq i \leq 52$), obtain a putative firing time by generating a random number from the exponential distribution with parameter $1/(k_i N_i)$, where k_i is the stochastic rate constant and N_i is the initial number of molecules of the reactant. If a reaction is not possible at this stage (i.e. if there are no molecules of the reactant present), set the putative firing time of this reaction equal to ∞. Set t1 equal to the lowest firing time.

Note that the first reaction to occur will be an RNAP molecule binding to a promoter, since no other events can occur until this has happened; therefore all other reaction types in this class have firing times of ∞ at this stage.

(f) The second order class:

There are 8 reactions in the second order class, which include protein dimerization (resulting in the formation of CI_2 and Cro_2 molecules) and association of proteins (either CII or CIII) with proteases (either P1 or P2).

For each second order reaction, a putative firing time is generated using (6.3.1).

Let t2 be the putative time at which the next second-order reaction fires. Since the first reaction to occur cannot be a second order reaction, set t2=∞.

(2) Time iterative loop.

(a) Identify which reaction will occur next, by determining which of t0, t1, and t2 has the lowest value. Label this reaction j.

(b) If reaction j is from the gamma class, set T=t0; else if the next reaction is from the exponential class, set T=t1; else if the next reaction is from the second-order class, set T=t2.

(c) Update the system state X according to reaction j.

(d) Calculate the new volume of the cell at time T, V_T. Note that the cell volume

increases with time such that at the end of the cell cycle the volume has doubled (i.e. the cell volume increases from 1 to 2 over the course of the cell cycle).

(e) If reaction j was from the gamma class, remove its firing time from the matrix L.

(f) Generate new putative firing times for each reaction in the exponential and second order classes. Let t1 and t2 be the lowest firing times for exponential and second order classes respectively.

(f) If reaction j has resulted in an RNAP molecule binding to a promoter or a ribosome binding to an mRNA transcript (both of which belong to the exponential class), then the next movement of this molecule will be a reaction belonging to the gamma class; therefore it is necessary to obtain the firing time of the corresponding gamma reaction as a random number from the appropriate gamma distribution. Then insert this firing time into the appropriate column of the matrix L.

(g) Set t0 equal to the lowest value in the matrix L.

(h) If the end of the cell cycle has not been reached (i.e. if T $<$ 35 minutes) go to step 2(a); otherwise stop.

Thus at each iteration of the algorithm, the algorithm moves forward in time to the next reaction event and updates the numbers of molecules of each substance (e.g. proteins, mRNA transcripts etc) accordingly. Whether the outcome of the run is lysis or lysogeny can be determined by comparing the final numbers of molecules of Cl_2 and Cro_2 at the end of the 35 minute cell cycle; if there are more molecules of Cl_2 than Cro_2 then a lysogen has been formed, otherwise the cell has been lysed. By running the algorithm many times for phage lambda and the Stx scenarios, the proportion of runs which result in lysogeny can be obtained for each phage type.

To obtain the results in this Chapter, Condor (The Condor Software Program) was used to distribute the algorithm to a large number of computers around the Liverpool University campus, so that multiple simulations could be carried out in parallel.

6.5 Results and Discussion

The algorithm described in the previous section was run many times for phage lambda and two Stx scenarios presented in Table 6.1. For each phage scenario 100 runs were initiated (via the Condor system), but not all of the runs were completed within the available time; the numbers of completed runs are given in Table 6.2. Thus, there is a possibility of bias in the results - it may be that runs which result in lysogeny generally take longer to complete than lytic runs, for example. However, this concern is lessened to some extent by the approximate agreement between the phage lambda

lysogenic proportion obtained here and that of Arkin et al (1998).

Figure 6.3 shows the final numbers of molecules of CI_2 and Cro_2 for each completed run of the algorithm, and for each of the three phage types. The plots also show the straight line along which $\#(CI_2)=\#(Cro_2)$; points above this line correspond to lytic outcomes, and points below correspond to lysogeny. The numbers of lytic and lysogenic outcomes are given in Table 6.2. For phage lambda the proportion of lysogenic outcomes is 0.45, which is in line with the results obtained by Arkin et al (1998) (for a multiplicity of infection of 6). For the two Stx scenarios this proportion is much lower (0.05 and 0.07), indicating that the reduced binding energies (as given in Table 6.1) have a significant impact on the probability of lysogeny. For both Stx scenarios, the final number of CI_2 molecules varies between approximately 30 and 260, while the number of Cro_2 molecules varies between 160 and 400 (with two outliers in the case of Stx1).

In Chapter 4 it was shown that the weaker binding energy between the operator site O_R2 and the repressor CI_2 in the Stx phage 933W (compared to phage lambda) contributes to the lower stability of its lysogens. The results of this Chapter confirm that this weaker binding energy also leads to a lower probability of lysogeny, and hence further increases the rate of toxin release.

One question which arises is whether the probability of lysogeny and the induction rate always evolve in tandem. Recall that in Chapter 3 a trade-off function was assumed to exist between these two parameters, such that a change in one of the parameters was always accompanied by a change in the other one. The results from Chapter 4 and Chapter 6 also indicate that changes in binding energies have an impact on both parameters. Since both parameters are determined by the same switching mechanism, any change which affects this mechanism is likely to affect both parameters simulatenously. There may be circumstances in which a phage population benefits from a change in only one of the parameters while keeping the other fixed, but whether this can be achieved in practice is not clear.

In Arkin et al (1998), the authors were able to carry out thousands of runs with the help of a supercomputer, whereas much smaller numbers of runs have been completed here. While it seems clear that the change in binding energy has an impact on the probability of lysogeny, the relatively small number of runs that have been completed mean that we cannot be certain as to the magnitude of this impact; part of the difference between the results for the three phage scenarios is attributable to random variation.

As in Chapter 4, it has been necessary to use phage lambda parameter values for modelling Stx phages, owing to the lack of experimentally determined values for Stx phages. It may be possible in the future to obtain the actual Stx values, and so to determine other parameters which may have a significant impact on the probability of

lysogeny.

Lower probabilities of lysogeny and lower lysogen stability are both associated with higher rates of toxin release into the environment, since toxins are only released when the host cell is lysed. While it is known that certain Stx lysogens have higher rates of induction than phage lambda (Livny and Friedman, 2004), there is currently no published data relating to probabilities of lysogeny for Stx phages. This is another important area for future experimental research.

Following Arkin et al (1998), a multiplicity of infection (MOI) of 6 has been assumed in this Chapter. The MOI is known to have a major effect on the probability of lysogeny in phage lambda (Kourilsky, 1973); for low MOI (i.e. 1 or 2), the probability of lysogeny is close to zero, and this is likely to be the case for Stx phages as well. Thus, for low MOI, any reduction in the probability of lysogeny resulting from the lower binding energy of 933W is likely to be negligible.

The approach used in this Chapter could theoretically be used to model the impact of environmental conditions on the probability of lysogeny. Given the very large number of parameters which appear in the model, a thorough analysis of the effect of temperature, say, would require a huge amount of experimental work to determine parameter values at different temperatures. However, changes in certain selected processes could be investigated - for example, if rates of transcription and translation were known to increase in response to increased temperature, then these rates could be adjusted accordingly in the model and the new probability of lysogeny determined.

It would be instructive to extend the model to include transcription and translation of the Shiga toxin gene. However, the biological knowledge of the mechanisms governing expression of the toxin gene in Stx phages such as 933W is not yet sufficient for this, and furthermore the greater complexity of such a model would require much greater level of computing resources.

In an exact stochastic simulation algorithm, such as the Gillespie algorithm (Gillespie, 1977), every reaction event is modelled seperately. Also, the algorithm must be run a large number of times in order to obtain statistically significant results. Therefore, stochastic modelling of complex cellular processes demands high levels of computational power, and this places severe restrictions on the amount of work that can be carried out in this area.

An alternative to exact algorithms is the use of approximate algorithms, which do not model every reaction event individually. These include hybrid algorithms in which some reactions are modelled stochastically while others are modelled deterministically (e.g. Puchalka and Kierzek, 2004), and leaping algorithms in which each time step may include more than one reaction event (e.g. Gillespie, 2001). In this Chapter, the use of the gamma distribution to model transcription and translation enabled simula-

Phage scenario	Total number of runs	Number of lytic runs	Number of lysogenic runs	Proportion of lysogenic runs
Lambda	69	38	31	0.45
Stx 1	41	39	2	0.05
Stx 2	57	53	4	0.07

Table 6.2: Table of results for phage lambda and the two Stx scenarios.

tion times to be reduced, but a single run of the algorithm still required several days to reach completion. Any attempt to capture cellular processes accurately requires the construction of highly complex models, and so there is still a need for developing methods which reduce the amount of time and computer power needed to carry out simulations.

To conclude, this Chapter has illustrated the impact on the probability of lysogeny of one aspect of the genetic switch in Stx phages. The structure and behaviour of the genetic switch in Stx phages plays a major role in determining the level of toxin release and hence the spread of disease, and the approach of this Chapter provides a basis for future modelling investigations in this area.

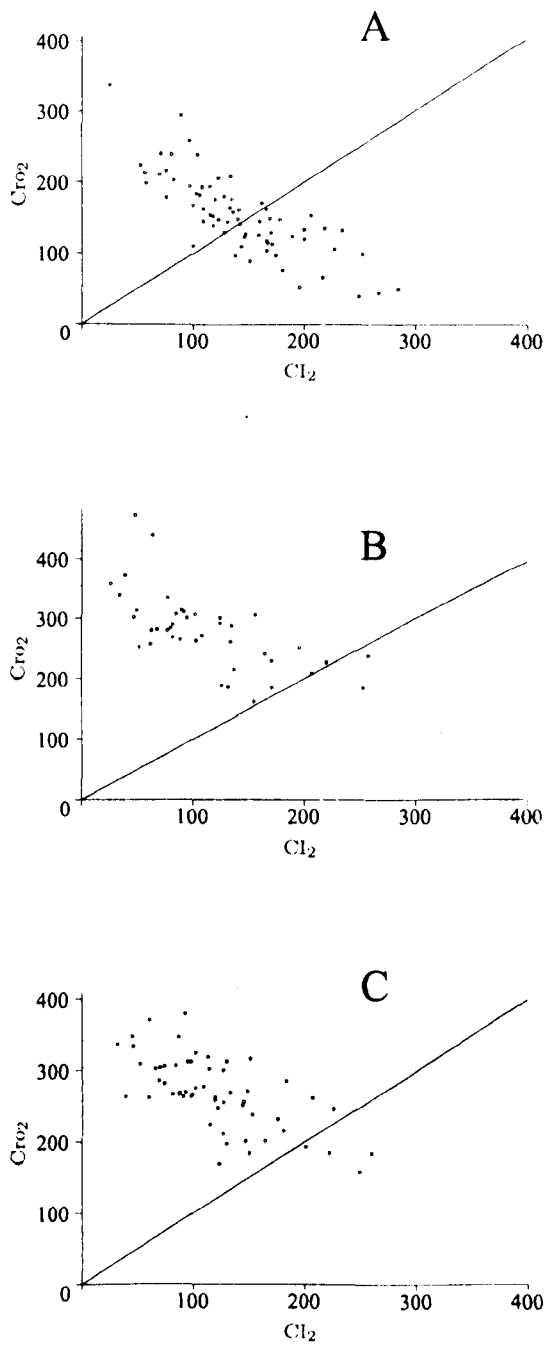

Figure 6.3: Scatter plots of the final numbers of molecules of CI_2 and Cro_2 for phage lambda (A), Stx1 (B), and Stx2 (C). Points above the diagonal line correspond to lysis, points below the line correspond to lysogeny.

Chapter 7

Conclusion

This thesis has considered models at both the population and molecular level in order to investigate the dynamics of temperate phages and their host cells, in particular Stx phages and the related phage lambda. Three timescales have been considered: cellular time, ecological time, and evolutionary time. Understanding the factors which influence the probability of lysogeny, and also the stability of lysogens, is especially important in the case of Stx phages because these characteristics are directly related to the rate at which Shiga-toxins are released into the environment, and hence the risk of outbreaks of disease in humans.

A Jacobian stability analysis was applied to the population dynamical model of phages and bacteria of Stewart and Levin (1984). The full model included temperate and virulent phages, and two bacterial populations, one of which was sensitive to phage infection and one which was resistant; a number of sub-models were also considered. For each model it was possible to identify equilibrium points, containing all possible types of phage and bacteria, at which the populations would remain constant. Simulations were carried out in order to illustrate different scenarios such as the coexistence of temperate and virulent phages, and the successful invasion of a virulent phage population by temperate phages; this was achieved by varying parameters such as the adsorption rates and burst sizes of the two phage strains, the rate at which resources flow into the environment, and the rate of growth of the bacterial populations. The results of the simulations were supported by analytical derivations of feasibility and stability criteria for the model equilibria, where possible. It was shown that the outcome of competition between a virulent and a temperate phage strain depends on particular parameter values, in particular the adsorption rates and burst sizes of the two strains, and also the probability of lysogeny and the induction rate of the temperate strain.

An adaptive dynamics approach was applied to the Mittler (1996) population dynamical model of temperate phages and bacteria, in order to investigate the evolution of temperate phages. A trade-off relationship was introduced such that the induction

rate of lysogens was an increasing function of the probability of lysogeny. This type of modelling is used to identify evolutionary singularities, which are points which evolution moves either towards or away from. It was shown that attractor and repellor singularities are possible, but branching points, which are associated with sympatric speciation, do not arise. Further research is needed to investigate whether the absence of branching points is simply a feature of the particular model considered, or reflects an actual characteristic of temperate phage populations. An initial approach could be to identify a different trade-off relationship, perhaps involving the probability of lysogeny as before, but replacing the induction rate with a different quantity (e.g. burst size, adsorption rate etc.), and then to find out whether branching occurs.

The stability of Stx lysogens was also investigated. It was shown how a model of the lambda molecular switch (Santillan and Mackey, 2004) could be extended to model Stx phages as well. In the literature it has been reported that there are Stx phages which differ from phage lambda in terms of the numbers of binding sites at the molecular switch, and also the binding energies between binding sites and key regulatory proteins. Hence, various Stx 'scenarios' were constructed which reflected these known characteristics. It was found that the difference in molecular binding energies between Stx and lambda phages does account for the lower stability of Stx lysogens. There is scope for further modelling work to be done in this area, once all the relevant binding energies have been measured and genome structures determined for particular Stx phages.

The influence of selected environmental conditions on Stx lysogens was also explored, again using a scenario-based approach. Both temperature and nutrient level in the environment influence the growth rate of the host cell (Bremer and Dennis, 1996), and this in turn may influence the stability of the lysogen. Results showed that the degradation rate of the phage regulatory protein CI, γ_{cI}, plays a significant role in determining whether changes in temperature or nutrient level result in an increase or decrease in stability. With both temperature and nutrient level fixed, it was found that an increase in γ_{cI} leads to lower stability. This may be explained in terms of a threat to the host survival: high values of γ_{cI} occur when there is a threat to the host, such as the presence of UV light (Ptashne, 2004), and reduced lysogen stability under these conditions is likely to improve the fitness of the phage population; the new phages which are released on induction may have the opportunity to infect new cells and so increase the chances of survival of the phage population.

The situation is more complicated when γ_{cI} is fixed, and either temperature or nutrient level is allowed to vary. For the ranges of temperatures and nutrient levels considered, it was shown that for low values of γ_{cI}, an increase in temperature or nutrient level tended to increase lysogen stability; however, for high values of γ_{cI}, an

increase in temperature or nutrient level resulted in a reduction in lysogen stability. Progress was made in understanding the mathematical reasons for the occurence of these interesting patterns; however, the implications in a biological context are less clear. Therefore experimental work would be useful to confirm the results in practice.

A stochastic model of the lambda genetic switch (Arkin et al, 1998) was modified in order to investigate the probability of lysogeny in Stx phages. Stx scenarios were constructed with different values of the binding energy constant, and the results showed that weaker binding energies were associated with lower probabilities of lysogeny. Thus the weaker binding energy in Stx phages (compared to phage lambda) leads to a greater proportion of lytic infections and hence increases the rate of toxin release into the environment.

There are many possibilities for future research. Studies in adaptive dynamics could be extended to considering the coevolution of temperate phages and bacteria. The modelling of competition between known Stx phage strains such as 933W and H19B could also be developed, in conjunction with experimental work. An important question to be considered is niche differentiation amongst Stx strains and the degree to which competition influences niche overlap.

It is currently not clear whether or how Stx phages derive fitness advantage from their ability to synthesize toxins (Herold et al, 2004). However, it may be speculated that the presence of the released toxins alters the environment in such a way that there is a benefit to the host, such as an increase in available resources. The phage population would then benefit from having a greater supply of uninfected host cells to infect. It is also likely that Stx phages confer many other functions upon their hosts, and thereby increase host fitness, but few such functions have as yet been discovered (Allison, 2007). Future experimental and modelling work may shed light on these questions.

Given appropriate data, there is also plenty of scope for further investigations into the impact of environmental conditions on both individual cells and populations of Stx lysogens. In particular, this thesis has considered seperately the influence of nutrient level and temperature on lysogen stability indirectly (i.e. via their influence on the host growth rate), but it would be interesting to study their combined effect - for example, what happens if an increase in temperature is accompanied by a decrease in nutrient level. Experimentally determining the *E. coli* growth rate at different nutrient levels and temperatures (i.e. extending the work of Bremer and Dennis (1996)) would enable a preliminary investigation of this question.

There is currently a shortage of experimental data relating to Stx phages, and therefore much of the modelling work in this thesis has relied on knowledge of phage lambda. In the future, the binding energies and other parameters involved in the Stx molecular switch will be determined, and other differences between the Stx and lambda

switches will emerge besides those considered in this thesis - for example, the function of the anti-repressor gene in the Stx phage $\Phi 24_B$ (Fogg et al. 2007). As knowledge of the Stx switch increases there will be an opportunity for revisiting the models considered in this thesis in order to achieve a closer correspondence with reality.

New Stx strains continue to be discovered regularly and outbreaks of Stx-mediated disease continue to occur (Allison, 2007). Theoretical work, such as that presented in this thesis, represent an important contribution in determining how these phages interact with their hosts in cellular, ecological and evolutionary time; this thereby contributes to a better understanding of the evolution of phage strains with consequences for limiting the spread of disease among humans.

Bibliography

Ackers, G.K., Johnson, A.D., Shea, M.A., 1982. Quantitative model for gene regulation by λ phage repressor. Proc. Nat. Acad. Sci. USA 79, 1129-1133.

Adler, H.I., Haskins, S.D., 1960. Heterogeneity of cultures of *Escherichia coli* B/r. Nature 4748, 249-251.

Allison, H.E., 2007. Stx-phages: drivers and mediators of the evolution of STEC and STEC-like pathogens. Future Microbiol. 2 (2), 165-174.

Allison, H.E., Sergeant, M.J., James, C.E., Saunders, J.R., Smith, D.L., Sharp, R.J., Marks, T.S., McCarthy, A.J., 2003. Immunity profiles of wild-type and recombinant Shiga-like toxin-encoding bacteriophages and characterization of novel double lysogens. Infect. and Imm. 71 (6), 3409-3418.

Arkin, A., Ross, J., McAdams, H.H., 1998. Stochastic kinetic analysis of developmental pathway bifurcation in phage λ-infected *E. coli* cells. Genetics 149, 1633-1648.

Aurell, E.S., Brown, S., Johnson, J., Sneppen, K., 2002. Stability puzzles in phage λ. Phys. Rev. E 65, 051914.

Bille, E., Zahar, J.R., Perrin, A., Morelle, S., Kriz, P., Jolley, K.A., Maiden, M.C.J., Dervin, C., Nassif, X., Tinsley, C.R., 2005. A chromosomally integrated bacteriophage in invasive meningococci. J. Exp. Med. 201, 1905-1913.

Boots, M., Haraguchi, Y., 1999. The evolution of costly resistance in host-parasite systems. Am. Nat. 153(4), 359-370.

Bowers, R.G., Hoyle, A., White, A., Boots, M., 2005. The geometric theory of adaptive evolution. J. Theor. Biol. 233, 363-377.

Bowers, R.G., White, A., 2002. The adaptive dynamics of Lotka-Volterra systems with trade-offs. Math. Biosci. 175, 67-81.

Bremer, H., Dennis, P.P., 1996. Modulation of chemical composition and other parameters of the cell by growth rate. *Escherichia coli* and Salmonella: Cellular and Molecular Biology. Neidhart, F.C. (ed.). Washington, DC: American Society for Microbiology. 1553-1569.

Campbell, A., 1961. Conditions for the existence of bacteriophage. Evolution 15, 153-165.

Canchaya, C., Fournous, G., Brussow, H., 2004. The impact of prophages on bacterial chromosomes. Mol. Microbiol. 53, 9–18.

Cheng, H.H., Muhlrad, P.J., Hoyt, M.A., Echols, H., 1988. Cleavage of the CII protein of phage lambda by purified HflA protease: control of the switch between lysis and lysogeny. Natl. Acad. Sci. USA 85, 78882-7886.

Christiansen, F.B., 1991. On conditions for evolutionary stability for a continuously varying character. Am. Nat. 138, 37-50.

Christiansen, F.B., Loeschcke, V., 1980. Evolution and intraspecific competition 1. One-locus theory for small additive genetic effects. Theor. Popul. Biol. 18 (3), 297-313.

The Condor Software Program. Computer Sciences Department of the University of Wisconsin-Madison. http://www.cs.wisc.edu/condor/.

Cooper, S., Helmstetter, C.E., 1968. Chromosome replication and the division cycle of *Escherichia coli* B/r. J. Mol. Biol. 31, 519-540.

Dodd, I.B., Perkins, A.J., Tsemitsidis, D., Egan, B., 2001. Octamerization of lambda CI repressor is needed for repression of P_{RM} and efficient switching from lysogeny. Gene. Dev. 15, 3013-3022.

Dziva, F., van Diemen, P.M., Stevens, M.P., Smith, A.J., Wallis, T.S., 2004. Identification of *Escherichia coli* O157:H7 genes influencing colonization of the bovine gas-

trointestinal tract using signature-tagged mutagenesis. Microbiology 150, 3631-3645.

Eshel, I., 1983. Evolutionary and continuous stability. J. Theor. Biol. 103, 99-111.

Evans, T.W., Bowers, R.G., Mortimer, A.M., 2007. Modelling the stability of Stx lysogens. J. Theor. Biol. 248, 241-250.

Fogg, P.C.M., Gossage, S.M., Smith, D.L., Saunders, J.R., McCarthy, A.J., Allison, H.E., 2007. Identification of multiple integration sites for Stx-phage $\Phi 24_B$ in the *Escherichia coli* genome, description of a novel integrase and evidence for a functional anti-repressor. Microbiol. 153, 4098-4110.

Geritz, S.A.H., Kisdi, E., Meszena, G., Metz, J.A.J., 1998. Evolutionarily singular strategies and the adaptive growth and branching of the evolutionary tree. Evol. Ecol. 12, 35-57.

Giafis, A., 2007. Unpublished PhD thesis.

Gibson, M.A., Bruck, J., 2000. Efficient exact stochastic simulation of chemical systems with many species and many channels. J. Phys. Chem. A 104, 1876-1889.

Gillespie, D.T., 1976. A general method for numerically simulating the stochastic time evolution of coupled chemical reactions. J. Comp. Phys. 22(4), 403-434.

Gillespie, D.T., 1977. Exact stochastic simulation of coupled chemical reactions. J. Phys. Chem. 81(25), 2340-2361.

Gillespie, D.T., 2001. Approximate accelerated stochastic simulation of chemically reacting systems. J. Chem. Phys. 115, 1716-1733.

Gyles, C.L., 2007. Shiga toxin-producing *Escherichia coli*: an overview. J. Anim. Sci. 85, E45-E62.

d'Herelle, F., 1917. Sur un microbe invisible antagoniste des bacilles dysenterique. Acad. Sci. Paris. 165, 373-375.

Herold, S., Karch, H., Schmidt, H., 2004. Shiga toxin-encoding bacteriophages - genomes in motion. Int. J. Med. Microbiol. 294, 115-121.

Herskowitz, I., Hagen, D., 1980. The lysis-lysogeny decision of phage λ: explicit programming and responsiveness. Annu. Rev. Genet. 14, 399-445.

Howe, M.M., Bade, E.G., 1975. Molecular biology of bacteriophage Mu. Science 190, 624-632.

Johannessen, G.S., James, C.E., Allison, H.E., Smith, D.L., Saunders, J.R., McCarthy, A.J., 2005. Survival of a Shiga toxin-encoding bacteriophage in a compost model. FEMS Microbiol. Lett. 245, 369-375.

Johnson, A.D., Meyer, B.J., Ptashne, M., 1979. Interactions between DNA-bound repressors govern regulation by the lambda phage repressor. Proc. Natl. Acad. Sci. USA 76, 5061-5065.

Karmali, M.A., Petric, M., Lim, C., Fleming, P.C., Steele, B.T., 1983. *Escherichia coli* cytotoxin, haemolytic-uraemic syndrome, and haemorrhagic colitis. Lancet 2, 1299-1300.

Kihara, A., Akiyama, Y., Ito, K., 1997. Host regulation of lysogenic decision in bacteriophage lambda: transmembrane modulation of FtsH (HflB), the cII degrading protease, by HflKC (HflA). Proc. Natl. Acad. Sci. USA 94, 5544-5549.

Koudelka, A.P., Hufnagel, L.A., Koudelka, G.B., 2004. Purification and characterization of the repressor of the Shiga toxin-encoding bacteriophage 933W: DNA binding, gene regulation, and autocleavage. J. Bacteriol. 186, 7659-7669.

Kourilsky, P., 1973. Lysogenization by bacteriophage lambda. I. Multiple infection and the lysogenic response. Molec. Gen. Genet. 122, 183-195.

Lederberg, E.M., 1951. Lysogenicity in *E. coli* K-12. Genetics 36, 560.

Leon-Garcia, A., 1994. Probability and Random Processes for Electrical Engineering. Addison-Wesley Publishing: Reading, MA.

Levin, B.R., Stewart, F.M., Chao, L., 1977. Resource limited growth competition and predation: a model and some experimental studies with bacteria and bacteriophage. Amer. Natur. 111, 3-24.

Little, J.W., Shepley, D.P., Wert, D.W., 1999. Robustness of a gene regulatory circuit. EMBO J. 18, 4299-4307.

Livny, J., Friedman, D.I., 2004. Characterizing spontaneous induction of Stx encoding phages using a selectable reporter system. Mol. Microbiol. 51 (6), 1691-1704.

The MathWorks, Inc., 1984-2008. http://www.mathworks.co.uk/.

Maynard Smith, J., Price, G.R., 1973. The logic of animal conflict. Nature 246, 15-18.

de Mazancourt, C., Dieckmann, U., 2004. Trade-off geometries and frequency-dependent selection. Am. Nat. 164(6), 765-778.

Metz, J.A.J., Nisbet, R.M., Geritz, S.A.H., 1992. How should we define "fitness" for general ecological scenarios? Trends Ecol. Evol. 7, 198-202.

Miller, M.R., White, A., Boots, M., 2005. The evolution of host resistance: tolerance and control as distinct strategies. J. Theor. Biol. 236, 198-207

Mittler, J.E., 1996. Evolution of the genetic switch in temperate bacteriophages. I. Basic theory. J. Theor. Biol. 179, 161 172.

Monod, J., 1949. The growth of bacterial culture. Annu. Rev. Microbiol. 3, 371-394.

Muniesa, M., Lucena, F., Jofre, J., 1999. Comparative survival of free Shiga toxin 2-encoding phages and *Escherichia coli* strains outside the gut. Appl. Environ. Microbiol. 65, 5615-5618.

Novick, A., Szilard, L., 1950. Experiments with the Chemostat on spontaneous mutations of bacteria. Proc. Natl. Acad. Sci. USA 36(12), 708-719.

Oppenheim, A.B., Kobiler, O., Stavans, J., Court, D.L., Adhya, S., 2005. Switches in bacteriophage lambda development. Annu. Rev. Genet. 39, 409-429.

Powell, E.O., 1956. Growth rate and generation time of bacteria, with special reference to continuous culture. J. Gen. Microbiol. 15, 492-511.

Powell, E.O., 1967. The growth rate of microorganisms as a function of substrate concentration. In Microbial Physiology and Continuous Culture (edited by E.O. Powell et al). HMSO, London.

Ptashne, M., 1986. A Genetic Switch, Gene Control and Phage Lambda. Cell Press, Cambridge, MA.

Ptashne, M., 1992. A Genetic Switch: Phage Lambda and Higher Organisms. Cell Press and Blackwell Scientific Publications.

Ptashne, M., 2004. A Genetic Switch: Phage Lambda Revisited, third ed. Cold Spring Harbor Laboratory Press, New York.

Ptashne, M., Gann, A., 2000. Genes and Signals. Cold Spring Harbor Laboratory Press, New York.

Puchalka, J., Kierzek, A.M., 2004. Bridging the gap between stochastic and deterministic regimes in the kinetic simulations of the biochemical reaction networks. Biophys. J. 86(3), 1357-1372.

Reinitz, J., Vaisnys, J.R., 1990. Theoretical and experimental analysis of the phage lambda genetic switch implies missing levels of co-operativity. J. Theor. Biol. 145, 295-318.

Riley, L.W., Remis, R.S., Helgerson, S.D., McGee, H.B., Wells, J.G., Davis, B.R., Herbert, R.J., Olcott, E.S., Johnson, L.M., Hargrett, N.T., Blake, P.A., Cohen, M.L., 1983. Hemorrhagic colitis associated with a rare *Escherichia coli* serotype. N. Engl. J. Med. 308, 681-685.

Rosner, J.L., 1972. Formation, induction, and curing of bacteriophage P1 lysogens. Virology 48, 679-689.

Rueffler, C., van Dooren, T. J., Metz, J. A. J., 2004. Adaptive walks on changing landscapes: Levins' approach extended. Annu. Rev. Microbiol. 65(2), 165-178.

Santillan, M., Mackey, M.C., 2004. Why the lysogenic state of phage λ is so stable: a mathematical modeling approach. Biophys. J. 86, 75-84.

Schneider, D., Duperchy, E., Depeyrot, J., Coursange, E., Lenski, R.E., Blot, M., 2002. Genomic comparisons among *Escherichia coli* strains B, K-12, and O157:H7 using IS elements as molecular markers. BMC Microbiology 2:18.

Shea, M.A., Ackers, G.K., 1985. The O_R control system of bacteriophage lambda, a physical-chemical model for gene regulation. J. Mol. Biol. 181, 211-230.

Smith, D.L., Wareing, B.M., Fogg, P.C.M., Riley, L.M., Spencer, M., Cox, M.J., Saunders, J.R., McCarthy, A.J., Allison, H.E., 2007. Multilocus characterization scheme for Shiga toxin-encoding bacteriophages. Appl. Environ. Microb. 73(24), 8032 8040.

Stewart, F.M., Levin, B.R., 1984. The population biology of bacterial viruses: why be temperate. Theor. Popul. Biol. 26, 93 117.

Twort, F., 1915. An investigation on the nature of ultramicroscopic viruses. Lancet, 11, 1241.

Tyler, J.S., Mills, M.J., Friedman, D.I., 2004. The operator and early promoter region of the Shiga toxin type 2-encoding bacteriophage 933W and control of toxin expression. J. Bacteriol. 186 (22), 7670-7679.

Unkmeir, A., Schmidt, H., 2000. Structural analysis of phage-borne *stx* genes and their flanking sequences in Shiga toxin-producing *Escherichia coli* and *Shigella dysentariae* type 1 strains. Infect. Immun. 68 (9), 4856-4864.

Verhulst, P.F., 1838. Notice sur la loi que la population poursuit dans son accroisement. Correspondance mathematique et physique 10, 113-121.

Waldor, M.K., Mekalanos, J.J., 1996. Lysogenic conversion by a filamentous phage encoding cholera toxin. Science 272, 1910-1914.

Watarai, M., Sato, T., Kobayashi, M., Shimizu, T., Yamasaki, S., Tobe, T., Sasakawa, C., Takeda, Y., 1998. Identification and characterization of a newly isolated Shiga toxin 2-converting phage from Shiga toxin-producing *Escherichia coli*. Infect. Immun. 66 (9), 4100-4107.

White, A., Bowers, R.G., 2005. Adaptive dynamics of Lotka-Volterra systems with trade-offs: the role of interspecific parameter dependence in branching. Math. Biosci.

193, 101-117.

White, A., Greenman, J.V., Benton, T.G., Boots, M., 2006. Evolutionary behaviour in ecological systems with trade-offs and non-equilibrium population dynamics. Evol. Ecol. Res. 8, 387-398.